E77-10123

"Made available under NASA sponsorship
In the interest of early and wide dissemination of Earth Resources Survey
Program information and without liability
for any use made thereof."

# APPLICATIONS OF SKYLAB DATA TO LAND USE AND CLIMATOLOGICAL ANALYSIS

CR-151196

T-5290B

By

Robert H. Alexander
John E. Lewis, Jr.
Harry F. Lins, Jr.
Carol B. Jenner
Sam I. Outcalt
Robert W. Pease

U.S. Geological Survey

(E77-10123) APPLICATIONS OF SKYLAB DATA TO LAND USE AND CLIMATOLOGICAL ANALYSIS Final Report (Geological Survey, Reston, Va.) 237 p HC A11/MF A01 CSCL 05B

N77-19556

Unclas
G3/43 00123

## FINAL REPORT
## SKYLAB/EREP INVESTIGATION NO. 469
## URBAN AND REGIONAL ENVIRONMENTAL INFORMATION SYSTEM DEVELOPMENT:
## PART A, CENTRAL ATLANTIC REGIONAL ECOLOGICAL TEST SITE EXPERIMENT

Original photography may be purchased from:
EROS Data Center
10th and Dakota Avenue
Sioux Falls, SD 57198

ORIGINAL CONTAINS
COLOR ILLUSTRATIONS

SPONSORED BY
National Aeronautics and Space Administration
Johnson Space Center
Houston, Texas 77058
and
U.S. Geological Survey
Reston, Virginia 22092

1976

# APPLICATIONS OF SKYLAB DATA TO LAND USE AND CLIMATOLOGICAL ANALYSIS

By Robert H. Alexander, Carol B. Jenner, John E. Lewis, Jr., Harry F. Lins, Jr., Sam I. Outcalt, Robert W. Pease

U.S. Geological Survey

February 1976

Final Report
Skylab/EREP Investigation No. 469
NASA-USGS Order No. T-5290B
Urban and Regional Environmental Information System Development:
CARETS and Census Cities Experiments
Part A: CARETS Experiment

| BIBLIOGRAPHIC DATA SHEET | 1. Report No. | 2. | 3. Recipient's Accession No. |
|---|---|---|---|
| 4. Title and Subtitle Applications of Skylab Data to Land Use and Climatological Analysis | | | 5. Report Date February 1976<br>6. |
| 7. Author(s) R. H. Alexander, C. B. Jenner, J. E. Lewis, Harry F. Lins, Jr., S. I. Outcalt, R. W. Pease | | | 8. Performing Organization Rept. No. |
| 9. Performing Organization Name and Address U.S. Geological Survey<br>Geography Program<br>Mail Stop 710<br>Reston, VA 22092 | | | 10. Project/Task/Work Unit No.<br>11. Contract/Grant No. T-5290-B |
| 12. Sponsoring Organization Name and Address Rigdon E. Joosten<br>NASA Johnson Space Center<br>Houston, TX 77058 | | | 13. Type of Report & Period Covered Type III Final Report<br>14. |

15. Supplementary Notes Sponsored jointly by the National Aeronautics and Space Administration and the U.S. Geological Survey

16. Abstracts

The Skylab investigation in the Central Atlantic Regional Ecological Test Site (CARETS) encompassed two separate but related tasks: (1) Evaluation of photographic sensors S-190A and S-190B as sources of land use information required for planning and managing the land resources in a major metropolitan region, and (2) evaluation of the multispectral scanner S-192, when used in conjunction with associated data and analytical techniques, as a source of information on urban climates and the surface energy balance in an urbanized area.

Photographs from the Skylab S-190B Earth Terrain Camera were of greatest interest in the land use analysis task; they were of sufficiently high resolution to identify and map many Level II and III land use categories. Such photography approaches in discrimination capability that of the high-altitude aircraft photography, but still falls short of being able to supply many of the detailed information needs of local or county-level planning agencies. (Abstract continued on following page)

17. Key Words and Document Analysis. 17a. Descriptors

Land use mapping
Climatology
Remote Sensing
Surface-temperature simulation
Urban studies
Skylab
Energy balance

17b. Identifiers/Open-Ended Terms

17c. COSATI Field/Group

| 18. Availability Statement | 19. Security Class (This Report) UNCLASSIFIED | 21. No. of Pages 210 |
|---|---|---|
| | 20. Security Class (This Page UNCLASSIFIED | 22. Price |

FORM NTIS-35 (REV. 10-73) ENDORSED BY ANSI AND UNESCO. THIS FORM MAY BE REPRODUCED USCOMM-DC 8265-P74

Abstract, continued

After being corrected to allow for the effects of the atmosphere, output from thermal and visible bands of the S-192 multispectral scanner was employed in constructing computer map plots of albedo and surface temperature.

A "predicted" temperature map produced by a surface climate simulation model showed fair correlation with the "observed" map produced from the S-192 data. Results indicate that, with improved methods of manipulating and mapping spaceborne thermal scanner data, land use related components of urban climates, such as the heat island effect, can be measured and modeled more effectively. Skylab-type data systems can thus aid urban land use planning by making information on the climatological consequences of proposed land use patterns available as input to future urban design.

## Preface

This report is one product of a large and complex effort attempting to bring space technology down to Earth--literally--by investigating ways in which information obtained from the Earth-viewing sensors carried aboard Skylab can be used to increase our understanding of the land use and energy transformations at the Earth's surface. The complexity of the effort has dictated a team approach, with each member of the team bringing specialized skills to the common effort. Not all of the members of the team are listed as co-authors; some team members are indeed not even known by the authors, such as the astronauts and the other members of the NASA organization responsible for getting the sensing apparatus into space and safely back to Earth again, and the data processing technicians who saw to it that we received copies of the data as necessary to perform our analysis.

Acknowledgments are hereby given to all of the above unnamed individuals without whose contributions this research would not have been possible. In addition, we wish to acknowledge assistance and support of USGS colleagues James R. Wray, Valerie Milazzo, and Daniel Gallagher, who performed the companion Skylab Census Cities investigation, and from whom we derived much support and assistance throughout the entire adventure. Thanks also are due to John Arnfield and John N. Rayner of the Ohio State University, who examined early drafts of project results and provided a critique of the project. Brian J. L. Berry of the University of Chicago provided guidance on the sampling design for measuring the accuracy of land use maps, and also provided a critical reading of the entire manuscript

in its final stages. Karen S. Letke produced and/or coordinated the production of all final graphics. Responsibility for typing, assembling, correcting and keeping in touch with all of the authors and others who had to approve of the final results, fell to Katherine A. Cook, who was assisted in these tasks by Cynthia L. Cunningham.

Special thanks and acknowledgments go to Rigdon E. Joosten of the NASA Johnson Space Center, who, as Technical Monitor of the project, assisted us in innumerable instances and who displayed commendable patience and understanding in the face of the many frustrating problems we encountered along the way.

By way of explanation of how the many co-authors functioned to bring this effort to fruition, it should first be noted that we were widely dispersed, geographically, throughout the lifetime of this project. For the tasks that required more than one of the authors, this meant cumbersome back-and-forth communication which would have been greatly facilitated if we had had closed circuit television with ability to transmit and display graphics including intermediate computer output. This dispersion of researchers is not recommended in general for the conduct of such projects, but until some organization assembles people in one place with the requisite skills to perform land use and climatological analysis based upon the use of remote sensing data, it will have to suffice.

Each section of the report was made the primary responsibility of certain designated co-authors, but there were of course some benefits obtained from critical reading of the entire manuscript by all of us. Lins was primarily responsible for Chapter 2; Pease, for the portion of

Chapter 3 dealing with the radiation-related maps produced from the Skylab S-192 data, including the "gray-window" calibration to account for atmospheric interference; Lewis, Outcalt, and Jenner for the portion of Chapter 3 dealing with the simulation experiment. Appendix A was written by Pease and appendix B by Jenner and Lewis. Alexander was primarily responsible for Chapters 1 and 4, and for administration and coordination of the entire effort. As to project direction, you do not "direct" a project like this, you merely try to keep up with all the various actors and hope that they end their performance together.

Contents

Page

Abstract---------- 1
Chapter 1: Introduction----------1-1
Development of the project as part of an integrated geographic research package----------1-1
The Geography Program CARETS and Census Cities experiments---------1-5
CARETS component of investigation 469: subject of this report-----1-6
Broad objectives----------1-6
Land use analysis----------1-8
Land use climatology----------1-9
Organization of the report----------1-11

Chapter 2: Assessment of data value for land use inventory and analysis----------2-1
Methodology for conducting the analysis----------2-6
Systematic aligned sample----------2-17
Area measurement comparison----------2-24
Visual assessment of photo characteristics----------2-27
S-190A photography----------2-27
Urban and built-up land----------2-27
Agricultural land----------2-29
Forest land----------2-29
Water----------2-29
Wetland----------2-30
Barren land----------2-30
S-190B photography----------2-30
Urban and built-up land----------2-31
Nonurban land----------2-34
Agricultural land----------2-34
Forest land----------2-34
Water----------2-34
Wetland----------2-35
Barren land----------2-35
Comparisons with aircraft and Landsat data----------2-35
User applications and evaluation----------2-63
Evaluation of Skylab data vis-a-vis future USGS Geography Program needs----------2-68
Evaluation of USGS remote sensor land use classification scheme---2-75

Chapter 3: Land use climatology--a coupled modeling and observational experiment----------3-1
Land use climatology----------3-2
Pre-Skylab developments----------3-5
Early mapping experiments----------3-6
Modeling in land use climatology----------3-8
Radiation-related maps from S-192 data----------3-13
The S-192 data----------3-13
The problem of atmospheric modification--the gray-window model----------3-17
Surface-collected data of use for calibration----------3-19

Contents--Continued

Page

Experiments with a two-target thermal IR calibration - band 13----3-22
Calibration using the atmospherics of the optical path - band 13----3-25
Data correction factor----3-30
Turbidity and other active air components----3-31
The necessity of the gray-window calibration----3-40
A map of the thermal state - distribution of radiation temperatures----3-41
A map of terrestrial albedos----3-41
Commentary about the mapping experiment----3-48
The simulation experiment----3-53
Modeling the spatial pattern----3-53
Scale considerations----3-55
Sources of land use information----3-55
Land use data collection----3-58
Surface characteristics----3-61
Building configuration----3-61
Surface roughness for vegetation----3-63
Surface wet fraction----3-63
Substrate thermal diffusivity and conductivity----3-63
Surface albedo----3-63
Emissivity----3-65
Data input into simulated surface radiant temperature map---3-65
Comparison of simulated and observed surface temperatures----3-67

Chapter 4: Summary and recommendations----4-1
Land use analysis----4-1
Summary----4-1
Recommendations----4-4
Land use climatology----4-8
Summary----4-8
Evaluation by review panel----4-10
Recommendations----4-13

References----R-1
Appendix A----A-1
Appendix B----B-1
Appendix C----C-1

## Illustrations


Page

Figure 2.1. Index map showing location of ground trace, S-190A camera system, Skylab 3 pass over CARETS, August 5, 1973----2-2

2.2. Index map showing location of ground trace, S-190B camera system, Skylab 3 pass over CARETS, August 5, 1973----2-3

2.3. Index map to S-190B frame 83-166, Skylab 3 pass over CARETS, August 5, 1973----2-5

2.4. Enlarged print of S-190A photograph, Fairfax, Virginia. EDC-010120----2-11

2.5. Enlarged print of S-190B photograph, Fairfax, Virginia. EDC-010121----2-13

2.6. Enlarged print, high-altitude photograph of Fairfax, Virginia. EDC-010122----2-15

2.7. Level III land use map, based on interpretation of Skylab S-190B photography, Fairfax, Virginia----2-18

2.8. Level III land use map, based on interpretation of high-altitude aircraft photography, Fairfax, Virginia----2-19

2.9. Location of points for comparing Skylab and aircraft-derived land use data, Fairfax, Virginia----2-21

2.10a - 2.10m. Illustrations of selected land use types in the CARETS area as imaged by high-altitude aircraft, Skylab S-190B, and Landsat-1:

2.10a. Single-family residential. EDC-010123----2-37

2.10b. Multi-family residential. EDC-010124----2-39

2.10c. Industrial. EDC-010125----2-41

2.10d. Central business district. EDC-010126----2-43

2.10e. Commercial strip. EDC-010127----2-45

2.10f. Shopping centers. EDC-010128----2-47

2.10g. Airport. EDC-010129----2-49

Illustrations--Continued

Page

2.10h. Industrial and commerical complexes. EDC-010130---------2-51

2.10i. Strip mines, quarries and gravel pits. EDC-010131--------2-53

2.10j. Transitional (and single-family residential). EDC-010132----------2-55

2.10k. Cropland and pasture. EDC-010133----------2-57

2.10L. Mixed forest land. EDC-010134----------2-59

2.10m. Utility rights-of-way. EDC-010135----------2-61

Figure 3.1. Distribution of PCM counts from S-192 output - band 13---3-23

3.2. Rawinsonde profile for 7:15 a.m. EST, August 5, 1973, Washington, D.C.----------3-27

3.3. Extinction coefficients ($\gamma$) at a wavelength of 10.591 μm for various visibility ranges----------3-34

3.4. Absorption spectrum of Peroxyacetyl Nitrite (PAN)--------3-36

3.5. Location of mapped areas, thermal mapping experiment-----3-42

3.6. Map showing distribution of surface radiation temperatures, Washington-Baltimore area, derived from band 13, S-192 (SDO channel 21), August 5, 1973---------3-43

3.7. Distribution of generalized surface albedos for the Washington-Baltimore area, derived from band 6, S-192 (SDO channel 7), August 5, 1973----------3-45

3.8. Land use map of study area for simulation of surface temperatures----------3-59

3.9. Map of surface radiation temperatures for the Baltimore area made by simulation procedure described in text-----3-69

3.10. Map of surface radiation temperatures for the Baltimore area made from Skylab S-192 data, band 13, as calibrated by procedure described in text----------3-71

## Tables


Page

Table 2.1. Summary of data from remote sensors used in this study---2-7

2.2. Version of the Anderson multilevel land use classification system for use with remote sensor data, used in this study----------2-9

2.3. Matrix listing the number of occurrences of land use categories interpreted from S-190A photography versus land use categories interpreted and field checked from aircraft photography for the city of Fairfax, Virginia--2-22

2.4. Matrix listing the number of occurrences of land use categories interpreted from S-190B photography versus land use categories interpreted and field checked from aircraft photography for the city of Fairfax, Virginia--2-23

2.5. Comparison of area measurements of Level III land use categories derived from aircraft and Skylab S-190B data sources, Fairfax, Virginia, in hectares and percent of total area mapped----------2-26

2.6. Relative comparison of sensor detection capabilities-----2-64

2.7. Comparison of wavelength bands for Landsat and Skylab photographic systems----------2-69

3.1. Necessary simulation data----------3-9

3.2. Computation of geographical parameters, as used in surface climate simulation model----------3-11

3.3. Urban terrain factors, as used in surface climate simulation model----------3-12

3.4. Ground correlation data collected for land use climatology experiment----------3-20

3.5. Temperature/water vapor profile from rawinsonde data, Washington, D.C., 11:15 a.m. GMT, August 5, 1973-------3-29

3.6. Atmospheric profile for gray-window calibration of Skylab data including the effects of turbidity----------3-37

3.7. Procedure for converting PCM counts to T°C----------3-39

3.8. Procedure for constructing albedo map----------3-49

3.9. USGS land use classification system as presented in Circular 671----------3-57

Tables--Continued

Page

3.10. Values of surface characteristics used as input for each land use category----------3-62

3.11. Land use associated values of surface wet fraction-------3-64

3.12. Meteorological conditions for August 5, 1973----------3-66

3.13. Simulated surface temperatures of each land use----------3-68

## ABSTRACT

The Skylab investigation in the Central Atlantic Regional Ecological Test Site (CARETS) encompassed two separate but related tasks: (1) evaluation of photographic sensors S-190A and S-190B as sources of land use information required for planning and managing the land resources in a major metropolitan region, and (2) evaluation of the multispectral scanner S-192, when used in conjunction with associated data and analytical techniques, as a source of information on urban climates and the surface energy balance in an urbanized area.

Photographs from the Skylab S-190B Earth Terrain Camera were of greatest interest in the land use analysis task; they were of sufficiently high resolution to identify and map many Level II and III land use categories. Such photography approaches in discrimination capability that of the high-altitude aircraft photography, but still falls short of being able to supply many of the detailed information needs of local or county-level planning agencies.

After being corrected to allow for the effects of the atmosphere, output from thermal and visible bands of the S-192 multispectral scanner was employed in constructing computer map plots of albedo and surface temperature.

A "predicted" temperature map produced by a surface climate simulation model showed fair correlation with the "observed" map produced from the S-192 data. Results indicate that, with improved methods of manipulating and mapping spaceborne thermal scanner data, land use related components of urban climates, such as the heat island effect, can be measured and modeled more effectively. Skylab-type data systems can thus aid urban land use planning by making information on the climatological consequences of proposed land use patterns available as input to future urban design.

# CHAPTER 1

## INTRODUCTION

This report summarizes results of a series of experiments with data provided by the National Aeronautics and Space Administration (NASA) under the Skylab Earth Resources Experiment Package (EREP). These experiments involved the applications of remote sensor data in analyzing patterns and processes of land use on the surface of the Earth, as observable from above, with special reference to the study of man-induced climatic changes in urban areas.

In addition to the specific focus on data actually obtained by the Skylab mission, the research activities reported on here represent a portion of a broader program of close cooperation between two Federal agencies, NASA and the U.S. Geological Survey (USGS) extending over the past 10 years. This cooperation involved a variety of research, coordination, and information exchange activities, in which each agency contributed its specialized expertise toward a common goal of improving the quality and usefulness of information needed to monitor critical changes in Earth-surface environments, and to assist in the solving of a variety of pressing environmental problems.

## DEVELOPMENT OF THE PROJECT AS PART OF AN INTEGRATED GEOGRAPHIC RESEARCH PACKAGE

The research reported on here was conducted as part of an integrated environmental experiment in the Central Atlantic Regional Ecological Test Site (CARETS), the purposes of which were to bring together several diverse lines of investigative effort that had grown over the past few

years--to bring these together in the context of applications to the solution of environmental problems growing out of practices of human use of the land and water resources. Thus the effort is multidisciplinary, a coordination and cooperation among investigators having quite different specialized scientific and technical skills. The investigation has many of the strengths and weaknesses of such a team approach.

One of the research fields or discipline specialty areas that is brought together in this investigation is the one running through modern geographic analysis, the application of the tools and techniques of geography and spatial analysis to the study of spatial processes affecting both the physical and socioeconomic environments of man. Those whose knowledge of the science of geography is derived primarily from times prior to the mid-1950's might gain brief insight into more recent developments in the field by reference to some of the summary papers and compendia. See, for example, Ackerman (1958), Berry and Marble (1968), and Taaffe (1970).

Another line of research joined in this investigation is remote sensing, which received impetus from military surveillance and intelligence data-gathering requirements in the post World War II period, and which was further developed in the civilian economy by the considerable body of research supported by the various NASA Earth observation programs from orbiting satellites. A summary statement of geographic research potential resulting from these developments is in National Academy of Sciences (1966).

A third line of research has been the development of computerized information systems applied to the handling of map data, a development

that is essential to the utilization of the very large information-gathering capabilities of orbiting remote sensors. For a recent summary of this field as it pertains to remote sensing systems, see Steiner and Salerno (1975).

A fourth research field or subdiscipline brought into this investigation is that of energy and water balance climatology, as described or summarized in such references as, for example, Miller (1965), Geiger (1965), Sellers (1965), Hare (1973).

Admittedly, the technology for monitoring changes in the environment has lagged behind the technology for producing those changes, through increases in population concentrations and massive construction works associated with the building of a modern industrial society. However, the kinds of experiments conducted under the auspices of the Skylab program are a step in the right direction toward closing those technological gaps.

The CARETS project was already in existence when Skylab experiments were initiated. Funding other than Skylab was provided by the NASA Earth Resources Aircraft Program, a major NASA ERTS (later renamed Landsat) investigation, and by the EROS and Geography Programs of the U.S. Geological Survey.

The underlying assumption of the CARETS model is that changes on the Earth's surface that can be observed from remote sensors are related to environmental consequences in ways that can be established through a program of correlated observations. Although the experimentation in the 1960's and early 1970's with a variety of remote sensors has proven

that those sensors have a capability of obtaining a wide variety of information on significant environmental parameters and processes, the obtaining, processing, handling, and using of such data would be a very expensive activity indeed for any significant portion of the critical environmental areas undergoing change within the area of the United States. However, one data set that is readily extractible from the remote sensors is one that has been called "land use," or more properly "land use/land cover," i.e., the surface configuration of the terrain, both land and water, which is directly or indirectly a consequence of some particular use category invented by man.

Forest land may be observed essentially in the natural state. But the potential use of forest land as a source of forest products, or as recreational area, or as a watershed protection area, can be defined in terms of man's use or potential use. More obvious categories of use are those showing the direct artifacts or consequences of human habitation--houses, streets, factories, major transportation arteries, utility corridors, large built-up areas. These land use phenomena, according to the CARETS model, are observed from the remote sensors, and then related empirically (or calibrated) to environmental consequences such as runoff, sedimentation, air pollution, and changes in the local or regional climates (Alexander and others, 1975). The set of experiments reported here deals with the combination of observations of land use categories and one of the environmental consequences of those land use patterns--namely changes in climate in and around cities. This effect is sometimes called the urban heat island effect. Though documented for

some time in the literature, e.g. Landsberg (1956) and Lowry (1967), only recently has there been more widespread recognition that urban heat island effects may be significant for energy expenditures for heating and cooling. Thus a practical reason exists for pursuing research efforts that may yield more information on this land use related phenomenon. The term "land use climatology" is used here to encompass the study of thermal and micro-climatological consequences of land use patterns and their changes.

The combination of remote sensors carried aboard the Skylab EREP proved to be valuable for gathering essential information both on studies of land use and on studies of the climatological consequences of land use change.

## THE GEOGRAPHY PROGRAM CARETS AND CENSUS CITIES EXPERIMENTS

The development of this Skylab investigation grew out of NASA-USGS negotiations beginning in 1971 to consider a program "package" of experiments with Skylab data, all attuned to the needs of the USGS Geography Program as it existed at that time. As a result of those negotiations, a large package proposal entitled "Regional and Urban Environmental Information System Experiment" was submitted, under the direction of the Geography Program Chief at that time, Dr. Arch C. Gerlach.

After review of all Skylab proposals, the USGS Geography Program package was reduced to two of its component experiments: the CARETS experiment directed by Robert H. Alexander, and the Census Cities experiment directed by James R. Wray. These two experiments benefitted

considerably from being located in the same program office, but they were, in fact, conducted as two separate research efforts, with each principal investigator responsible for his portion. This report therefore concerns only the CARETS portion of Skylab Investigation No. 469, NASA Order T-5290 B.

## CARETS COMPONENT OF INVESTIGATION 469: SUBJECT OF THIS REPORT

### Broad Objectives

The overall objectives of this investigation were to test the hypothesis that data from Skylab can be made an integral part of a regional environmental information system, encompassing both inventory of the resource base and monitoring of changes along with their effects on the quality of the environment. Along with the Landsat demonstration project in the CARETS region (Earth Resources Technology Satellite Investigation SR-125), this Skylab project was to have been conducted as a prototype of a new land use and geographic analysis function within the USGS. The CARETS project was carried out in cooperation with Federal, State, and local agencies having resource and environmental monitoring interests in the test region.

The goals of the demonstration project, and the operational programs that are expected to grow out of it, are to make accurate and timely environmental information available to those who make decisions affecting the use of the land, water, and air resources, and thus to improve the environmental complex that develops from those decisions. Implementation will be by means of an integrated three-pronged approach: (1) The establishment of a land use data base and monitoring of its

change; (2) the assessment, monitoring, and modeling of changes in the total environmental complex relating to the land use change; and (3) the linking of (1) and (2) in a regional information service for the institutions that will be users of the information derived from Skylab sensor systems, in conjunction with appropriate aircraft and ground observations.

The ultimate objective of the demonstration project is to develop both an integrated multidisciplinary ecological outlook and a new kind of information service for the Federal, State, regional, and local level institutions with environmental decisionmaking responsibilities in the region. The ecological outlook will enable the decisionmakers to see the likely environmental effects of changes or proposed changes in resource use patterns, such as air and water pollution resulting from conversion of land from nonurban to urban uses, or such as changes in the local microclimates resulting also from land use changes. The information derived from remote sensing will be integrated with information from other sources, such as the census of population, geological maps, and meteorological data, as required for the problem-solving and decisionmaking models that are to be used. The institutions that make those decisions will participate in a demonstration and evaluation of the remote sensing techniques as aids in solving environmental problems resulting from the impact of increasing human use of the land, water, and air resources of the region.

The test region for the CARETS project is defined to encompass a major segment of the Central Atlantic coastal and estuarine physiographic province plus a heavily populated and closely interdependent hinterland, which includes the national capital area and the other major urbanized

areas of Philadelphia, Baltimore, Richmond, and Norfolk. This test region approximates the southern half of an area that has previously been studied and defined as Megalopolis, one of the world's major concentrations of urban and industrial activities (Gottmann, 1961).

Just to the south of Megalopolis is an area, part of the CARETS test region, which is already being subjected to megalopolitan land use pressures and rapid change. This area may be spared some of the most undesirable consequences of uncontrolled development only by the most urgent regional planning and management efforts. The test zone thus provides an excellent regional laboratory for monitoring the land use and related environmental change and for demonstrating to the decision-makers the values of obtaining rapid and timely environmental information from orbiting remote sensors.

## Land Use Analysis

Within the broad framework of the larger objectives stated in the previous section, two separate but interrelated portions of the investigation were undertaken: land use analysis and land use climatology. The objectives of the land use analysis portion were to test the ability of the Skylab photographic sensors (S-190A and S-190B) to replicate land use categories already developed for the region using the two-digit USGS land use classification scheme, and further, to examine the adequacy of the resulting land use information for the requirements of key users at the State, county, and local levels within the region. The user evaluation was to be accomplished through 1-day workshops, during which representatives of user institutions were invited to the USGS National

Center for presentations on the data systems and examples of aircraft, Landsat, and Skylab data that were available in several formats for inspection. In addition, follow-up interviews, usually at the offices of the user institutions, were carried out after users had had an opportunity to examine samples of data that were distributed at the workshops. The intention of the land use analysis component of the experiment was to evaluate the Skylab results as the space component of a three-part, space-air-ground data system of land use analysis in a metropolitan area.

## Land Use Climatology

A key portion of the environmental problem-solving strategy of the CARETS model is the establishment of relationships between land use/land cover as detected by the Skylab sensors and certain environmental consequences of those land use patterns, such as stream runoff, water quality, erosion, and changes in the local climates of urbanized areas. The land use climatology portion of the investigation addresses the latter type of environmental change, taking advantage of the ability of the Skylab multispectral scanner system (S-192) to obtain information in both visible and thermal portions of the electromagnetic spectrum. Building upon prior NASA-funded experiments utilizing multispectral scanners carried aboard aircraft, this experiment had as one of its objectives to determine the extent to which Skylab data can be used to assess energy exchange parameters crucial to the measurement of the climatological impact of drastic land use changes such as urbanization and land clearing. A convenient vehicle for investigating this change is the so-called heat island effect, experienced by those living in and

around urban areas and already well documented in the scientific literature. Specifically, the intent of the investigation was to combine observed and simulated surface temperatures to develop procedures for routinely using data from spaceborne platforms to obtain quantitative information on the distribution of solar energy received at the surface. Such information is fundamental to the establishment of local microclimates that have a bearing on human comfort, to the supply of energy for such key processes as evaporation and photosynthesis, and possibly in the future to the direct supply of solar energy for heating.

The land use climatology experiment approach involved two major tasks. First, investigators used Skylab S-192 data with simultaneously collected ground data and pertinent meteorological data for developing calibration procedures to account for the attenuation of the signal caused by properties of the intervening atmosphere. Second, we combined the new calibration procedures with an effort to apply a surface climatological simulation model to the same area as that observed by the Skylab sensor. The use of the simulation modeling technique in conjunction with observations from remote sensors was expected to greatly enhance and improve the utility of remote sensor data, which cannot necessarily be collected often enough or at specific times in the diurnal or annual cycle for extrapolation to true energy balance values. Thus, the simulation technique enables extrapolation of results of remote sensing measurements at a specific instant to other times of the day or year, with variations in the astronomical, meteorological, or surface terrain factors supplied by changing input parameters to the simulation procedure.



REPRODUCIBILITY OF THE
ORIGINAL PAGE IS POOR

## Organization of the Report

Chapter 1 has presented introductory and background material setting the experiment in the context of related work and program objectives. Chapter 2 presents the results of the land use analysis portion of the experiment, based upon evaluation of the photographic sensor experiments, S-190A and S-190B. In addition, Chapter 2 contains a discussion of the user response to this material, an evaluation of Skylab photographic data for meeting information needs of the USGS Geography Program, and a comment on the USGS land use classification scheme and its applicability with data such as those supplied by the Skylab and related sensor systems. Chapter 3 contains the summary results of the land use climatology portion of the experiment. The first portion of the chapter deals with the development of radiation-related maps from the S-192 data, as built upon experiments conducted prior to the Skylab mission, and as corrected by the Pease gray-window model for atmospheric calibration of the signal received from the thermal channel of the S-192 scanner. The second portion of Chapter 3 presents the results of the simulation experiment and the simulated surface temperature data sets and map produced by that effort. Chapter 4 contains summary, conclusions, and recommendations. Two technical appendices are also included to provide more detail on certain aspects of the land use climatology experiment. Appendix A contains the results of the Baltimore aircraft mission flown in 1972 by the NASA aircraft program utilizing the Environmental Research Institute of Michigan's aircraft and multispectral scanner. Appendix B contains the technical details of the simulation model. A list of other reports sponsored by our NASA Skylab investigation and by pre-Skylab NASA funding of energy balance studies in the USGS Geography Program constitutes appendix C.

CHAPTER 2

## ASSESSMENT OF DATA VALUE FOR LAND USE INVENTORY AND ANALYSIS

This chapter contains the summary results of examination of the Skylab photographic sensors (S-190A, multispectral camera system, and S-190B, Earth Terrain Camera) for their applications to the inventory and analysis of land use in the Central Atlantic region.

The analysis contained herein is based upon data received from the Skylab 3 pass over the CARETS area on August 5, 1973. Other passes over the test region did not produce data suitable for the analysis. The ground trace of the Skylab 3 "footprint" over the CARETS region for the photographic sensors is shown in figures 2.1 and 2.2.

In the early planning stages for this experiment, before the Skylab launch, it was hoped that complete photographic coverage for the region could be obtained. Such coverage could have been the data source for land use mapping and uniform evaluation throughout the test region, as well as an update of the land use data base for 1970, which had been prepared from high-altitude aircraft data as part of the CARETS-Landsat experiment. When it was learned that only a portion of the CARETS test region could be covered by Skylab photography a different strategy was devised, namely, to map only a selected sample area, to make detailed quantitative study of the accuracy of the resulting map, and to examine other portions of the test site coverage for suitability of data as applied to identification and mapping of various land use classes and levels of detail.

The Skylab photographic data of most interest to the investigators and the users of CARETS land use informtion were photographs taken by the S-190B Earth Terrain Camera experiment. This photography was of sufficient

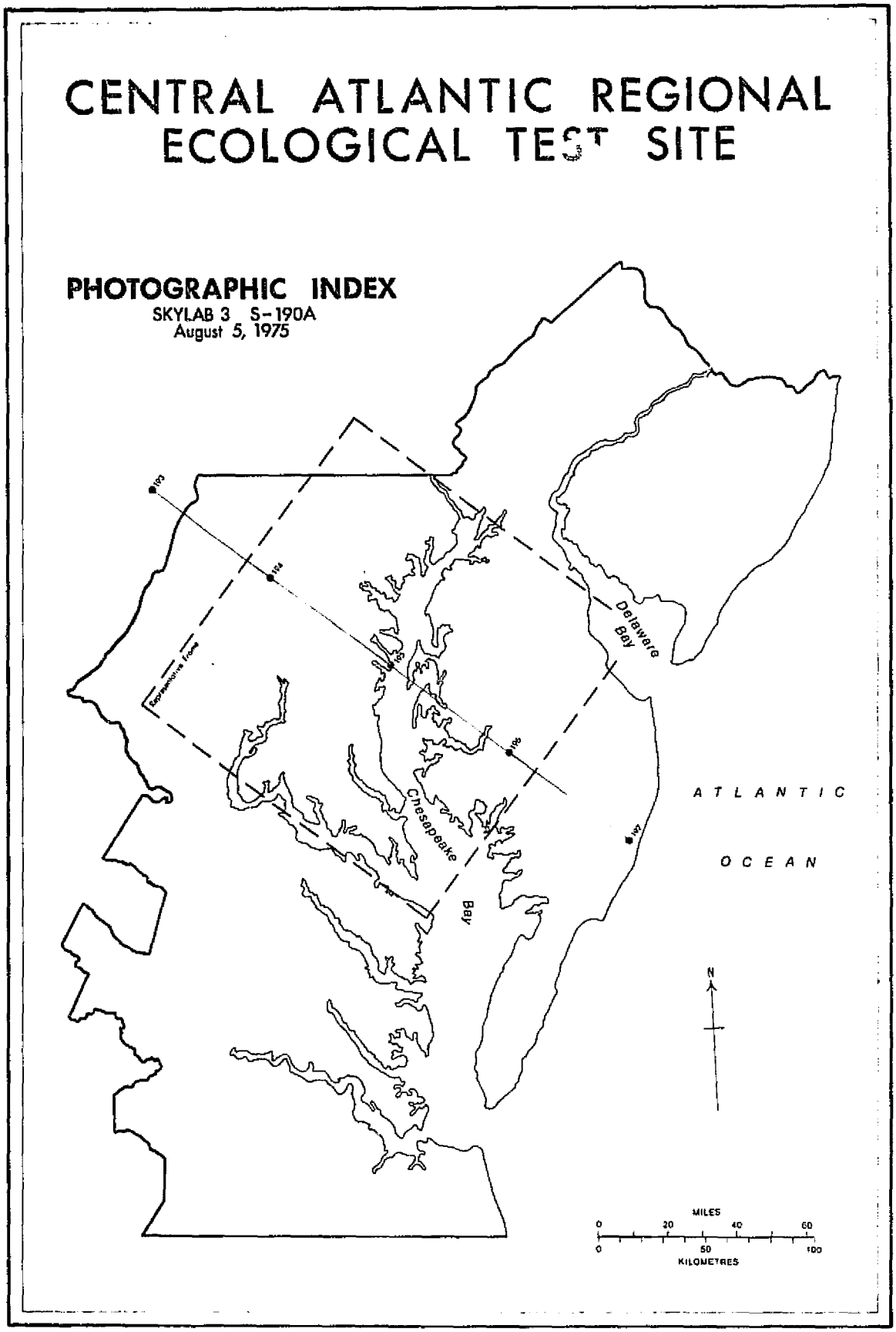


Figure 2.1--Index map showing location of ground trace, S-190A camera system, Skylab 3 pass over CARETS, August 5, 1973.

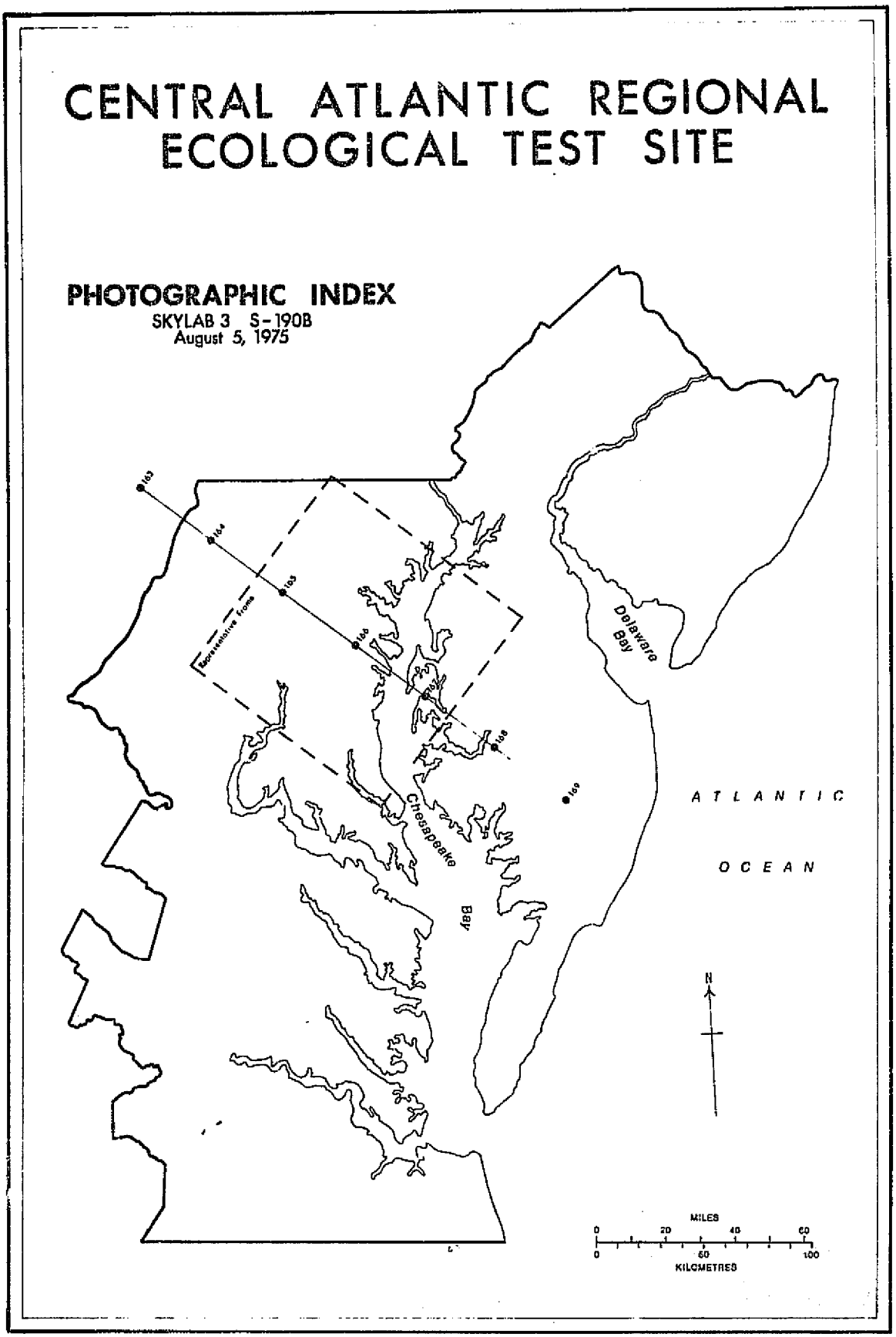


Figure 2.2--Index map showing location of ground trace, S-190B camera system, Skylab 3 pass over CARETS, August 5, 1973.

spatial resolution to allow identification of most of the Level II categories, and many Level III categories. It even approached in capability the resolution of the high-altitude aerial photography. The S-190B photography was found to provide relatively high resolution data, which can be a valuable source of information for land use maps and inventories, in urban as well as nonurban areas. These results indicate that photography of the caliber of S-190B could be of considerable value in the work of planning agencies at State or regional levels. It is not quite of sufficient resolution, however, to be used for many local and urban land use data requirements or for many environmental impact applications.

Because of this greater interest in the S-190B photography, as compared to the S-190A photography, the major portion of the effort in this analysis is devoted to the S-190B. That is, the greater spatial resolution was considered to be of more interest, for purposes of this experiment, than the multispectral capability of the S-190A. In any operational system, the best combination of the two systems would be employed to take advantage of both spatial resolution and spectral discrimination and enhancement, as dictated by the objectives of the operation.

The examples of land use applications cited in this study were taken from a single frame of S-190B photography, number 83-166 taken on the Skylab 3 pass over the CARETS test site on August 5, 1973. Figure 2.3 contains an index map of this frame of photography, marked to show location of sites selected for detailed analysis.

After discussing the methodology for analyzing the detailed land use map of Fairfax, Virginia, the chapter deals with specific land use categories and their suitability for extraction from the S-190A and S-190B photography. Following that is a series of comparisons with aircraft and Landsat data,



REPRODUCIBILITY OF THE
ORIGINAL PAGE IS POOR

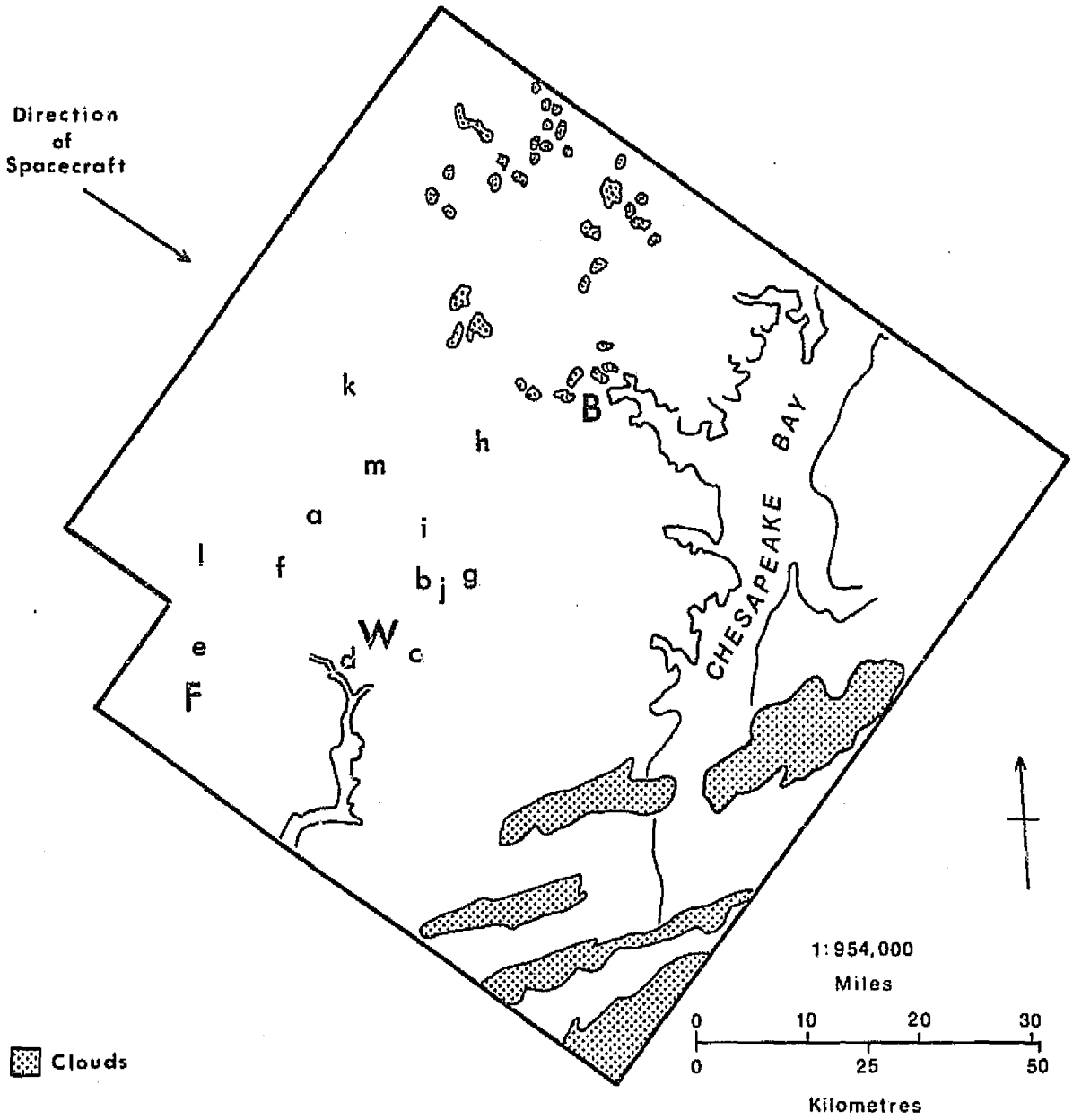


Figure 2.3--Index map to S-190B frame 83-166, Skylab 3 pass over CARETS, August 5, 1973; F = Fairfax, Va.; W = Washington, D.C.; B = Baltimore, Md.; a through m = locations of land use illustrations contained in figures 2.10a through 2.10m.

followed by the results of the user evaluation, and a discussion of an evaluation of Skylab data in terms of future USGS Geography Program operational needs and requirements. Finally, as requested by the NASA project scientific monitor, the chapter concludes with an evaluation of the USGS Circular 671 land use classification scheme for deriving land use information from remotely sensed data.

## METHODOLOGY FOR CONDUCTING THE ANALYSIS

Investigators used manual photointerpretation techniques to compile land use data from the Skylab photography. The high quality of the S-190B photos facilitated photointerpretation and required only a minimum amount of interpretation time for the interpreter to become familiar with the appearance of different types of land use on the photography. A summary of data sources is given in table 2.1.

Familiarization was enhanced by the use of U-2 underflight photography and selected field checking. In an automobile traverse investigators found that one could locate his position directly on a seven-times (7x) enlargement of the S-190B Earth Terrain Camera (ETC) photograph. Prior knowledge of the region under study was also employed by the investigators; such a situation is realistic for the actual use that would be made of the data by planning agencies.

The starting point for the land use analysis performed in this study was the two-level classification system presented in USGS Circular 671 (Anderson and others, 1972). This classification scheme has been widely reviewed since its publication, and a revision has been published as USGS' Professional Paper 964. The categories and definitions used in the

Table 2.1--Summary of data from remote sensors used in this study

| | SKYLAB S-190A | SKYLAB S-190B | HIGH-ALTITUDE AIRCRAFT (U-2) |
|---|---|---|---|
| Image Type | CIR Photos* | Color Photography | Color Infrared Photography |
| Image Acquisition Format | 70 mm | 114.3 mm | 228.6 mm |
| Acquisition Scale | 1:3,000,000 | 1:970,000 | 1:130,000 |
| Altitude | 435 km | 435 km | 21 km |
| Ground Resolution | 55 m | 10 m | 3.5 m |
| Image Date | 05 Aug. 73 | 05 Aug. 73 | 27 Oct. 73 |
| Image Time (GMT) | $15^h\ 03^m\ 54^s$ | $15^h\ 03^m\ 54^s$ | $18^h\ 12^m\ 37^s$ |

*Color Infrared Photos

Professional Paper are employed here, with the addition of third-level categories where applicable to the analysis of the ETC data (table 2.2).

Using the appropriate levels of this three-level classification system to derive a variety of data sets and descriptions from the Skylab photography, investigators developed measures and comparisons along three independent approaches: (1) Systematic aligned sample; (2) area measurement comparison of classification elements (S-190B only); and (3) visual assessment of photo characteristics (S-190A and S-190B). High-altitude aircraft data were used for comparison. Each method was employed in different circumstances for measuring the accuracy of a land use map covering an urban test site in Fairfax, Virginia, a part of the Washington, D.C. metropolitan area.

The analysis began with the compilation of three land use maps of the same area, using the USGS land use classification system: one from Skylab S-190A color-infrared photography, one from Skylab S-190B color photography, and one from high-altitude aircraft (U-2) color-infrared photography. For mapping bases and photointerpretation, photographic enlargements at a scale of 1:24,000 covering the city of Fairfax, Virginia, were made from NASA-supplied Kodak Aerochrome Infrared (SO-127) S-190A, Kodak Aerial color (SO-242) S-190B, and Kodak Aerochrome Infrared (2443) RC-10, camera high-altitude aircraft photographs. The Skylab photos were taken on August 5, 1973, and the U-2 photo on October 27, 1973. Figures 2.4, 2.5, and 2.6 contain prints made from the aircraft and Skylab photographs.

The land use map produced from aerial photography was field checked and corrected so that, for comparative purposes in this research, it was

Table 2.2--Version of the Anderson multilevel land use classification system for use with remote sensor data, used in this study.

| LEVEL I | LEVEL II | LEVEL III |
|---|---|---|
| 1 Urban and Built-Up | | |
| | 11 Residential | |
| | | 111 Single Family |
| | | 112 Multi-Family |
| | 12 Commercial and Services | |
| | | 121 Wholesale trade |
| | | 122 Retail trade |
| | | 123 Business, Professional and personal services |
| | | 124 Cultural, entertainment and recreational activities |
| | | 125 Educational facilities |
| | | 127 Religious facilities |
| | | 129 Government, administration, and services |
| | 13 Industrial | |
| | | 136 Non-classified industrial |
| | 14 Transportation, Communication and Utilities | |
| | | 141 Highways, auto parking, bus terminals, motor freight and other facilities. |
| | | 146 Electric, water, gas, sewage disposal, solid waste, and other facilities. |
| | 15 Industrial and Commercial Complexes | |
| | 16 Mixed | |
| | 17 Other | |
| | | 171 Improved Open space |
| | | 172 Unimproved Open space |
| 2 Agricultural Land | | |
| | 21 Cropland and Pasture | |
| | 22 Orchards, groves, vineyards, nurseries and ornamental horticultural areas | |
| | 23 Combined feeding operations | |
| | 24 Other | |

Table 2.2--Continued

| LEVEL I | LEVEL II | LEVEL III |
|---|---|---|
| 4 Forest Land | | |
| | 41 Deciduous | |
| | | 411 Afforesting deciduous |
| | | 412 Light crown deciduous |
| | 42 Evergreen | |
| | 43 Mixed | |
| | | 431 Afforesting mixed |
| 5 Water | | |
| | 51 Streams and Canals | |
| | 52 Lakes | |
| | 53 Reservoirs | |
| | 54 Bays and Estuaries | |
| | 55 Other | |
| 6 Wetland | | |
| | 61 Forested | |
| | 62 Non-forested | |
| 7 Barren Land | | |
| | 71 Salt Flats | |
| | 72 Beaches and Mudflats | |
| | 73 Sandy areas other than beaches | |
| | 74 Bare Exposed Rock | |
| | 75 Strip Mines, Quarries and Gravel Pits | |
| | 76 Transitional Areas | |
| | 77 Mixed | |

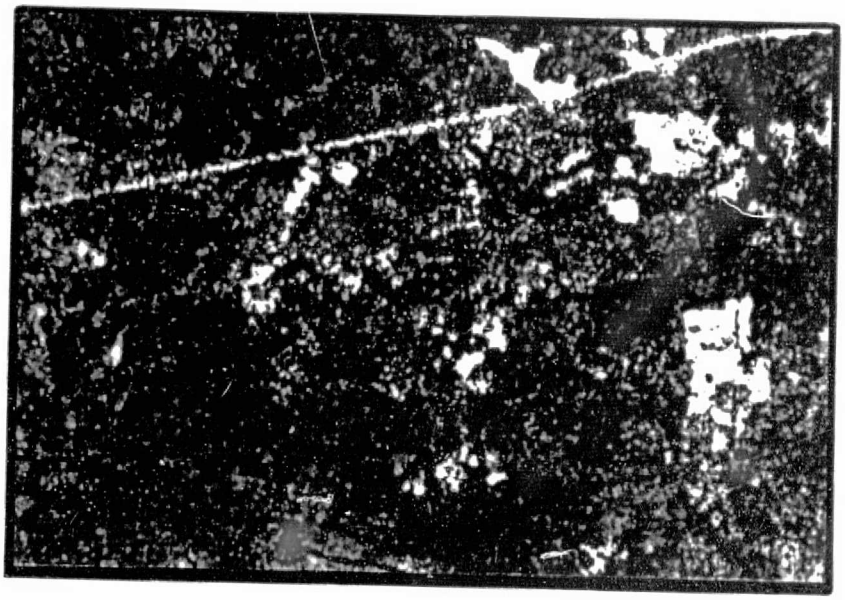


REPRODUCIBILITY OF THE
ORIGINAL PAGE IS POOR

Figure 2.4--Enlarged print of S-190A photograph, Fairfax, Virginia. EDC-010120.

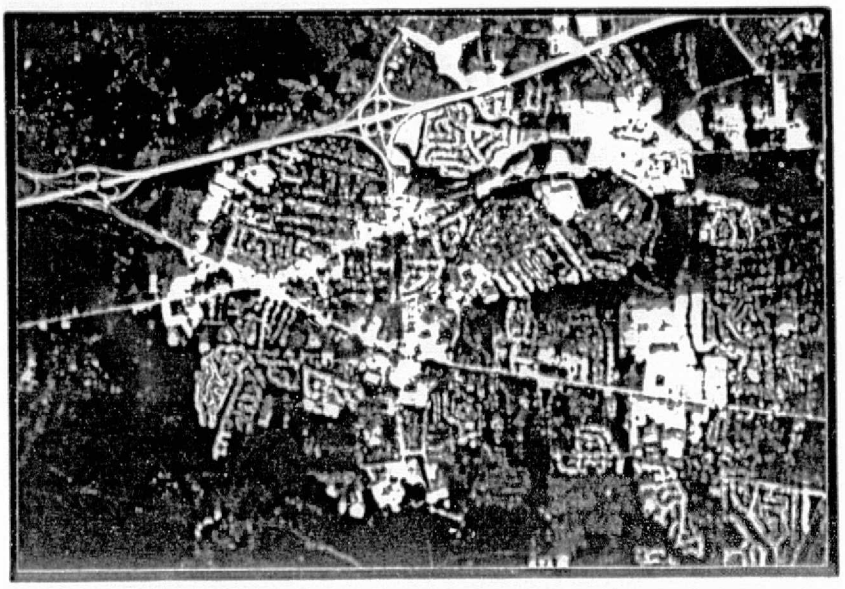


2-12

PAGE INTENTIONALLY BLANK

2-12

PRECEDING PAGE BLANK NOT FILMED

Figure 2.5--Enlarged print of S-190B photograph, Fairfax, Virginia. EDC-010121.

Figure 2.6--Enlarged print, high-altitude photograph of Fairfax, Virginia. EDC-010122.

2-14
PAGE INTENTIONALLY BLANK
2-14
PRECEDING PAGE BLANK NOT FILMED

considered error free. This correction process facilitated the comparison of the map produced from Skylab photography to the map produced from aerial photography for accuracy determination. Figures 2.7 and 2.8 depict two of the land use maps, those made from S-190B and aircraft photography, respectively.

## Systematic Aligned Sample

One method of comparison applied a systematic aligned sample strategy, which compared two spatial data sets by using a corresponding point sample drawn from each (Berry and Baker, 1968). For example, consider two polygon maps, A and B, which cover exactly the same geographical area and use the same units of classification. Map A results from the interpretation of sensor X data and map B from analysis of sensor Y data. By observing points on one and then the other, one can determine which points, if any, have classification differences. If one assumes further that map A, because of certain characteristics in sensor X, combined with more detailed information from additional sources (other maps, field work, etc.), is accurate, and if the two maps are temporally similar, then any point on map B whose interpretation differs from that of its corresponding point on map A, can be considered a misinterpretation. The quotient of the number of points found to be the same on both maps divided by the total number of points examined can thus be considered a measure of accuracy.

Misinterpretations, however, are considered at a single level of classification or generalization. No credit is given to an incorrect interpretation that is correct at a higher level of aggregation.

2-16
PAGE INTENTIONALLY BLANK
2-16
PRECEDING PAGE BLANK NOT FILMED

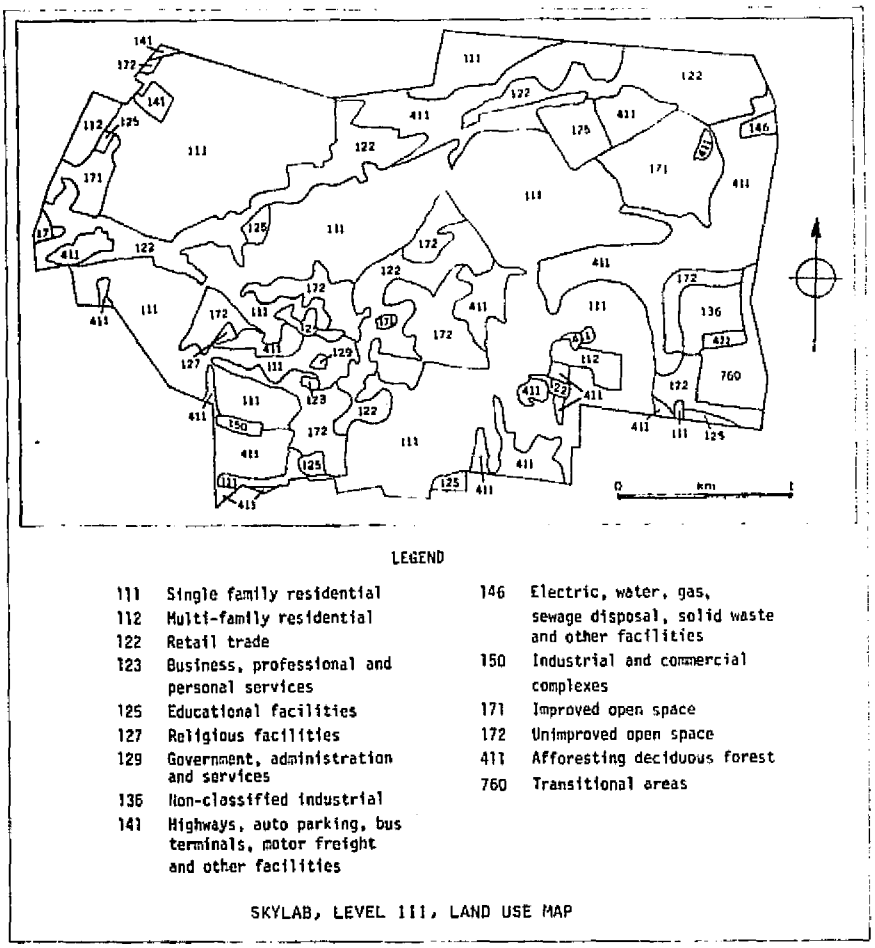


Figure 2.7--Level III land use map, based on interpretation of Skylab S-190B photography, Fairfax, Virginia.

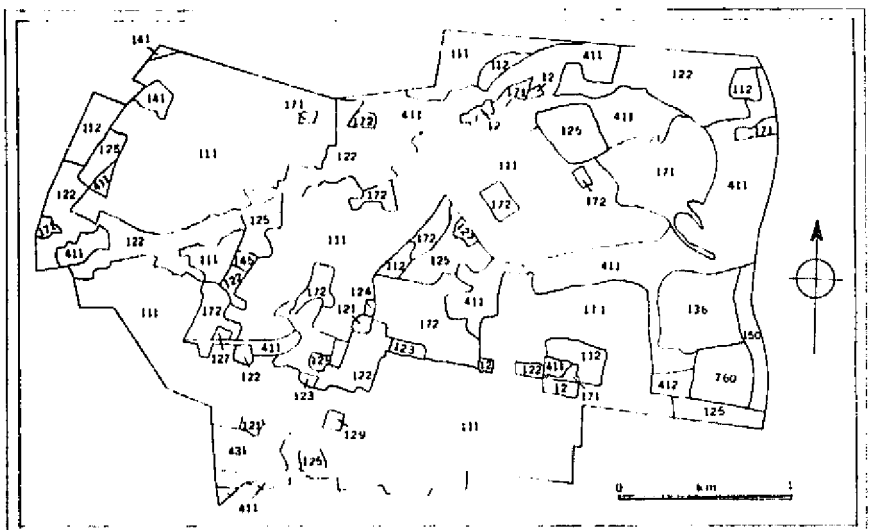

LEGEND

| | | | |
|---|---|---|---|
| 111 | Single family residential | 140 | Transportation, communication and utilities |
| 112 | Multi-family residential | 141 | Highways, auto parking, bus terminals, motor freight, and other facilities |
| 12 | Commercial and services | 150 | Industrial and commercial complexes |
| 121 | Wholesale trade | 171 | Improved open space |
| 122 | Retail trade | 172 | Unimproved open space |
| 123 | Business, professional and personal services | 411 | Afforesting deciduous forest |
| 124 | Cultural, entertainment and recreational activities | 412 | Light crown deciduous forest |
| 125 | Educational facilities | 431 | Afforesting mixed forest |
| 127 | Religious facilities | 760 | Transitional areas |
| 129 | Government, administration and services | | |
| 136 | Non-classified industrial | | |

AIRCRAFT, LEVEL III, LAND USE MAP

Figure 2.8--Level III land use map, based on interpretation of high-altitude aircraft photography, Fairfax, Virginia.

Primary source: U-2 flight 73-181, RC-10 color infrared photograph, frame 5296, 27 October 1973.

Supplementary source: U.S. Geological Survey, 7½-minute topographic map of Fairfax, Virginia, 1971 photorevised edition.

The systematic aligned or grid sample was employed in this example since the mapped data did not appear to contain any regularly repeated pattern or spatial periodicity. In the absence of spatial periodicity in the mapped data, the grid sample has been found to be the simplest and most efficient type. The geographical area analyzed was overlain by a grid of equal-sized cells, the center points of each serving as the observation points (figure 2.9). The cell size was arbitrarily established based on the scale of the interpreted data. In this example 69 points were examined for an area of 1,600 ha at a scale of 1:24,000.

Table 2.3 indicates relatively good performance by the interpreter in working with S-190A photography in identifying residential land use; fair performance in identifying commercial and services, and deciduous forest land uses; and poor performance in recognizing the other land uses in this urban setting. Most errors were a function of the lower resolution of the S-190A compared to the high-altitude aircraft photography. For example, a tank farm containing large circular tanks for storage of petroleum products was misclassified as commercial (12) based on the brightness of the reflected signal and its location along a transportation artery. On the aircraft photography (and, even on the S-190B photography) the outlines of the individual tanks could be seen clearly, permitting the correct classification as industrial (13).

Land-use classification data comparisons between S-190B and high-altitude aircraft sources are illustrated in table 2.4, which shows that of 69 points examined, 57 were found to be alike on both maps. Based on the stratified aligned sampling method, the accuracy of the S-190B land use maps using Level III categories is 83 percent. Of the

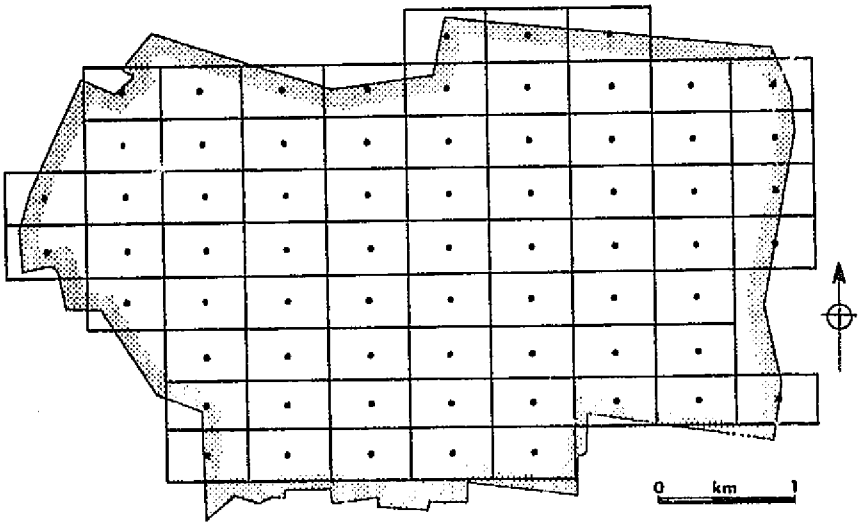


Figure 2.9--Location of points for comparing Skylab and aircraft-derived land use data, Fairfax, Virginia.

Table 2.3--Matrix listing the number of occurrences of land use categories interpreted from S-190A photography versus land use categories interpreted and field checked from aircraft photography for the city of Fairfax, Virginia. Diagonal is the axis of correct S-190A interpretations.

Land Use Categories as Determined from Skylab S-190A Photography

Land Use Categories as Determined from Aircraft Photography

| Categories | | 11 | 12 | 13 | 14 | 15 | 17 | 41 | 43 | 76 |
|---|---|---|---|---|---|---|---|---|---|---|
| Residential | 11 | 36 | 3 | | | | | | | |
| Commercial and Services | 12 | 2 | 7 | | | | | | | |
| Industrial | 13 | | 1 | | | | | | | 1 |
| Transportation, Communication & Utilities | 14 | | 1 | | | | | | | |
| Industrial & Commercial Complexes | 15 | | 1 | | | | | | | |
| Open Space | 17 | 2 | 1 | | | | 2 | 1 | | |
| Deciduous Forest | 41 | 2 | 1 | | | | 1 | 6 | | |
| Mixed Forest | 43 | | | | | | | 1 | | |
| Transitional Areas | 76 | | | | | | | | | |

Land-use categories correctly identified on Skylab S-190A, 74 percent

Table 2.4--Matrix listing the number of occurrences of land use categories interpreted from S-190B photography versus land use categories interpreted and field checked from aircraft photography for the city of Fairfax, Virginia. Diagonal is the axis of correct S-190B interpretations.

Land-Use Categories as Determined from Skylab S-190B Photography

| Land-Use Categories as Determined from Aircraft Photography | 111 | 112 | 122 | 125 | 136 | 15 | 171 | 172 | 411 | 412 | 76 |
|---|---|---|---|---|---|---|---|---|---|---|---|
| 111 | 34 | | 1 | | | | | 1 | 2 | | |
| 112 | | | 1 | | | | | | | | |
| 122 | | | 7 | | | | | | | | |
| 125 | | | | 1 | | | | 1 | | | |
| 136 | | | | | 1 | | | 1 | | | |
| 15 | | | | | | | | | | | 1 |
| 171 | | | 1 | | | | 2 | | | | |
| 172 | 1 | | | | | | | 3 | | | |
| 411 | | | | | | | | 1 | 9 | | |
| 412 | | | | | | | | 1 | | | |
| 76 | | | | | | | | | | | |

Land-use categories correctly identified on Skylab S-190B, 83 percent

| | | | |
|---|---|---|---|
| 111 | Single-family residential | 171 | Improved open space |
| 112 | Multi-family residential | 172 | Unimproved open space |
| 122 | Retail trade | 411 | Afforesting deciduous forest |
| 125 | Educational facilities | 412 | Light crown deciduous forest |
| 136 | Non-classified industrial | 76 | Transitional areas |
| 15 | Industrial and commercial complexes | | |

12 points in disagreement, 5 occurred in cases where the S-190B data were misclassified as unimproved open space. This misclassification appeared to be attributable to the spectral characteristics of the color film (SO-242) and the spatial resolution of the camera (S-190B). The colorimetry was such that suitable vegetation differences were imperceptible, and the lack of detail in the data inhibited the observation of certain residential and commercial structures. Positive identification of these features was difficult.

## Area Measurement Comparison

A second technique employed was a comparison of the area measurement of land use types. As an example, consider a classification system consisting of n land use categories. For any given map using this classification, the sum of the areas of each category used will equal 100 percent of the total area of the map. Consider further the case of three maps, E, F, and G, of the same geographical area, which are produced using the same classification system. Map E is derived from source R, map F from source S, and map G from source T. If map E, because of the superior source information, is considered correct, then by comparing the percentage of area in each land use category in maps F and G to the percentage of their corresponding areas in map E, the relative accuracy of maps F and G by each land use category can be determined. Suppose that a land classification with categories 1, 2, and 3 is employed and a hypothetical ground truth map is produced with 20 percent of its area in category 1, 30 percent in category 2, and 50 percent in category 3. Another map has constituents of 21 percent in 1, 31 percent in 2, and 48 percent in 3. Empirically the two are very similar. If, on the other hand, sizable discrepancies occur in the percentages, then a comprehensive look into

the reasons for such differences would be in order. The actual physical determination of area was accomplished in this case by using a dot planimeter (Yuill, 1970).

Table 2.5 presents the Level III tabulations of area measurements of the land use categories derived from Skylab S-190B data, compared with those derived from aircraft data. The table indicates a sizable discrepancy in residential land area. Interpretation of Skylab photography resulted in the delineation of approximately 120 ha less of residential land than did the analysis of aircraft photography. Both data sets were made by the same photointerpreter. Nearly all of the difference occurred in single-family residential areas, many of which are located in wooded or semiwooded areas. In this situation, the spatial resolution of the Earth Terrain Camera (S-190B) is not high enough to allow the detection of houses or other residential "keys" such as street patterns and sidewalks that are partially obscured by vegetative cover.

Areas of commercial and services land use, especially retail trade areas, were readily detectable from Skylab photography, apparently because of the distinctive spectral and spatial characteristics of shopping areas. Two main types of commercialized areas are usually found: suburban shopping centers and urban commercial strips along major thoroughfares. That less industrial area was interpreted from the Skylab data than from the aerial data appears mainly to be the result of interpreter inability, in some cases, to detect differences between the industrial category and the commercial and services category using Earth Terrain Camera (S-190B) photography.

Table 2.5--Comparison of area measurements of Level III land use categories derived from aircraft and Skylab S-190B data sources, Fairfax, Virginia, in hectares and percent of total area mapped.

| Land use type code | | AIRCRAFT Hectares | AIRCRAFT Percent | SKYLAB S-190B Hectares | SKYLAB S-190B Percent |
|---|---|---|---|---|---|
| Single family residential | 111 | 780.4 | 50.22 | 657.3 | 42.30 |
| Multi-family residential | 112 | 32.2 | 2.07 | 26.4 | 1.70 |
| Commercial & Services | 120 | 7.4 | 0.48 | -- | -- |
| Wholesale trade | 121 | 3.4 | 0.22 | -- | -- |
| Retail trade | 122 | 166.3 | 10.70 | 166.4 | 10.71 |
| Business, professional, & personal services | 123 | 3.6 | 0.23 | 1.4 | 0.09 |
| Cultural, entertainment, & recreational activities | 124 | 0.8 | 0.05 | -- | -- |
| Educational facilities | 125 | 60.7 | 3.91 | 99.8 | 6.42 |
| Religious facilities | 127 | 2.8 | 0.18 | 1.9 | 0.12 |
| Government, administration, & Services | 129 | 5.1 | 0.33 | 1.1 | 0.07 |
| Non-classified Industrial | 136 | 32.1 | 2.07 | 23.7 | 1.53 |
| Highways, auto parking, bus terminals, motor freight, & other facilities | 141 | 6.9 | 0.44 | 7.2 | 0.46 |
| Electric, water, gas, sewage disposal, solid waste & other facilities | 146 | -- | -- | 4.8 | 0.31 |
| Industrial & Commercial Complexes | 150 | 12.1 | 0.78 | 4.5 | 0.29 |
| Improved Open Space | 171 | 54.4 | 3.50 | 39.6 | 2.55 |
| Unimproved Open Space | 172 | 128.2 | 8.25 | 152.9 | 9.84 |
| Afforesting Deciduous Forest | 411 | 215.2 | 13.85 | 339.5 | 21.85 |
| Light Crown Deciduous Forest | 412 | 5.6 | 0.36 | -- | -- |
| Afforesting Mixed Forest | 431 | 16.2 | 1.04 | -- | -- |
| Transitional Areas | 760 | 20.6 | 1.33 | 27.5 | 1.77 |
| | | 1,554.0 | 100.0 | 1,554.0 | 100.00 |

The two systems showed a marked similarity in discriminating the improved and unimproved open space categories. Although their spatial discriminations differed, their spectral responses to open ground were, in many respects, similar.

Forest land interpretation, on the other hand, was less accurate with Skylab. The map generated from the Skylab photo had 58 percent more area in forest than did the map generated from the aircraft photo. This result was mainly attributable to the aforementioned tree-covered residential area where 120 ha of residential land were misinterpreted as forest land from the Skylab data.

## Visual Assessment of Photo Characteristics

### S-190A Photography

Since the investigators did not have access to specialized equipment and facilities for analysis of multispectral photography, they used only the S-190A photography taken with the color-infrared film. Because color-infrared film has slightly lower spatial resolution capabilities than the black-and-white films used in the other cameras of the multispectral photographic system, slightly improved detection of some features might result from analysis using the entire multispectral capability of the S-190A system. However, these advantages are probably not offset by the convenience, ease of manual photointerpretation, and lower cost attained in the use of the color-infrared presentation that had become familiar to and favored by the investigators in this project.

Urban and Built-up Land.--Suburban single-family residential developments at least 0.75 $km^2$ in area, with a density of about 500 houses per $km^2$, generally are distinguishable. On color-infrared film, such developments appear granular and pink as a result of the red signature of lawns

speckled with blue emanating from a combination of houses and street-sidewalks. Suburban multi-family residential areas appear similar to suburban commercial and services (building [roof] area and parking lots).

Multi-family residential areas surrounding and radiating out from the CBD (Central Business District) can be delimited, but with some difficulty. They can be differentiated from the CBD primarily by their finer texture. Their color is blue, although in neighborhoods with trees, speckles of red are visible.

Strip-type commercial and service areas are recognizable primarily because of their linear pattern and bluish color. The commercial areas within cities are more difficult to delineate, especially in fringe areas where commercial and residential mixes occur. They are bluish, similar to residential areas within cities, but they generally have a lighter tone. In most cases commercial areas are interspersed with bright white spots. Differentiating commercial from industrial areas is difficult. Industrial areas seem to have more large white spots, probably representing either tops of large buildings, or areas around buildings lacking landscaping.

Transportation, communication and utilities categories are also difficult to interpret, with the exception of the major freeways. Primary, hard surface roads as defined on USGS 1:250,000-scale topographic maps, mark the threshold for detection.

Industrial and commercial complexes are difficult to identify by spectral signature alone and are sometimes confused with transitional land. The large industrial-commercial complexes often exhibit a white return, frequently mixed with blue. A further clue is the locational context, often in a suburban setting, usually along major thoroughfares.

Other urban and built-up land as a collective category is identifiable. Land uses such as golf courses, driving ranges, zoos, drive-in theaters, parks, ski areas, cemeteries, waste dumps, and sanitary land fills, however, are not generally identifiable.

Agricultural Land.--This general category is delimitable. The subcategory cropland and pasture is likewise delimitable. Other uses, such as orchards, vineyards, bush fruit, and horticultural areas as well as feeding operations, are less easily defined. Signatures are similar enough so that they are usually interpreted as cropland and pasture. Moreover, these more discrete occurrences of land use are typically underestimated since a conscious decision is required to classify an area in such a category rather than to leave it in a "background" category.

Forest Land.--The signature produced by forest land on the S-190A photography is similar to that produced on Landsat imagery. As with the Landsat data, delimitation of deciduous, evergreen, and mixed Level II categories is difficult, if not impossible. The spectral discrimination seems adequate for differentiating these categories, but the spatial resolution is marginal. Winter and summer coverage would improve the interpreter's ability to distinguish deciduous and evergreen forest categories.

Water.--Delineation of water bodies and shorelines is attainable with S-190A color-infrared data. Further discrimination of the Level II categories, streams and waterways, lakes, reservoirs, and bays and estuaries, is also possible, providing a good example of a case where spectral resolution is more important than spatial resolution in the determination of a land cover category.

Wetland.--Nonforested wetlands, as with forest land, produced a signature resembling that of Landsat imagery. Delineation of this category is possible. Interpretation could, however, be difficult if a wetland area had undergone a "dry" period. This condition could result in a signature easily mistaken for cropland and pasture. The delimitation of forested wetlands, on the other hand, was not possible in the test area examined.

Barren Land.--The mapping of barren land faces several problems. This category, on small-scale photography and imagery, usually produced a bright or near-white signature. Accurate interpretation is hampered by the similar spectral return of freshly plowed fields (part of the cropland and pasture category) and many industrial sites. Subcategories, such as beaches, and sand other than beaches, may be interpretable with little difficulty, with the aid of locational clues. Transitional land, depending on its area, is generally identifiable. Smaller tracts of transitional land are easily confused with large plowed fields.

S-190B Photography

To an investigator who had examined photographic data from space, including the Mercury, Gemini, Apollo, and Landsat spacecraft experiments, the S-190B Earth Terrain Camera photography was instantly perceived to be an exciting culmination in terms of beauty of the photography and amount of spatial detail discernible. This photography is the most detailed photographic rendition of the surface of the Earth obtained from orbiting spacecraft that has yet been obtained by NASA. Even from the limited amount of coverage that was available from the Central Atlantic test site, it was apparent that the Earth Terrain Camera has an outstanding potential for the detailed imaging of the Earth's surface and gathering

of important land use and environmental information. The resolution is, in fact, so good and so nearly approaching that of the high-altitude photography that the temptation is great to recommend lengthening the focal length of future spaceborne photographic sensors beyond the 18 in. (457 mm) of the S-190B camera system.

Urban and Built-up Land.--Residential land is readily identifiable and delimitable in most cases, except where houses lie under a very heavy forest cover. The data permit the making of some housing quality or age statements or both. For example, older single-family residential (SFR) developments as well as newer, more expensive developments are distinguished by areas with substantial tree cover. Individual houses may appear as dots or as part of residential road patterns. The latter, however, are often difficult to define. Some houses appearing as dots are as small as 150 $m^2$. Such structures are visible mainly because of the high contrast ratio between them and their forest "background." Differentiation between the older homes and the newer, larger homes is very difficult.

Newer SFR subdivisions and moderate income SFR housing are easily distinguishable by their street patterns. The actual signature on S-190B data is a combination of generally brighter reflected signals from the streets and roofs, as contrasted with that from surrounding trees and lawns. Individual houses are rarely visible, except where spacing between houses combines with contrast between roof and surroundings to provide a separate image spot representing a detached dwelling unit. The width of these street-house-lawn complexes varies among subdivisions but generally appears to be in the 50- to 90-m range.

Individual multi-family dwelling units become identifiable as discrete structures when their area exceeds approximately 1,000 $m^2$ and when they have trees or shrubbery between the buildings. Trailer parks are distinguishable in low-density urban or rural areas but are very difficult to identify in high-density urban areas, unless they are large. Evidence of internal structure within the trailer parks exists, but individual trailers are indistinguishable. In a few cases the roads within the court (approximately 5 m in width) appear to be visible. This particular signature could be the entire area between the mobile homes including both the roads and the lawns.

Areas occupied by commercial and service activities are quite evident in strip development along roads and in complexes. However, delineation of these areas within cities is difficult unless the structure is large enough to differentiate from its surroundings. Although experience and intuition usually permit the mapping of these areas, positive identification of specific commercial activities is nearly impossible for all but a few high schools and colleges with adjacent open ground. Individual structures become sharp enough to outline accurately at about the 1,000 $m^2$ size when contrast conditions permit.

Industrial land uses are extremely difficult to differentiate from large commercial buildings. The one type of industrial use that is apparent on the S-190B data is tank farms associated with petroleum refining and storage. Individual tanks with diameters of 40 to 50 m, spaced only 10 m apart, are identifiable.

Transportation, communication and utility uses, because of their linearity, are usually easy to identify. The network of transportation



REPRODUCIBILITY OF THE ORIGINAL PAGE IS POOR

routes shows up well. In some cases, where the contrast ratio is high, the paths followed by light-duty improved roads of 10-m width are visible. Generally speaking, streets within subdivisions are not visible, but their patterns are clearly visible because of the combination of house and street albedos. These streets basically range from 8 to 12 m wide. The threshold size, above which streets themselves are visible, appears to be between 35 and 45 m. Large airports are easy to identify and map. The smaller airports, on the other hand, especially those with asphalt single runways less than 1,200 m in length, are usually difficult to delineate.

Power line rights-of-way, 50 to 60 m in width, are distinctive where they cut through forest tracts. In residential areas and especially in agricultural regions they are far more obscure and usually imperceptible.

The industrial and commercial complex category is, in general, one that is capable of being mapped. Such a complex has a bright spectral response, and the buildings comprising it are usually large enough to be seen individually. In some cases industrial and commercial complexes can be mistaken for apartment complexes. The threshold value for positive identification of an individual structure, as such, is approximately 1,000 $m^2$.

The category of other urban and built-up land consists of such uses as golf courses, driving ranges, zoos, drive-in theaters, some parks, ski areas, cemeteries, waste dumps, sanitary land fills, and undeveloped land within an urban setting. With the possible exception of golf courses and some undeveloped land, deciding what activity within this

category is occurring is difficult. Nevertheless, the open land category is identifiable primarily because, by definition, it appears within urban areas. It can, however, be confused with small plots of agricultural land.

Nonurban Land.--Categories of land use other than "urban and built-up" are significant in urban area analysis when they indicate the regional distribution of phenomena that interact with the city. For example, nonurban land uses in zones of possible urban expansion are significant.

Agricultural Land.--Cropland and pasture are relatively easy to map from the Skylab data. Except for context (away from built-up areas), agricultural land is sometimes difficult to distinguish from the urban-open category.

Forest Land.--In most cases, using the S-190B color photography, interpreters mapped forests as deciduous. The color film did not provide enough spectral differentiation to determine variations in forest type. Here again, as with cropland and pasture, color-infrared film will probably provide more spectral differences and thereby permit a more detailed breakdown. In a number of instances, the contrast between forest and open land was so low that accurate delineation of the two was difficult. Even so, the data did permit mapping of forest tracts down to the minimum mapping level of 2 x 2 mm (50 x 50 m on the ground).

Water.--Because of the nature of the color film, especially at orbital altitudes, the shoreline delineation of bays and estuaries and identification of lakes and reservoirs, is often difficult. All of these features are within the resolution capability of the sensor and,

with the use of color-infrared film, could be mapped with near perfect accuracy.

Wetland.--Nonforested wetland areas are generally identifiable. In some areas the actual border between wetland and water or wetland and agricultural land is difficult to demarcate. This difficulty, too, could be eliminated with the use of color-infrared film. Forested wetlands are virtually impossible to identify with the Skylab data.

Barren Land.--Strip mines, quarries, and gravel pits are visible on S-190B data but are almost impossible to categorize correctly without supplemental data such as topographic maps. Transitional areas, however, are identifiable because of a distinctive reddish hue they exhibit.

## Comparisons with Aircraft and Landsat Data

Figures 2.10a through 2.10m display examples of selected land use types in the Washington, D.C. metropolitan area, as imaged from high-altitude aircraft, Skylab S-190B, and Landsat. Locations of the example sites are indicated by the symbols "a" through "m" in the index map to the Skylab S-190B frame in which all are located (figure 2.3).

Careful study of these illustrations reveals that at each of the three levels of resolution, there is useful land use information that can be obtained in some categories, though such information may be only at a Level I detail for the coarse resolution Landsat. When enlarged, as in figure 2.10a through 2.10m, the Landsat image appears blurred in comparison to either the aircraft or Skylab photography. But Landsat imagery appears sharper when displayed at a smaller scale. It is

Figures 2.10a through 2.10m:

Illustrations of selected land use types in the CARETS area as imaged by high-altitude aircraft, Skylab S-190B, and Landsat-1.

Locations of each illustration are indicated by letters "a" through "m" in Index Map, figure 2.3.

Each illustration is identified in the caption by an EDC number. Copies of the original color are available for purchase from the EROS Data Center, Sioux Falls, South Dakota 57198, using the EDC number. Prices are available on request.

High-altitude aircraft
Mission 73-181, Frame 5271
October 27, 1973

0 .5 mi
0 .5 km

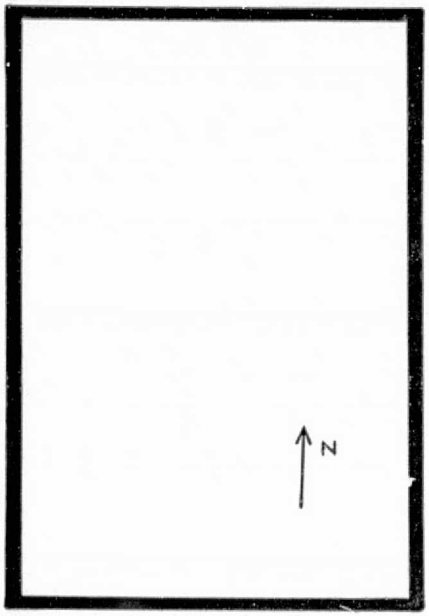

Skylab 3, S-190B
Photo 83-166,
August 5, 1973

0 .5 mi
0 .5 km

Landsat-1 color composite
of MSS Bands 4, 5, and 7;
E 1080-15192, October 11, 1972

0 .5 mi
0 .5 km

2.10a--Single-family residential. EDC-010123. (Areas shown on the three images are not exactly equivalent.)

High-altitude aircraft
Mission 73-181, Frame 5273
October 27, 1973

0 .5 mi
0 .5 km

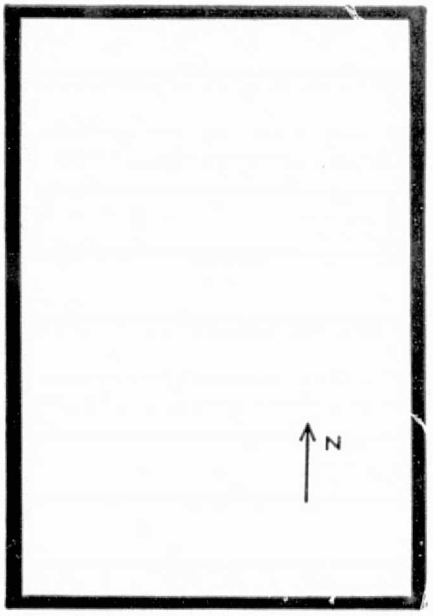

Skylab 3, S-190B
Photo 83-166,
August 5, 1973

0 .5 mi
0 .5 km

Landsat-1 color composite
of MSS Bands 4, 5, and 7;
E 1080-15192, October 11, 1972

0 .5 mi
0 .5 km

2.10b--Multi-family residential. EDC-010124. (Areas shown on the three images are not exactly equivalent.)

PAGE INTENTIONALLY BLANK
2-38 2-38
PRECEDING PAGE BLANK NOT FILMED

High-altitude aircraft
Mission 73-181, Frame 5293
October 27, 1973

0 .5 mi
0 .5 km

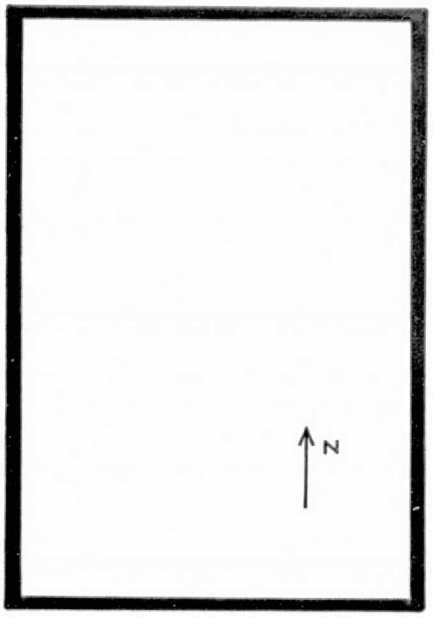

Skylab 3, S-190B
Photo 83-166
August 5, 1973

0 .5 mi
0 .5 km

Landsat-1 color composite
of MSS Bands 4, 5, and 7;
E 1080-15192, October 11, 1972

0 .5 mi
0 .5 km

2-40

PRECEDING PAGE BLANK NOT FILMED

2.10c--Industrial. EDC-010125. (Areas shown on the three images are not exactly equivalent.)

2-40

PAGE INTENTIONALLY BLANK

High-altitude aircraft
Mission 73-181, Frame 5293
October 27, 1973

0 .5 mi
0 .5 km

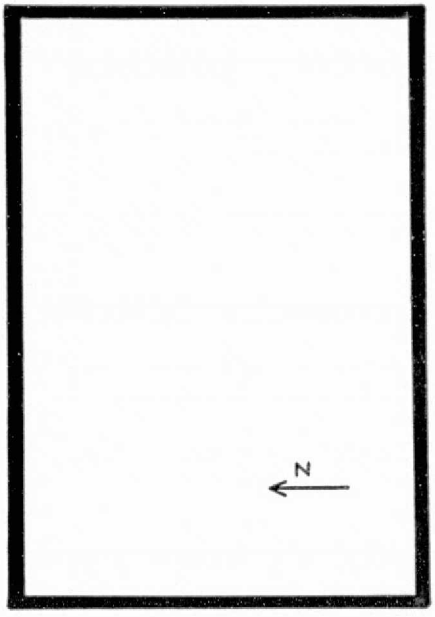

Skylab 3, S-190B
Photo 83-166
August 5, 1973

0 .5 mi
0 .5 km

Landsat-1 color composite
of MSS Bands 4, 5, and 7;
E 1080-15192, October 11, 1972

0 .5 mi
0 .5 km

2.10d--Central business district. EDC-010126. (Areas shown on the three images are not exactly equivalent.)

PAGE INTENTIONALLY BLANK
2-42
2-42
PRECEDING PAGE BLANK NOT FILMED

High-altitude aircraft
Mission 73-181, Frame 5294
October 27, 1973

0 .5 mi
0 .5 km

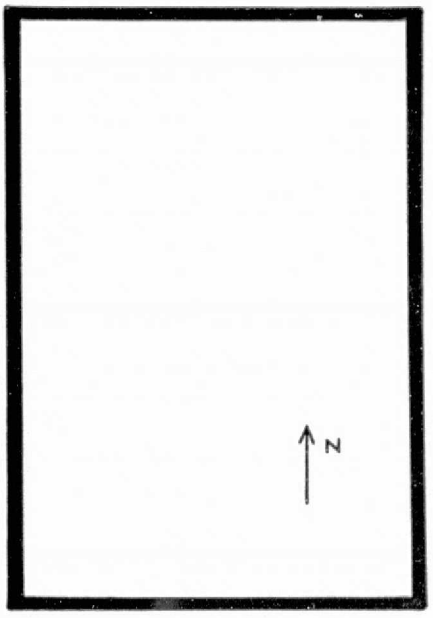


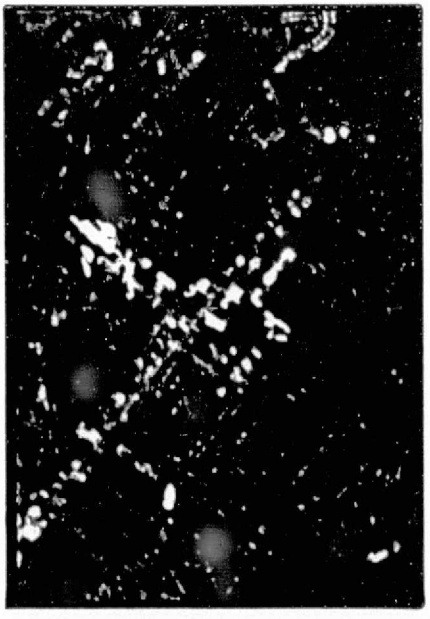

Skylab 3, S-190B
Photo 83-166
August 5, 1973

0 .5 mi
0 .5 km

Landsat-1 color composite
of MSS Bands 4, 5, and 7;
E 1080-15192, October 11, 1972

0 .5 mi
0 .5 km

2.10e--Commercial strip. EDC-010127. (Areas shown on the three images are not exactly equivalent.)

2-44

PAGE INTENTIONALLY BLANK

2-44

PRECEDING PAGE BLANK NOT FILMED

High-altitude aircraft
Mission 73-181, Frame 5271
October 27, 1973

0 .5 mi
0 .5 km

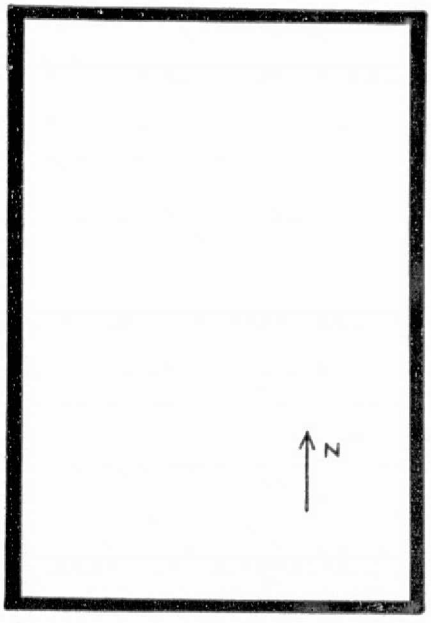

Skylab 3, S-190B
Photo 83-166
August 5, 1973

0 .5 mi
0 .5 km

Landsat-1 color composite
of MSS Bands 4, 5, and 7;
E 1080-15192, October 11, 1972

0 .5 mi
0 .5 km

2.10f--Shopping centers. EDC-010128. (Areas shown on the three images are not exactly equivalent.)

2-46

PAGE INTENTIONALLY BLANK

2-46

PRECEDING PAGE BLANK NOT FILMED

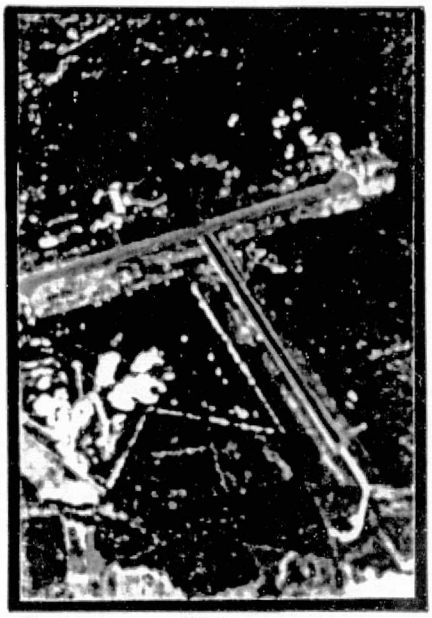

High-altitude aircraft
Mission 73-181, Frame 5274
October 27, 1973

0 .5 mi
0 .5 km

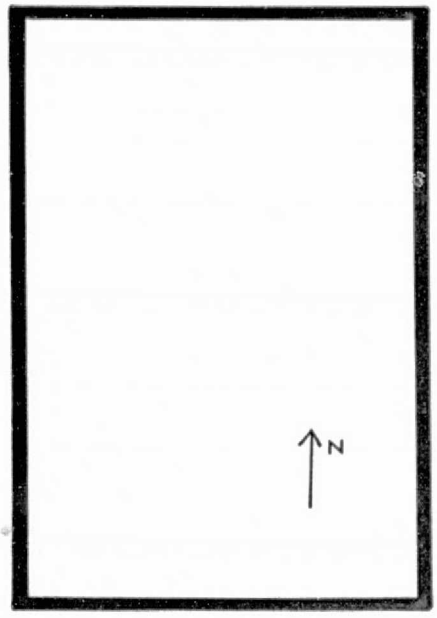

Skylab 3, S-190B
Photo 83-166
August 5, 1973

0 .5 mi
0 .5 km

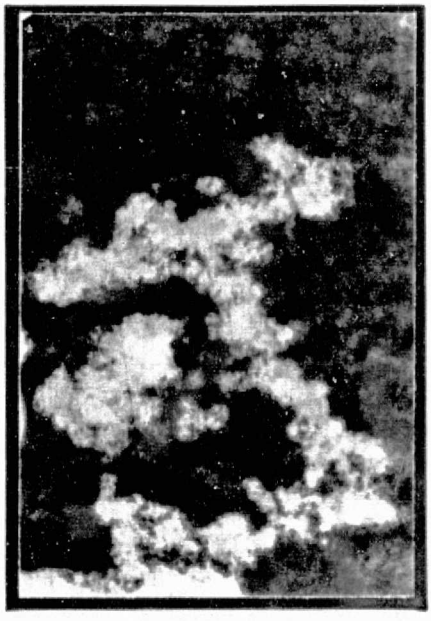

Landsat-1 color composite
of MSS Bands 4, 5, and 7;
E 1080-15192, October 11, 1972

0 .5 mi
0 .5 km

2.10g--Airport. EDC-010129. (Areas shown on the three images are not exactly equivalent.)

2-48
PAGE INTENTIONALLY BLANK



2-48
PRECEDING PAGE BLANK NOT FILMED

High-altitude aircraft
Mission 73-181, Frame 5258
October 27, 1973

0 .5 mi
0 .5 km

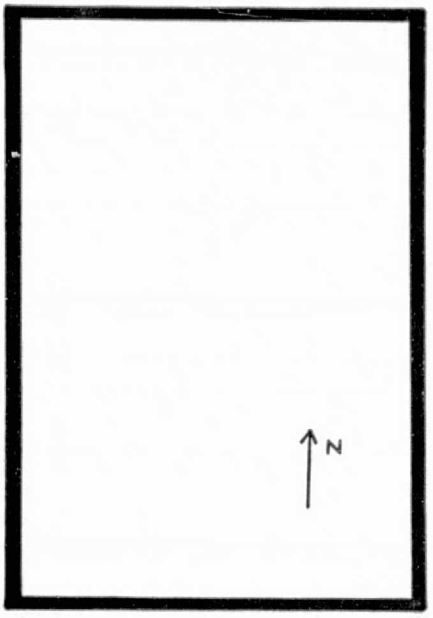

Skylab 3, S-190B
Photo 83-166
August 5, 1973

0 .5 mi
0 .5 km

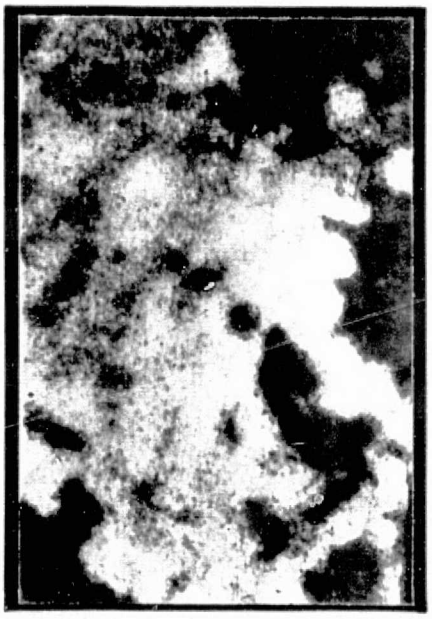

Landsat-1 color composite
of MSS Bands 4, 5, and 7;
E 1080-15192, October 11, 1972

0 .5 mi
0 .5 km

2.10h--Industrial and commercial complexes. EDC-010130. (Areas shown on the three images are not exactly equivalent.)

2-50

PAGE INTENTIONALLY BLANK

2-50

PRECEDING PAGE BLANK NOT FILMED

High-altitude aircraft
Mission 73-181, Frame 5273
October 27, 1973

0 .5 mi
0 .5 km

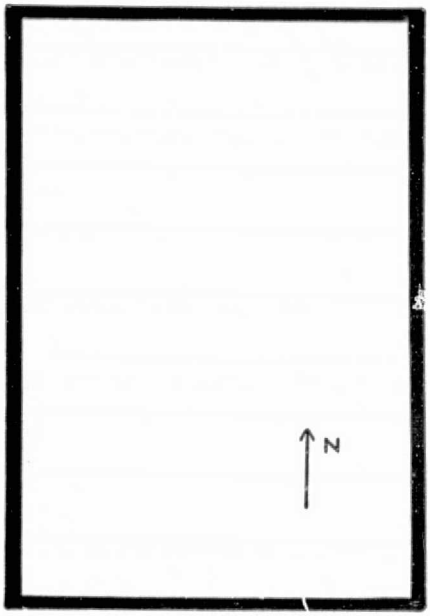


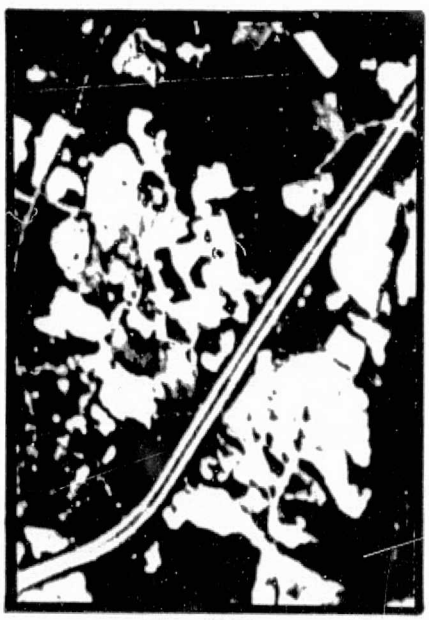

Skylab 3, S-190B
Photo 83-166
August 5, 1973

0 .5 mi
0 .5 km

Landsat-1 color composite
of MSS Bands 4, 5, and 7;
E 1080-15192, October 11, 1972

0 .5 mi
0 .5 km

2.10i--Strip mines, quarries and gravel pits. EDC-010131. (Areas shown on the three images are not exactly equivalent.)

2-52
PRECEDING PAGE BLANK NOT FILMED



2-52
PAGE INTENTIONALLY BLANK

High-altitude aircraft
Mission 73-181, Frame 5273
October 27, 1973

0 .5 mi
0 .5 km

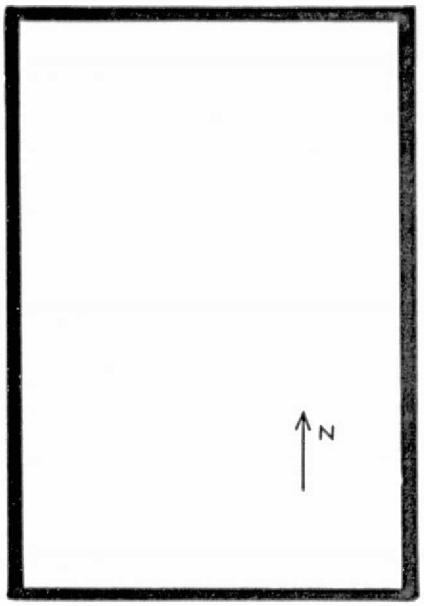


REPRODUCIBILITY OF THE
ORIGINAL PAGE IS POOR

Skylab 3, S-190B
Photo 83-166,
August 5, 1973

0 .5 mi
0 .5 km

Landsat-1 color composite
of MSS Bands 4, 5, and 7;
E 1080-15192, October 11, 1972

0 .5 mi
0 .5 km

2-54
PAGE INTENTIONALLY BLANK

2-54
PRECEDING PAGE BLANK NOT FILMED

2.10j--Transitional (and single-family residential). EDC-010132.
(Areas shown on the three images are not equivalent.)

High-altitude aircraft
Mission 73-181, Frame 5259
October 27, 1973

0 .5 mi
0 .5 km

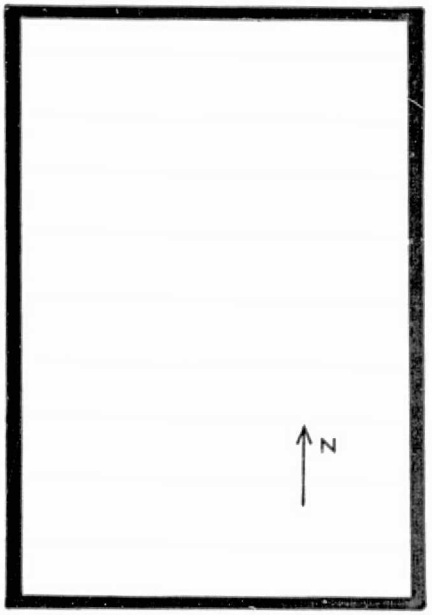

Skylab 3, S-190B
Photo 83-166,
August 5, 1973

0 .5 mi
0 .5 km

Landsat-1 color composite
of MSS Bands 4, 5, and 7;
E 1080-15192, October 11, 1972

0 .5 mi
0 .5 km

2.10k--Cropland and pasture. EDC-010133. (Areas shown on the three images are not exactly equivalent.)

2-56
PRECEDING PAGE BLANK NOT FILMED
2-56
PAGE INTENTIONALLY BLANK

High-altitude aircraft
Mission 73-181, Frame 5271
October 27, 1973

0 .5 mi
0 .5 km

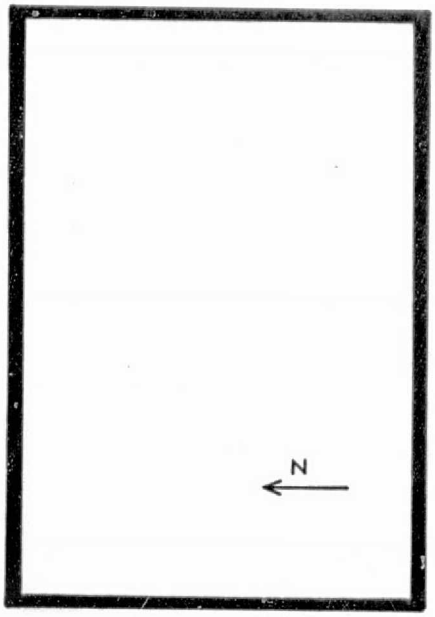


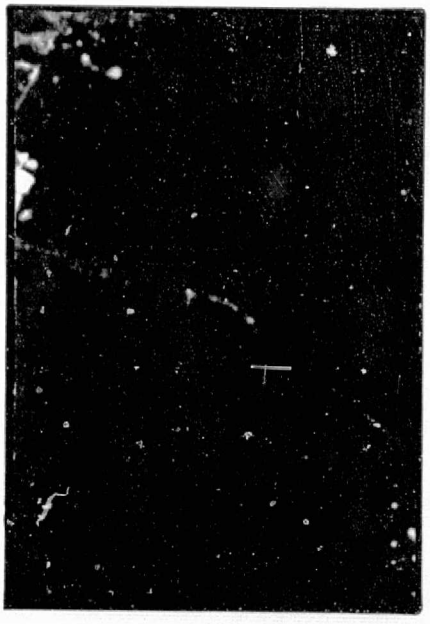

Skylab 3, S-190B
Photo 83-166,
August 5, 1973

0 .5 mi
0 .5 km

Landsat-1 color composite
of MSS Bands 4, 5, and 7;
E 1080-15192, October 11, 1972

0 .5 mi
0 .5 km

2.10L--Mixed forest land. EDC-010134. (Areas shown on the three images are not exactly equivalent.)

2-58
PAGE INTENTIONALLY BLANK
2-58
PRECEDING PAGE BLANK NOT FILMED

REPRODUCIBILITY OF THE
ORIGINAL PAGE IS POOR

High-altitude aircraft
Mission 73-181, Frame 5259
October 27, 1973

0 .5 mi
0 .5 km

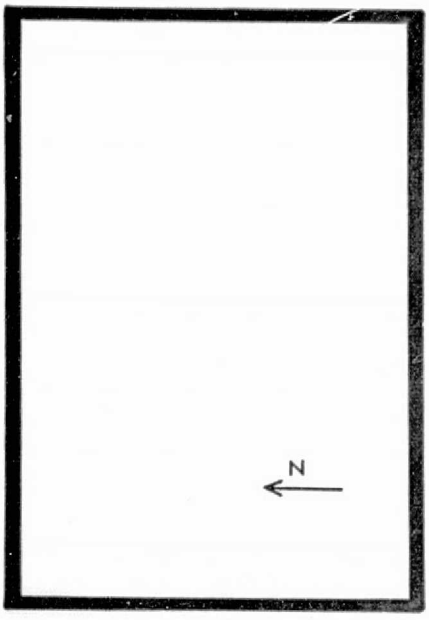

Skylab 3, S-190B
Photo 83-166,
August 5, 1973

0 .5 mi
0 .5 km

Landsat-1 color composite
of MSS Bands 4, 5, and 7;
E 1080-15192, October 11, 1972

0 .5 mi
0 .5 km

REPRODUCIBILITY OF THE
ORIGINAL PAGE IS POOR

2.10m--Utility rights-of-way. EDC-010135. (Areas shown on the three images are not exactly equivalent.)

PRECEDING PAGE BLANK NOT FILMED



2-60
PAGE INTENTIONALLY BLANK

purposely shown here in a more enlarged and hence grainier presentation to illustrate a range of sensor resolutions, each with its own advantages. Even the highest resolution format (high-altitude aircraft photography) does not go to the level of detail needed in many land use information applications in metropolitan areas. Comparisons of the three sets of illustrations also reveal that Skylab S-190B photography is much closer to the aircraft photography in sharpness and ability to resolve key features on the ground than it is to the Landsat. Further comparisons are detailed in table 2.6.

## USER APPLICATIONS AND EVALUATION

The evaluation of Skylab photography by users within CARETS took place as part of a broader analysis of all CARETS products. CARETS investigators conducted three user evaluation workshops for representatives of local, State, and Federal agencies respectively. At the workshop users received data packets containing sample CARETS products. They studied the products for several weeks and evaluated each on the basis of their data needs at subsequent interviews with CARETS personnel.

Objective and meaningful evaluation of Skylab data suffered from two serious constraints. The first was the lack of high quality images for users to take with them. They were able to see second generation prints and transparencies at USGS offices, but in the packet of data handouts the only type of Skylab imagery included was 35-mm slides. The second constraint was the area of noncoverage. The jurisdictions of many users did not fall within the limits of the Skylab sensors

2-62
PRECEDING PAGE BLANK NOT FILMED



2-62
PRECEDING PAGE INTENTIONALLY BLANK

Table 2.6--Relative comparison of sensor detection capabilities

| LAND USE CATEGORY | ERTS MSS | S-190A | S-190B | AIRCRAFT (U-2) |
|---|---|---|---|---|
| Urban and Built-Up | 2 | 2 | 1 | 1 |
| Residential | 3 | 3 | 2 | 1 |
| Commercial and Services | 3 | 3 | 2 | 1 |
| Industrial | 4 | 3 | 2 | 1 |
| Trans., Comm., & Utilities | 3 | 3 | 2 | 1 |
| Industrial and Commercial Complexes | 4 | 3 | 2 | 1 |
| Mixed | 3 | 3 | 2 | 1 |
| Agricultural Land | 2 | 2 | 1 | 1 |
| Cropland and Pasture | 2 | 2 | 1 | 1 |
| Forest Land | 2 | 2 | 2 | 1 |
| Deciduous | 3 | 3 | 4 | 2 |
| Evergreen | 3 | 3 | 4 | 2 |
| Mixed | 3 | 3 | 4 | 2 |
| Water | 1 | 1 | 2 | 1 |
| Streams and Canals | 1 | 1 | 3 | 1 |
| Lakes | 1 | 1 | 2 | 1 |
| Reservoirs | 1 | 1 | 2 | 1 |
| Bays and Estuaries | 1 | 1 | 1 | 1 |
| Wetland | 2 | 2 | 3 | 2 |
| Forested | 4 | 4 | 4 | 3 |
| Nonforested | 2 | 2 | 2 | 1 |

1 - Optimal, 2 - Adequate, 3 - Marginal, 4 - Unattainable

Note: ERTS data was in color composite form, S-190A in color infrared, S-190B in color, and Aircraft data in color infrared.

fields-of-view. Some user agencies, however, did find utility in Skylab data. In some cases these evaluations are based on the similarity of Skylab data to certain types of aircraft and satellite data.

CARETS researchers divided potential user agencies into three primary groups: local and regional planning agencies, State agencies, and Federal agencies. They further divided agencies into groupings based on the major function of each. These include land use planning, transportation planning, environmental protection, mineral and energy survey, disaster warning and assessment, outdoor recreation planning, water resource planning, fish and wildlife management, agricultural management, socioeconomic data collection, utility planning, economic and community development, and multipurpose resource management.

For the majority of users interviewed, the most useful CARETS product has been high-altitude color-infrared photography. In every case users saw these data as at least of secondary utility and sometimes of primary utility. Data of primary utility are here defined as having high value in the performance of agency functions. Data of secondary utility are useful but not necessary, and data of tertiary utility are of limited value in the performance of agency functions. Some State and Federal agencies found the aircraft photography of primary utility. These agencies include the Economic Development Council of Northeastern Pennsylvania; the Virginia Division of State Planning and Community Affairs; the Pennsylvania Department of Environmental Resources, Environmental Master Planning; the Maryland Department of Economic and Community Development; and the U.S. Department of Agriculture, Soil Conservation Service.

In contrast, most user groups expressed little interest in Landsat data in the formats and scales presented. Two agencies found Landsat to be of primary utility. The Interstate Commission on the Potomac River Basin saw both cost and time advantages to Landsat data and used them to produce a Level I land use map of the entire Potomac River basin. The U.S. Army Corps of Engineers, Baltimore District, in need of a good visual presentation of land use in the Chesapeake Bay region and unaware of the preparation of the CARETS Landsat maps, converted more detailed data (CARETS Level II maps, 1:100,000) into more generalized data (Level I, 1:250,000). Only after the fact did they realize that Landsat could have provided nearly all of their required information. Several other agencies found some value in Landsat for providing a generalized view. Most users, however, were interested in obtaining larger scale, more detailed data.

The majority of land use data users in CARETS require Level III detail at scales of 1:24,000 and larger. Of secondary utility to most is Level II data at scales ranging from 1:24,000 to 1:125,000. For most of the agencies expressing interest in Landsat (1:250,000 or smaller scale data), the utility of these data is tertiary.

In light of the aforementioned user responses, primary and secondary applications appear feasible with S-190B photography. The S-190B photos approach high-altitude aircraft photos in information content of significance for land use identification and mapping. As stated previously, many Level III categories can be identified accurately on S-190B data. The Skylab data, however, may not be as inclusive in fulfilling the first order needs of users as the aircraft data. At the State and

Federal levels, Skylab data could provide comparable results. Where Level II type data is of primary utility the S-190B system adequately provides the necessary information.

Discussions with numerous user groups indicate that data of the quality of S-190B are often useful but not necessary in the resource management decisionmaking processes. Organizations reporting a primary utility in such data, however, include the National Oceanic and Atmospheric Administration's Office of Coastal Zone Management, the U.S. Department of Agriculture's Soil Conservation Service, and several State land use and environmental planning agencies. In the cases where the data were reported not necessary--usually the sub-State planning agencies--the primary levels of detail needed for decisionmaking are Level III and Level IV, sometimes unobtainable by any remote sensing means or at scales smaller than 1:24,000.

S-190A data, containing much less detail, are primarily of tertiary utility. Although superior in spatial resolution to Landsat imagery, S-190A photography is similar to such imagery in that it is acquired at small scale, presents a synoptic view, and becomes grainy if photographically enlarged beyond a scale of approximately 1:250,000. In evaluating data utility, users generally establish broad categories of discrimination because small differences in resolution do not constitute significant changes in the total value of a product. Since there is not an order of magnitude difference in the quality of data between S-190A and Landsat, S-190A also falls into the small-scale information, tertiary utility category.

Another similarity between S-190A and Landsat is the acquisition of multispectral data. A summary of image bandwidths is given in table 2.7. Skylab investigators hoped that the S-190A multispectral photography, with its increased spectral discrimination capabilities, could serve as a complement to the S-190B photos. Most users, however, found the S-190A spatial resolution too low and the tradeoff in spectral vs. spatial discrimination not great enough to warrant using the S-190A data. The users finding the greatest use for this type of data are the oceanographers and hydrologists. Much of their work requires visible data in the blue and blue-green portions of the spectrum. In the CARETS user evaluation study, the most positive response to S-190A photography came from the American University Department of Biology, which found these data of value in wetland research. American University researchers reported that a false-color composite of three black-and-white bands of the S-190A photography, enlarged to 1:250,000, is more useful in some respects than the color-infrared film used in the same camera.

Much of the user response indicates that multispectral data with low spatial resolution, like S-190A (30 - 50 m), is not significantly more useful than lower resolution (70 - 100 m) multispectral data. If this is true, then multispectral scanners, such as the 13-channel Skylab S-192 system, could hold much more potential for users of such data, considering the increased spectral discrimination (i.e., number and range of wavebands).

## EVALUATION OF SKYLAB DATA VIS-A-VIS FUTURE USGS GEOGRAPHY PROGRAM NEEDS

The USGS Geography Program is entering a new phase of operations with the close of the NASA-funded research projects. Attention now has turned

Table 2.7--Comparison of wavelength bands for Landsat and Skylab photographic systems

| | Landsat | Band | Skylab S-190A |
|---|---|---|---|
| RBV 1 | 0.475 - 0.575 μm | 1 | 0.7 - 0.8 IR Aerographic (B&W) |
| RBV 2 | 0.580 - 0.680 μm | 2 | 0.8 - 0.9 IR Aerographic (B&W) |
| RBV 3 | 0.690 - 0.830 μm | 3 | 0.5 - 0.88 IR Aerographic (Color) |
| MSS 4 | 0.5 - 0.6 | 4 | 0.4 - 0.7 Aerial Color (High Resolution) |
| MSS 5 | 0.6 - 0.7 | 5 | 0.6 - 0.7 Panatomic X (B&W) |
| MSS 6 | 0.7 - 0.8 | 6 | 0.5 - 0.6 Panatomic X (B&W) |
| MSS 7 | 0.8 - 1.1 | | |
| | | | Skylab 190-B |
| | | | 0.4 - 0.7 (SO 242) |

to a broad based effort to compile and disseminate current land use information in map and digital tape form for the entire United States. This program will provide for the first time a systematic and comprehensive collection and analysis of land use information on a nationwide basis at map scales of 1:250,000 and 1:100,000 within a 6- to 7-year period. Periodic revisions are planned. Included within the program's framework is an experimental mapping effort at larger scales (1:24,000 and 1:50,000) in selected areas.

Geography Program research focuses primarily on the following tasks: (1) Technological improvement in the compilation, handling, and dissemination of current land use data; (2) interpretative or analytical studies relating current land use data to physical, socioeconomic, political, and demographic conditions; (3) prediction of future land use trends; and (4) urban and regional modeling of land utilization problems.

The USGS land use and land cover mapping effort depends primarily on remote sensor data as source materials, and Geography Program investigators designed and tested the USGS land use and land cover classification system to be used with remote sensor data. The land use and land cover operational mapping project requires systematic and reasonably current remote sensor coverage of the entire United States, a need accounting for the present decision to use classified source material, NASA U-2 photography, and other maps and statistics. The only feasible alternative to the use of these data has been Landsat, which would not provide as detailed ground resolution.

One of the most valuable land information gathering systems for geographic coverage data uniformity, and economic practicability, Landsat has suffered severely from misunderstanding and misuse. In many cases,

researchers have evaluated multispectral scanner imagery from what cannot be seen rather than by what can be seen. Furthermore, future optimal use of Landsat data most probably lies in the automated analysis of computer-compatible tapes. Researchers have been constantly refining these automation techniques and recently have attained land use interpretation accuracies, in some categories, of over 80 percent (Ellefsen, 1973, and Klemas and others, 1975). In some cases, accuracy has been increased with a concurrent reduction in the cost of machine processing by an order of magnitude. Admittedly, these techniques are not yet operational, but refining them to the point of operational status should not take long, given the proper support.

The USGS land use and land cover classification scheme is not entirely compatible with Landsat data. Many of its categories are activity oriented and are difficult to define by automated processing. The USGS land use and land cover categories, however, have been devised with the data user in mind rather than the acquisition system. Landsat data are not always interpreted correctly, especially with respect to the type of activity occurring at a particular location. But in most cases, such data can be used to correctly interpret land cover. The requirement that the maps conform to the USGS land use and land cover classification system restricts Landsat as a source of information for the nationwide mapping project. The Geography Program would incorporate Landsat data into its operational mapping program if accurate delineation of the Level II land use and land cover categories could be achieved.

REPRODUCIBILITY OF THE
ORIGINAL PAGE IS POOR

This preceding evaluation illustrates that the Geography Program places discrete resolution requirements on remote sensing systems. Results from Skylab S-190B research indicate that spaceborne sensors can meet operational resolution requirements. Moreover, the ability of the S-190B camera to discriminate certain ground features lies between that of the higher resolution aircraft and the lower resolution Landsat sensors. Research investigating the value of S-190B as a land use mapping system also reveals a close correlation between the quality of maps made from Skylab S-190B photography and those made from high-altitude aircraft photography at scales much larger than 1:250,000.

The Skylab EREP was not designed to provide complete photographic coverage of the United States nor to provide repetitive coverage of geographic areas over a long period of time. Rather it was designed to test several remote sensing systems as tools in resource information gathering. Skylab, therefore, did not offer an operational means of data gathering for the Geography Program. Its noteworthy contribution in this regard, however, was its ability to acquire data of high enough resolution to meet the criteria for operational land use and land cover mapping.

One can summarize guidelines for the development of the future operational systems capable of satisfying the needs of USGS land use and land cover mapping in two statements: (1) A spacecraft system or spacecraft-aircraft combination capable of providing repetitive coverage over a large geographical area is necessary; and (2) the system must be capable of obtaining interpretable data at the level of detail of the USGS land use and land cover classification. Landsat meets the first criterion but not the second. The opposite is true for Skylab. For system suitability the stage has therefore been set for the entrance of Landsat follow-on systems.

Turning from the operational mapping needs, we will now examine the wide range of Geography Program research needs. Some are in-house projects and others are multi-office, multidisciplinary projects. All involve the application of land use information. Examples of program thrusts include: (1) Continuing research on the application of Landsat computer-compatible tapes to operational land use mapping; (2) updating the land use classification system and expanding it to third and fourth level categories for specific user or regional requirements; (3) investigating the impact of land use on solar-terrestrial energy systems; (4) continuing involvement in the Office of Land Information and Analysis (LIA) and other USGS divisional multidisciplinary research efforts such as the Chattahoochee River Quality Study, Yampa River Study, and various urban area studies; and (5) participating in data gathering and environmental analysis in such areas of U.S. Geological Survey responsibility as oil shale deposits and strip mined land reclamation.

The types of remote sensing data of import to these thrusts are varied. In most cases high-resolution photography is the best source. The solar-terrestrial energy systems task, however, relies most heavily on multispectral scanner data in the thermal infrared wavelengths. A bilateral approach to the kinds of future operational remote sensing systems to apply to these research areas seems most functional. Such a system would incorporate both synoptic, small- to medium-scale information and site-specific, large-scale information. The former could be derived from the present Landsat system, whereas the latter could be derived from the NASA aircraft operation. In several investigations a combination of both systems would be desirable. For example, in the

multidisciplinary analysis of a critical environmental region like the Louisiana Gulf Coast, such factors as land use change could be monitored by Landsat, and such effects of land use change as increased sedimentation could be monitored by U-2 aircraft. This type of operational remote sensor system would provide the fastest, most economical mechanism for providing users with systematic and descriptive data. More importantly, however, these data are of high enough quality to be used in the resource management decisionmaking process.

The more specialized investigation dealing with the land use impact on solar-terrestrial energy systems with its requirements for thermal infrared data, has a number of possible sources. Landsat-C and Applications Explorer Mission-A (AEM-A), also designated as the Heat Capacity Mapping Mission (HCMM), will provide high-quality thermal data. Present plans for Landsat-C call for the thermal band to have an instantaneous field-of-view (IFOV) of approximately 250 m. The HCMM IFOV is intended to be 500 m. The data obtained from both of these missions will be detailed enough spatially and radiometrically to provide inputs into urban climate simulation models.

Prospects are also good for the possible application of thermal data obtained from the National Environmental Satellite Service's ITOS, TIROS, and GOES meteorological satellites. The spatial resolution of these systems is lower than either Landsat-C or HCMM, but is still high enough to provide synoptic thermal inputs to the climate simulators. Furthermore, these systems have the added advantage of presently functioning in an operational mode and providing information on a daily basis.

To summarize, a multistage (spacecraft/aircraft) monitoring system holds the most promise for providing certain Geography Program research projects with the necessary levels of remote sensor information. This monitoring system, in concert with other operational systems, could set the stage for optimal use of remote sensor data as inputs into resource and land information analysis systems.

## EVALUATION OF USGS REMOTE SENSOR LAND USE CLASSIFICATION SCHEME

In assessing the adequacy of the land use classification originally presented in USGS Circular 671 (Anderson and others, 1972), later modified in USGS Professional Paper 964 (Anderson and others, 1976), as a uniform scheme for application with space-acquired data, one must recognize the main shortcoming of all land use classification systems--their inability to meet the needs of all possible users. The diversity of land use information users, each desiring a certain type and level of detail, results in a necessary generalization of categories allowing the needs of the largest number of people to be satistied. This means that no ideal or universal classification of land use is likely to exist (Anderson and others, 1972).

The USGS land use classification grew out of the recommendations of the Inter-Agency Steering Committee on Land Use Information and Classification (Anderson and others, 1972). The committee developed the scheme on the assumption that different sensors provide information at different levels of classification. The scheme presented Level I categories that should be derivable from spacecraft data, Level II derivable from high-

altitude aircraft data, and Levels III and IV derivable from low-altitude aircraft and ground data. Prior to the completion of the scheme as presented in Circular 671, Anderson (1971) stated that a land use classification system for use with spacecraft data should meet the following criteria:

1. The minimum level of accuracy in the interpretation of imagery should be about 85 to 90 percent.

2. The accuracy of interpretation for the several categories should be about equal.

3. Repeatable or repetitive results should be obtainable from one interpreter to another and from one time of sensing to another.

4. The classification system should be usable or adaptable for use over an extensive area.

5. The categorization should permit vegetation and other types of land cover to be used as surrogates for activity.

6. The classification scheme should be suitable for use with imagery taken at different times during the year.

7. Effective use of subcategories that can be obtained from the use of larger scale or enhanced imagery should be possible.

8. Collapse of categories must be possible.

9. Comparison with land use information compiled in the past or to be collected in the future should be possible.

10. Multiple use of land use should be recognized when possible.

Using the above criteria and the experience of research in the Central Atlantic region, investigators have assessed the USGS land use classification scheme. The accuracy analysis of various CARETS maps reveals that the classification falls short of achieving the first criterion--permitting a minimum accuracy level of 85 percent using

high-altitude aircraft-derived Level II land use maps. At three different scales, 1:24,000, 1:100,000, and 1:250,000, Level II land use maps revealed respective map accuracies of 84.9, 77.4, and 73.0 percent. Investigators also found a 1:250,000-scale Level I map derived from aircraft photography to have an accuracy of 76.5 percent and a 1:250,000 Level I map derived from Landsat-I imagery to have a 69.5 percent accuracy (Fitzpatrick, 1975).

Another study found the accuracy of a 1:24,000-scale Level III map derived from Skylab S-190B color photography to be 82.6 percent (Lins, 1975). The Skylab analysis, however, was much narrower in scope, covering an area of only 16 $km^2$ as opposed to the entire area of CARETS (75,000 $km^2$) mapped in the other examples. If similar Skylab photography had been interpreted for the entire test site, one would expect the accuracy to have been lower.

The first three percentages mentioned above reflect the direct relationship between map accuracy and scale--that is, map accuracy increases as scale increases, given the same source and classification system. The next two percentages show an increase in accuracy corresponding to an increase in data source resolution. Research, therefore, indicates that a change or modification of certain USGS land use categories could result in an increase in the total accuracy of the CARETS land use maps (Fitzpatrick, 1975).

The second criterion, that all categories be interpretable to the same degree of accuracy, also causes problems for the USGS classification. A test of the CARETS land use maps revealed several repetitive

errors, occurring at three different scales and indicating a basic difficulty in recognizing certain signatures on the remote sensor data. For example, interpreters misclassified residential land as cropland or forest land by as much as 35 percent at a scale of 1:250,000. For cropland and pasture, one can most likely attribute the error to recognition and mapping of the land according to the predominating surrounding use. In forested areas, the problem is mainly one of determination of usage, i.e., how dense is the residential pattern beneath the trees? Also, nonforested wetlands are frequently confused with adjacent land use categories, especially tidal water and forest land.

Two significant interpretation problems interfere with the USGS classification's meeting the third criterion--that results be replicable from one interpreter to another and from one time to another. Nonforested wetlands, for example, are subject to tidal fluctuations and undergo a seasonal change in appearance. Proper and consistent identification of this category requires seasonal remote sensor coverage. Similarly, the identification of deciduous and coniferous forest requires seasonal coverage, since color-infrared photography taken in summer reveals little distinction between signatures of the two types of forest land.

The USGS land use classification successfully meets criteria 4 and 5. The scheme is applicable over a large geographical area, and it does permit land cover types to be applicable as surrogates to activity. A prime example of the use of land cover types as surrogates in the CARETS research has been the use of land use categories to estimate and predict

the sulfur dioxide and particulate emissions in the Norfolk-Portsmouth Standard Metropolitan Statistical Area (Reed and Lewis, 1975).

Criterion 6, that the classification scheme be suitable for use with imagery taken at different times of the year, is similar to criterion 3, concerning the repeatability of results, and certain examples apply to both criteria. For nonforested wetlands, a rainy or dry season greatly affects the signature recorded on the photography or imagery. Wetlands lying beneath a foot of water will render a signature similar to tidal water on color-infrared photography because water absorbs rather than reflects light in the infrared wavelengths. The deciduous/coniferous forest land delineation is another special case that may require both summer and winter coverage. Interpreting forest land from summer photography is easy, providing no further breakdown is required. If more detail is needed, however, then winter data are necessary. The lack of foliage on deciduous trees in winter is easily discernible from the coniferous forests' bright spectral return on color-infrared film.

The USGS classification adhered well to criteria 7 and 8. Categories are mutually independent, and each category within a given classification level provides approximately the same degree of generalization as the other categories within that level. Moreover, the Circular 671 classification was designed to allow more detailed categories to be collapsed into the more generalized categories.

Few occasions have arisen where the USGS classification could be tested for the ninth criteron--the ability to compare land use data collected with information collected in the past or to be collected in

the future. This criterion may cause problems for urban and built-up categories which, in many instances, combine land use types.

Finally, the tenth criterion, concerning multiple-use aspects of land use, is extremely difficult to meet. Ground survey classification schemes are hard put to handle this case so that the USGS system cannot be criticized heavily for its deficiency here.

In reflecting on the particulars of this evaluation, one discovers that the USGS land use classification system, like all other schemes, has some strong points and some weaknesses. The system is coherent, inclusive, and adaptable for use over a large geographical area. Even with these strengths, the USGS classification does not provide the most uniform classification system for use with space-acquired remotely sensed data. It may, however, be the best scheme presently available. A classification system, or systems, which is based on analyzing an image and asking "What land use causes this signature?" will maximize the utility of remotely sensed data. This approach was initially used in developing the USGS system. Then compromises were made in defining some categories in order to provide a better fit with existing usage. Continuing evaluation and feedback from users is also an essential component in the development of land use classification schemes.

CHAPTER 3

## LAND USE CLIMATOLOGY--A COUPLED MODELING AND OBSERVATIONAL EXPERIMENT

A key environmental challenge that faces man is the achievement of more hospitable climates in urbanized regions while conserving energy expenditures to maintain these climates. This is admittedly a large challenge involving complex natural and man-modified environmental systems--systems which range from those governed by large-scale atmospheric processes to those of the artificial microclimates we maintain inside the buildings where we live, work, and play. Somewhere in between those scale extremes lies a mesoscale range where energy-exchange and related climatological phenomena can be described in relation to the terrain units into which the large urbanized regions are subdivided--the functional concentrations of residential, commercial, industrial, park land, and other land types. Moreover, each land use type has distinctive physical and human use characteristics that affect surface energy-exchange and climatological response.

Early in the planning stages for the Skylab Earth Resources Experiment Package, it became evident that the Skylab sensors would be well-suited to observations of phenomena and study of processes operating at this mesoscale level in an urbanized region. It was thought that direct mesoscale measurements of surface energy-exchange phenomena might prove a more efficient method of forecasting climatological effects of proposed land use changes than either extrapolating from point observations at existing weather stations or looking to the large-scale atmospheric

process models that are too coarse for the level of spatial detail required. Therefore, the "land use climatology" portion of this Skylab investigation was carried out, using a combined modeling and observational approach, with the goal of assessing the application of remote sensors to improve our understanding of the relationships between surface properties and the mesoclimates of urbanized regions. It is hoped that results will be useful aids to land use planners who may be required to consider energy use and climatological impacts of proposed changes within their planning jurisdictions. The Washington-Baltimore urbanized area has been chosen as a test site.

## LAND USE CLIMATOLOGY

The climate of an urbanized region has been described somewhat simplistically as a group of heat islands set in a matrix of cooler, nonurban land uses. By implication these heat islands are considered monolithic, whereas in fact they may be a matrix of thermal elements that differ according to the various land uses within a city, such as business districts, manufacturing districts, parks, and residential areas. Surrounding nonurban lands may also be matrices of diverse thermal elements related to various suburban and rural land uses. Thus the simple regional view becomes complicated by the variety of terrain elements that impact upon local and regional climates and that interact mutually as well. More is involved than merely an analysis of surface thermal state. Insight is also needed into such things as the role of albedos as controls of energy absorbed by the surface. Energy absorbed

by the surface is in turn a component of net radiation--that balance between energy absorbed and energy emitted--which acts as a broad indicator of energy retained by a terrestrial thermal system.

New methods are needed to study the dynamics of these complex surface energy relationships. The monolithic concept of the urban heat island, for example, may well be an artifact of traditional slowly-made spot observations that tend to smooth out both spatial and temporal diversities within a city. Due to equipment and manpower limitations, measurements are usually averages between a few data points made over a considerable period of time. If a synoptic approach has been desired, transects by automobile typically have been made in the radiation traps of thermal canyons between buildings. Measurements by such transects, however, exclude the radically different environments away from streets, such as building roofs, and the true diversity of the energy-related patterns is not recorded.

In contrast, a calibrated electro-optical scanner, airborne or in a satellite, acts as an imaging radiometer; its linescan image records energy states of active meteorological surfaces, not only in the business districts containing high topographic gradients but for other urban and nonurban land uses as well. In addition, it circumvents one of the troublesome problems that confront the traditional ground observer--that of representative site selection that must be made for logistic reasons. No representative sites may exist in a heterogeneous terrain. But a scanner, acting as an imaging radiometer, substitutes a matrix of values so complete as to include essentially all sites--a matrix

unequalled by any attempted ground measuring program. Such a complete array of data permits a superior alternative to representative sites, i.e., the use of averages taken over different sectors of the terrain. This array of data is particularly useful for urban surfaces which constitute a mosaic of small and exceedingly diverse elements. The remote collection of information by calibrated scanners can provide a magnetic tape for processing directly into digital computers where spatial smoothing or other averaging procedures can be applied without laborious keypunch or other manual inputs.

Although the use of calibrated linescan data provides a way to study the dynamics of surface energy-exchange processes as they relate to land use, these data give no direct insight into the various subprocesses acting to produce the observed changes. Useful inputs to achieve this can be obtained from corollary ground observations, but here again are many of the obstacles that face a ground observer. Analytical tools that parallel the remote gathering of information from above are the numerical computer models which combine existing knowledge of involved processes to simulate the energy-related phenomena that occur at the surface. Such an approach is particularly useful in the study of the processes as they relate to land use. Remotely observed data can serve not only to test the accuracy of simulation models but to provide necessary inputs to them as well.

Possibly the greatest single value of a simulation model is its potential to test the sensitivity of a phenomenon to changes in its various subprocesses. A simulation model incorporates subroutines that

have been derived from analytical relationships formulated by earlier investigators. By changing inputs to these subroutines to simulate either natural or man-induced forces, the investigator can cause the model to indicate possible effects upon the larger energy-exchange system.

The combined capabilities afforded by the remote measurement of surface energy phenomena from above and the simulation modeling of these same phenomena become the base for a new subdiscipline or area of inquiry, cogent to man's concern for his impact on the environment. This subdiscipline has been termed "land use climatology." The Skylab S-192 scanner has provided a useful vehicle for lifting the new inquiry from a microclimatic perspective afforded by airborne scanners to the mesoscale or regional view of the satellite. It has provided satellite data for this use, although the fact that only one usable set of data was received has reduced the scope of the experiment to developing systems of application rather than actually observing the dynamics of surface energy phenomena in a variety of synoptic states. The following sections detail systems developed, technical problems overcome, and technical problems still to be tackled. They then evaluate the use of a satellite platform to gather information for these purposes.

## PRE-SKYLAB DEVELOPMENTS

Previous work leading to the coupled land use climatology experiment has followed two paths: (1) Development of techniques for mapping radiation-related phenomena from electro-optical scanner outputs, and

(2) the development of the simulation model. Early work is summarized in the following two subsections, and appendix A presents details of "The Baltimore Mission."

## Early Mapping Experiments

First attempts of these investigators to map from scanner data involved those data imaged in 1969 by the NASA RS-14 (Texas Instruments Scanner) over the Island of Barbados in conjunction with the larger Barbados Oceanographic and Meteorological Experiment (BOMEX). Maps showing the distribution of radiation temperatures and surface radiances were made from a calibrated image of a single flight across the northern edge of the city of Bridgetown and adjacent sugar cane fields. The technique of block filtering to generalize data was developed optically for transparencies. The centroids of the blocks provided values for contouring data into isarithms (Pease and others, 1970). That air in the optical path modifies the surface signal, even in the so-called water vapor window, was recognized during the experiment with the discovery that an airport runway with a radiation temperature of 52°C recorded only 42°C from an altitude of 1,000 ft. Although calibration of the imagery to adjust for this discrepancy was essentially accomplished by ground targets, the theory of the "gray-window" effect of the atmosphere in the scanner optical path was hypothesized, and a model for converting values received aloft to their true surface equivalents was formulated. Theoretical groundwork for eventual calibration of data without surface targets was established.

The second mapping experiment was performed in an effort designed specifically as a precursor to this Skylab climatology investigation. As part of the NASA Earth observations aircraft program, the Environmental Research Institute of Michigan (ERIM) made imaging flights with the M-7 multispectral scanner over the city of Baltimore at three different times in a single diurnal cycle on May 11, 1972. Not only did this experiment show that the dynamics of energy-exchange processes could be examined by time-sequential imagery, but that surface energy phenomena other than thermal state could be observed as well. Maps of surface albedos, energy emitted and absorbed by the surface, and net radiation were created. A summary of results of this effort is presented in appendix A. For the maps shown in appendix A, target calibration was used.

In a separate but parallel inquiry with the same Baltimore data, ERIM used the self-calibration potential of their scanner to achieve absolute radiance values aloft. They still depended substantially upon targets to check the alteration of signals by the air. Their project demonstrated that radiation maps could be made directly from magnetic tape rather than from photographic scanner outputs, which led the way for the use of tapes in the Skylab mapping experiment.

That calibration targets have not been available for the mapping from Skylab S-192 data, as will be described, has led to significant further development of the gray-window model using instead the atmospherics of the optical path. The use of this model should prove desirable because satellite scanners are difficult to calibrate by ground target methods, and frequently the decision to use data may come after the imaging pass has occurred.

## Modeling in Land Use Climatology

The development of any research program is essentially dependent upon questions to be answered. In land use climatology, the central question involves the ways various uses of the land interact with local weather to modify surface climate (Outcalt, 1972a). The mean temperature of the surface in any area of terrain, for example, is a unique response to local weather and the physical properties of the Earth's surface and substrate. Present modeling technology permits the numerical simulation of surface thermal and energy balance regimes as a function of local meteorological observations and of the radiative, aerodynamic, and thermal properties of the near-surface environment. Specific data in these categories, necessary for simulation, are listed in table 3.1.

Simulation strategies used in the Skylab experiment were initially developed from techniques described in the literature (Lettau, 1969; Myrup, 1969; Outcalt, 1972b). Briefly, the method hinges on the specification of all variables needed to calculate the components of surface energy transfer based on the meteorological (M) and geographical (G) data listed in table 3.1. The four components of surface energy transfer [net radiation (R), soil heat flux (S), sensible heat flux (H), and latent heat flux (L)] can be specified as transcendental in surface temperature (T) in the familiar energy conservation equation,

$$R(G,M,T) + S(G,T) + H(G,M,T) + L(G,M,T) = 0 \qquad (3.0)$$

A temperature equilibrium model (interval halving or secant numerical algorithm) carries out a search for that surface temperature which will drive the equation to a zero sum condition. This search is followed

Table 3.1--Necessary simulation data

Meteorological Variables

Station Pressure

Incoming Solar Radiation

Incoming Thermal Radiation

Mean Air Temperature

Mean Relative Humidity

Mean Wind Velocity

Geographical Terrain Parameters

Substrate Thermal Diffusivity

Substrate Thermal Conductivity

Surface Albedo (Effective)

Surface Aerodynamic Roughness

Surface Wetness

by an explicit or implicit finite difference algorithm which generates an update soil temperature/depth profile. At each iteration, the surface temperature and all of the components of surface energy transfer are output in addition to the substrate (soil) thermal profile.

A second version of the model utilized estimates of the geographical terrain parameters listed in table 3.1. Such estimates were easily made by using land tracts for urban centers which included several city blocks. Related to features that can be abstracted from remote sensing imagery, these parameters are summarized in table 3.2. In addition, three terrain parameters which mold the geographic parameters are listed in table 3.3. Researchers tested the use of estimates as simulation inputs in Ann Arbor, Michigan, and environs, using an integrated thermal response means derived from thermal imagery collected by ERIM. The test used a simulation of thermal response for two times, 11:44 a.m. and 2:25 p.m. EST on August 6, 1970 (Outcalt, 1972a). In all cases the thermal rank was correct in the simulation, and maximum differences were in the realm of 15 percent of the total thermal range. Results were extremely encouraging and contradicted the concept of a monolithic heat island previously noted. The model was later tested using winter conditions. Results indicated that surface wetness was largely responsible for heat island contrasts in the summer, whereas the absorption of beam radiation by vertical walls was the most potent environmental factor in winter.

The Skylab simulation experiment described in a later section of this chapter refines the model still further. Many problems of the initial model have been removed, and spatial application of the technique

Table 3.2--Computation of geographical parameters, as used in surface climate simulation model

| Parameter | Definition | A function of |
|---|---|---|
| Substrate thermal diffusivity and conductivity | Traditional definition | Wetness fraction |
| Surface albedo (effective) | Includes radiation absorption from vertical surfaces | Silhouette ratio, obstruction height |
| Surface aerodynamic roughness | Used in computation of turbulent fluxes | Silhouette ratio, obstruction height |
| Surface Wetness | Direct | Surface wetness |

Source: Lettau, 1969, and Myrup, 1969

Table 3.3--Urban terrain factors, as used in surface climate simulation model

| | |
|---|---|
| Wet Fraction | --That fraction of a terrain tract covered by vegetation (freely transpiring) or by a wet surface. |
| Silhouette Ratio | --The ratio of the vertical silhouette area in a tract to the horizontal area of that tract. |
| Obstruction Height | --The mean height of building and vegetation which forms an obstruction to air flow and creates a vertical silhouette which collects radiation in addition to the radiation absorbed on horizontal surfaces. |

has yielded completely simulated maps of the Washington-Baltimore area, which parallel those made from scanner data. The reader is referred to appendix B for a more detailed description of the energy budget simulation model.

## RADIATION-RELATED MAPS FROM S-192 DATA

The opportunity to make synoptic maps of surface radiation related phenomena on a regional scale came with the receipt of Experiment S-192 tapes in December 1974. The August 5, 1973 pass was the only satellite overflight (Skylab 3) to obtain data in the thermal infrared that could be processed to reduce system noise sufficiently so as not to impede surface measurements and therefore to be of use to the land use climatology experiment. With this satellite-acquired information, maps of the surface thermal state and surface albedos at the time of imaging (10:00 a.m. EST) have been made. The following sections describe the techniques used and problems overcome in carrying out this mapping experiment.

### The S-192 Data

The S-192 system is an electro-optical multispectral scanner with 13 bands, or spectral sensitivities that encompass a total wavelength interval from 0.41 to 12.5 micrometres (μm). Thirteen detectors are simultaneously irradiated by energy from the Earth's surface, with each producing an electronic output signal corresponding to the average radiance received from the spot on the terrestrial surface contained in the instantaneous field-of-view. These surface spots, which become pixels in the scanner output, are either 36.3 or 72.6 m apart on centers, depending on whether a high or low scan rate

is used. The system has a conical-scan geometry, which produces a circular scan-line trace on the surface, skewed by the forward motion of the satellite and the rotation of the Earth that occur while a scan is being recorded. This geometry gives both an optical path of constant length and a constant angle to the horizon plane, two characteristics of significant interest to the mapping project. The imaged path is approximately 69 km (43 miles) wide.

Data were recorded in the satellite on 24 tracks of a 28-track tape in an S-192 pulse code modulation (PCM) Miller-encoded form at a density of 16,177.86 bits per inch and at a speed of 60 inches per second. Most shortwave or "reflected" information was recorded at a high scan rate (2,480 samples per scan line) with some of the weaker near-infrared and violet wavelengths at a slow rate, 1,240 samples per scan line. Thermal infrared data of band 13 (10.2 - 12.5 μm) were recorded at both scan rates. That at the low rate (SDO channel 21)[1/] was used in this study for making the map of thermal state of the surface.

Tapes were returned to Earth at the end of each mission in the command module. Surface processing of the tape data included reformatting and skew removal, decommutation, conversion to Greenwich Mean Time, and transferral to an edited 14-track tape copy. After initial principal investigator evaluation, the data were subjected to line straightening in addition to other modifications to suit various users. Line straightening by choosing pixels from a sequence of circular lines creates new lines that are straight and easier to use. The number of pixels per line is reduced to approximately

---

[1/] SDO (Scientific Data Output) is the designation given for channels in the reformatted tape that correspond to specific tracks in the original EREP tape for Experiment S-192. The SDO channels do not bear the same numbers as the Skylab tape tracks from which they are taken nor are they the numbers of the spectral bands. For example, band 6, with a spectral range from 0.68 to 0.76 μm, was recorded in Skylab on tracks 9 and 10. In the reformatting process, the data appears on SDO channels 7 and 8. All references to channels will be to SDO channels.

1,033 and some information is thereby lost. High sample rate channels are converted to two low sample rate channels by choosing alternate pixels for each of the two. Whether it occurred in the initial data calibration or in the line straightening process, an error of approximately 5 percent seems to appear in final radiance values from band 13, as will be subsequently discussed.

The initial problem of reading the computer tapes was resolved with the assistance of Mr. Robert McNelly of the USGS Computer Center Division. However, because of constraints on his time, making of surface energy exchange maps was transferred to the Department of Earth Sciences, University of California, Riverside, and carried out under the supervision of R. W. Pease. Techniques used to derive maps from the line-straightened NASA-192 tapes are described in the following.

In the format of the NASA-supplied tapes, data blocks are by scan lines: that is, all data from the several SDO channels for a discrete scan line are grouped together. Also included for each scan line are such ancillary data as latitude and longitude of the first pixel, orthogonal location of the satellite nadir point, direction azimuth, and velocity. Only the locations of nadir and the first pixel are accurate. The locations of other points (centers of scan lines, etc.) read out as useless numbers. All data are in a hexadecimal code which permits PCM counts from 1 to 255--a more than sufficient number of digital levels to accomodate all data recorded.

The first step in making use of the NASA-supplied tape data, therefore, was to separate scan lines from line data blocks into channel files. This step consumed the greatest amount of computer time in the entire mapmaking process, since it required reading all data to obtain what was pertinent and desired. The job was reduced by addressing the extraction of data only to

those lines needed for the imaging area of concern, which utilized portions of two tape reels out of four supplied. Data files by discrete channels were made for approximately 1,000 scan lines out of approximately 4,000 on the tapes. In so doing, it was necessary to account for a measure of overlap of lines between tapes 2 and 3.

With the desired SDO data in files according to the discrete channels, the first chore was to make PCM-count averages for 100-pixel blocks (10 adjacent pixels in 10 adjacent lines). Block filtering was performed only for the two SDO channels desired for the mapmaking, channel 21 for the map of surface radiation temperatures and channel 7 for the map of surface albedos. The 100-pixel blocks are the basic mapping unit used in this phase of the project. Average values for the blocks for the two channels used have been placed on tape for permanent storage along with all pertinent ancillary data.

Data-cell maps have been made for both surface radiation temperatures, as they existed for the few moments of the overpass of the data-gathering Skylab satellite, and surface albedos. Procedures and problems for translating the SDO channel 21 PCM-count block averages into the temperature map are discussed first in the following sections. Surface radiation temperatures are momentarily transient, and the map of them is truly synoptic in nature. Although the data were collected in a synoptic manner, albedos are relatively conservative surface characteristics which change with the time of year rather than with the time of day as do temperature values.

The map products (figures 3.6 and 3.7 discussed later), display the discrete data cells in a value-intervalled hierarchy. They have been made on a vector line plotter with contiguous cells of the same value shown as a

polygon on which the cell pattern shows conspicuously. A further sophistication can include smoothing interval boundaries to yield conventional isarithms, a process that can be accomplished either on the computer and plotter or quite easily by eye. Less costly line-printed graymaps have been made where each cell is represented by a 2 x 2½ character printout to make the map planimetric, but these are not included in the report.

The Problem of Atmospheric Modification--the Gray-Window Model

In the pre-Skylab Baltimore experiment, calibration of scanner thermal infrared (IR) values to the surface was accomplished by using ground targets sufficiently large to be discriminated by the 1-mm aperture of a MacBeth densitometer, or identifiable as pixel values when analysis was made directly from digitized magnetic tapes. In the Baltimore experiment, the aircraft imaged comparatively close to the surface (1.63 km, or 5,000 ft.), and target image elements were therefore comparatively large. It was recognized, however, that with satellite images the targets would not be large. Specific calibration targets, such as those used for Baltimore, would be smaller than a pixel and thus almost impossible to find, much less discriminate from their surroundings. Calibration of data to the surface therefore depends upon analysis of the processes whereby the surface signal is modified by the atmospherics of the optical path, here termed the gray-window calibration model. Of most concern are the conditions of water vapor content, turbidity (aerosols), and gaseous pollution of the air.

The original gray-window model developed from Schwarzchild's Equation for the Barbados (BOMEX) experiment (Pease and others, 1970) can be written in Skylab terms as follows:

$$R_z = \epsilon[\varepsilon_{bb}(\overline{T})] + (1 - \epsilon)\ R_o \qquad (3.1)$$

where $R_z$ is the radiance in $W/cm^2/\mu m/sr$ (steradian) received aloft by the scanner (scanner output value), $R_o$ is the radiance of the surface represented by its emitted signal, $\varepsilon$ is the emissivity of the air column of the optical path, $(1 - \varepsilon)$ the transmissivity of the air column, and $[\varepsilon_{bb}(\bar{T})]$ the equivalent blackbody radiance of the air in the column for a mean temperature in °K $(\bar{T})$. Application of this model to a signal received by a scanner moving above the Earth's atmosphere leads to a simpler and more understandable model.

The surface signal, when passing through the atmosphere, is modified in two ways: (1) The surface signal is attenuated according to the atmosphere transmissivity, and (2) the upward radiance of the air in the optical path is added to the attenuated signal. With the substitution of R↑a for $\varepsilon[\varepsilon_{bb}(\bar{T})]$ and T for $(1 - \varepsilon)$, equation 3.1 becomes:

$$R_z = T\,R_o + R\uparrow a \tag{3.2}$$

where T is the overall transmissivity of the optical path and R↑a is the energy radiated by the atmosphere upward along the path in the spectral band of the scanner sensitivity. It follows, then, that radiance values received at the satellite can be converted to the corresponding radiances emitted by the surface by a transposition of the terms of equation 3.2 to

$$R_o = \frac{R_z - R\uparrow a}{T} \tag{3.3}$$

which becomes the basic relationship for calibrating S-192 data.

The value of $R_z$ is supplied by the scanner through proper manipulation of PCM counts, but R↑a and T are values that must be supplied either from a fit to high and low ground calibration targets or by the analysis of the atmospherics of the optical path.

## Surface-Collected Data of Use for Calibration

Surface data, collected during Skylab passes, were of several types: (1) The radiances (radiation temperatures) of possible targets which could be discriminated on S-192 outputs, (2) kinetic temperatures of these targets, and (3) pyranometric measurements of solar energy both for beam and diffuse values. Data collected by John Lewis of the University of Maryland on three dates, June 12, August 5, and September 12, 1973, are shown in table 3.4. Usable scanner outputs for only one Skylab pass, August 5, were received.

Three attempts were made to establish large water bodies as targets. On June 12 the radiation temperatures of Burke Lake in Fairfax County, Virginia, were measured. Loch Raven Reservoir, Maryland, was similarly measured on August 5 and Chesapeake Bay on September 12. Radiometric measurements of temperatures were made with a Barnes PRT-5 radiometer with a custom 10 - 12 μm bandpass which matched the scanner band 13 sensitivity fairly closely. Unfortunately, the August 5 target, Loch Raven Reservoir, was north of the scanned path and could only be used in the experiment for reference.

Lack of adequate calibration target data for August 5 suggested the desirability of obtaining the temperature of Chesapeake Bay from other sources. The most useful values are those measured radiometrically by the Johns Hopkins University oceanographic research vessel, the Ridgely Warfield on August 3, 2 days prior to the Skylab date. The temperature of the waters of the bay is considered not to have changed significantly between August 3 and 5. These data indicate a considerable range of temperature over the bay--temperatures that extend from 26°C to 29°C. Diversity is also apparent

Table 3.4--Ground correlation data collected for land use climatology experiment

June 12, 1973
Burke Lake, Fairfax, Virginia

| Solar Rad. ly/min. | Albedo | Temperature Air | Temperature Water($T_r$) | Time EDT |
|---|---|---|---|---|
| 0.45 | 0.02 | 80°F | 28.7°C | 8:15 EDT |
| .51 | .02 | 81 | 28.7 | 8:30 |
| .59 | .02 | 81 | 28.7 | 8:45 |
| .64 | .02 | 82 | 29.0 | 9:00 |
| .71 | .02 | 83 | 29.0 | 9:15 |
| .75 | .02 | 86 | 29.0 | 9:30 |
| .82 | .02 | 85 | 29.0 | 9:45 |
| .82 | .02 | 86 | 29.0 | 10:00 |
| .90 | .02 | 85 | 29.0 | 10:15 |
| .95 | .03 | 86 | 29.5 | 10:30 |
| 1.10 | .02 | 85 | 29.0 | 10:45 |

Notes: At 10:45 ratio of global to diffuse radiation = .33

Water temperatures are radiation temperatures
Air temperatures are kinetic temperatures

August 5, 1973
Loch Raven Reservoir, Maryland

| Solar rad. ly/min. | Water kinetic temp. in °F | Air kinetic temp. °F | Water radiant temp. °C | Time EDT |
|---|---|---|---|---|
| 1.07 | 78°F | 91°F | 26.0°C | 10:30 |
| 1.17 | 80 | 92 | 26.0 | 10:45 |
| 1.19 | 81 | 91 | 26.0 | 11:00 |
| 1.23 | 82 | 93 | 26.5 | 11:15 |
| 1.26 | 82 | 92 | 26.0 | 11:30 |
| 1.29 | 80 | 90 | 27.0 | 11:45 |
| 1.33 | 78 | 90 | 27.0 | 12:00 |
| 1.29 | 79 | 91 | 27.0 | 12:15 |
| 1.29 | 80 | 93 | 27.0 | 12:30 |
| 1.29 | 83 | 93 | 27.0 | 12:45 |
| 1.29 | 81 | 92 | 28.0 | 13:00 |
| 1.33 | 81 | 94 | 28.0 | 13:15 |
| 1.31 | 82 | 95 | 28.0 | 13:30 |
| 1.29 | 84 | — | 27.0 | 13:45 |
| 1.26 | 82 | | 27.0 | 14:00 |

Note: Radiometric temperature measurements made with Barnes PRT-5 Precision Radiation Thermometer with 10-12 μm sensitivity.

Table 3.4--Continued

August 5, 1973 (contd.)
Loch Raven Reservoir

| Time EDT | Diffuse (sky) radiation-ly/min. | Radiation reflected from water-ly/min. |
|---|---|---|
| 11:30 | 0.22 | 0.10 |
| 12:30 | .24 | .14 |
| 13:30 | .22 | .12 |

Notes: All solar radiation readings made with a silicon cell pyranometer

Cloud cover at 11:00 EDT, Cumulus humilus, 10-15 percent

September 12, 1973
Chesapeake Bay

| Time EDT | Water TIR temp °C | Shortwave (solar) radiation global | diffuse | reflected |
|---|---|---|---|---|
| 11:50 | 25.0 | | | |
| 11:55 | 24.5 | 5.00 mv[1] | 0.85 | 0.6 |
| 12:00 | 25.0 | | | |
| 12:05 | 25.0 | | | |
| 12:10 | 24.0 | 5.25 | 1.0 | .6 |
| 12:15 | 25.0 | | | |
| 12:20 | 25.0 | 5.40 | 1.0 | |
| 12:25 | 25.0 | | | |
| 12:30 | 25.0 | 5.30 | 1.0 | .6 |
| 12:35 | 25.0 | | | |
| 12:40 | 25.0 | 5.50 | 1.0 | |
| 12:45 | 24.5 | | | |
| 12:50 | 25.0 | 5.40 | 1.0 | |

[1]Values never converted to ly/min (langleys per minute).

Notes: Surface water (skin) temperature at 1215 h--26.2°C
Salinity 15.9 ppth
Current-flood conditions
Tide-flood conditions



...RODUCIBILITY OF THE
... PAGE IS POOR

on the S-192 band 13 image. A spatial plot was made of PCM values of the digitized tape as line-printed map, gated to show the diversity of bay temperatures. This plot suggested that a PCM count of 149 was a widespread value that corresponds to a radiation temperature of 27°C (300°K). The measured radiation temperature of Loch Raven Reservoir had been 26°C to 27°C. The histograms of PCM counts helped to ascertain value ranges and identify counts that matched various surface terrain elements (figure 3.1).

Experiments with a Two-Target Thermal IR Calibration - Band 13

If a high temperature calibration target as definitive as Chesapeake Bay had been available, a two-target calibration of scanner data would have been possible without an analysis of the atmospherics of the scanner optical path. Such a calibration was attempted on an experimental basis by assuming 27°C for the bay and 40°C for the centers of the urban districts of Washington and Baltimore, which comprise the "hot spots" of the imagery. Choice of this high value is based upon previous experience with the Baltimore experiment (appendix A) and with general values predicted by the simulation model. If no other means for calibration had been available, an approximation could have been achieved by the method. Use of the simulation output, however, would have eliminated its value as part of a coupled modeling and observational experiment. Documentation of the calibration would not have been convincing and acceptance of values so derived would be based upon an educated guess.

A two-target calibration has both numerical and analytical aspects in its solution. Essentially, one finds the combination of atmospheric transmissivity (T) and upward atmospheric longwave radiation ($R\uparrow a$) for the scanner spectral window that will convert appropriate scanner radiance

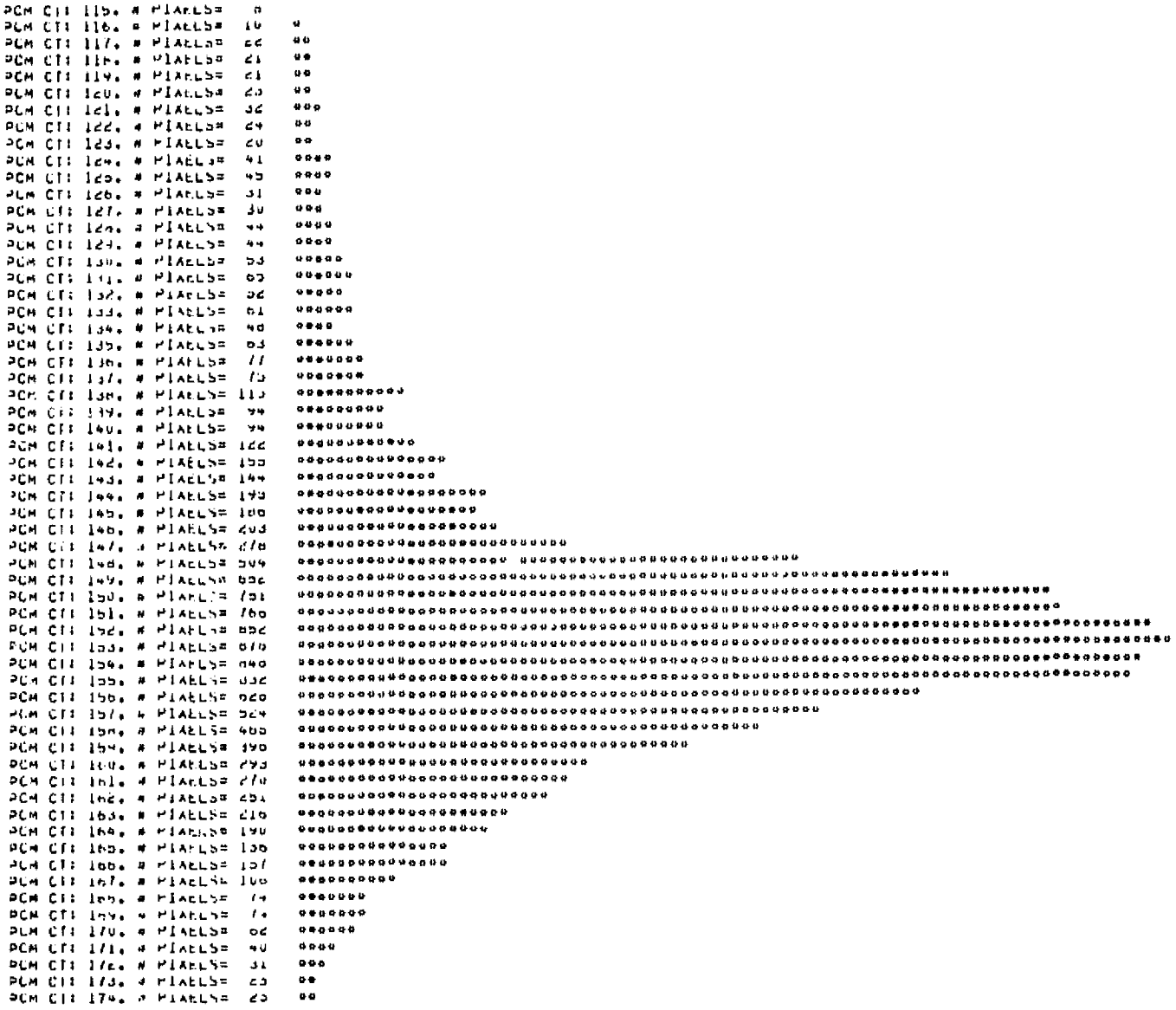


Figure 3.1--Distribution of PCM counts from S-192 output - Band 13

ORIGINAL PAGE IS
OF POOR QUALITY

values ($R_z$) to two corresponding target temperatures ($R_o$) using equation 3.3. These two values, however, are mutually dependent according to the transposed relationship,

$$R\dagger a = R_z - T\,R_o \tag{3.4}$$

and, for specific values of $R_z$ and $R_o$ which match the two target temperatures, T cannot be changed without changing R†a. Although these values can be found by iteration, the process can be made analytical by first determining the value of $R_o$ for each target temperature, using Planck's Equation converted to a spectral radiance per steradian form by adding the value (¶) to the denominator. The basic form used is modified from Hudson (1969) with

$$N_\lambda\ (sr) = R_o = \frac{c_1}{\P\lambda 5} \quad \frac{1}{e^{\,c_2/\lambda t}-1} \tag{3.5}$$

$c_1$ and $c_2$ the first and second radiation constants with values of 3.7415 ex 4 (W $cm^{-2}$ $\mu m^4$) and 1.43875 ex 4 ($\mu m$ $^oK$) respectively and 11.5 $\mu m$ the central wavelength of the scanner spectral sensing window. The value of $R_o$ for a temperature in $^oK$ then becomes

$$R_o = \frac{.05921}{e^{1251/t}-1} \tag{3.6}$$

when constants and the wavelength have been entered. Temperature (t) is in $^oK$. When values for $R_o$ have been ascertained from target temperatures and $R_z$ from scanner output, the transmissivity of the atmosphere (T) in the sensing band will be

$$T = \frac{(H)\ R_z - (L)\ R_z}{(H)\ R_o - (L)\ R_o} \tag{3.7}$$

with (H) and (L) designating values for the high and low radiance targets, respectively. The value (T) can then be used along with those for $R_z$ and $R_o$ to obtain R†a in accordance with equation 3.4.

Calibration Using the Atmospherics of the Optical Path - Band 13

The calibration model used for mapping in this experiment involves the atmospherics in the optical path and their effects upon the surface emitted signal. A rawinsonde profile, made 3 h before the satellite passage, describes the water vapor in the optical path, the primary modifying agent. Synoptic weather conditions indicated by both the profile and daily weather map, consisted of a surface moist and turbid layer separated by a temperature inversion from a deep capping layer of dry subsiding air. The surface weather map for the day shows a high pressure cell centered over the Central Atlantic States. The sounding indicates the inversion to be at 740 mb or 2.45 km. The inversion inhibited cumulus humilus cloud buildup although bands of cold high cirrus extend on the image southwest to northeast across Chesapeake Bay well to the south of the Washington-Baltimore area.

Use of atmospherics reduces dependence upon calibration targets. Indeed, if sufficient data were available and all scanner measurements were completely accurate, need for targets would be eliminated. However, this i not the case and Chesapeake Bay has provided a reference for tying the model to the surface, a use which suggests the measure of inaccuracy of the NASA supplied radiances.

Water vapor in the optical path acts both as an absorber and emitter of radiant energy between 10.2 and 12.5 μm even though this spectral band ostensibly is in the so-called "water vapor window." Absorption is a

function of transmissivity which is defined in terms of water vapor by the Bouguer-Beers Law as $e^{-ku}$ where e is the natural log base, u the water vapor expressed as precipitable centimetres ($gm/cm^2$), and k is a mass absorption coefficient with a value of 0.1 for the 10.2-12.5 μm sensing band (Kondratyev, 1969). Water vapor in precipitable centimetres (u) can be determined by the following equation:

$$u = \frac{\bar{m}\ (p_2 - p_1)}{g} \tag{3.8}$$

when $\bar{m}$ is the mean mixing ratio of the layer of atmosphere under consideration in grams of water per kilogram of dry air, $p_2 - p_1$ is the pressure depth of the layer in millibars, and g is the acceleration of gravity, 980 $cm/s^2$. The sounding lists temperatures for various pressure heights and dew points as depressions from kinetic (sensible) temperatures, elements which are diagrammed in figure 3.2. A pseudoadiabatic chart is the simplest way to obtain mixing ratios although a form of Teton's Equation can be used for this purpose:

$$m \approx Q = \frac{(3798)\ (10^{7.5\,t/t\,+\,237.3})}{P} \tag{3.9}$$

where the value (t) is the dew point in °C and P is the pressure in millibars. The value ($\bar{m}$) is very close to Q, the specific humidity, and for our purposes can be considered the same. Units are in grams per kilogram.

Since upward emission from each small but finite layer of the atmosphere is modified by the layer above through attenuation and additional emission, a high resolution numerical integration of values upward will yield the most accurate value of up-radiance (R↑a) into space. Analysis is more easily accomplished, however, by treating the atmosphere as a fewer number

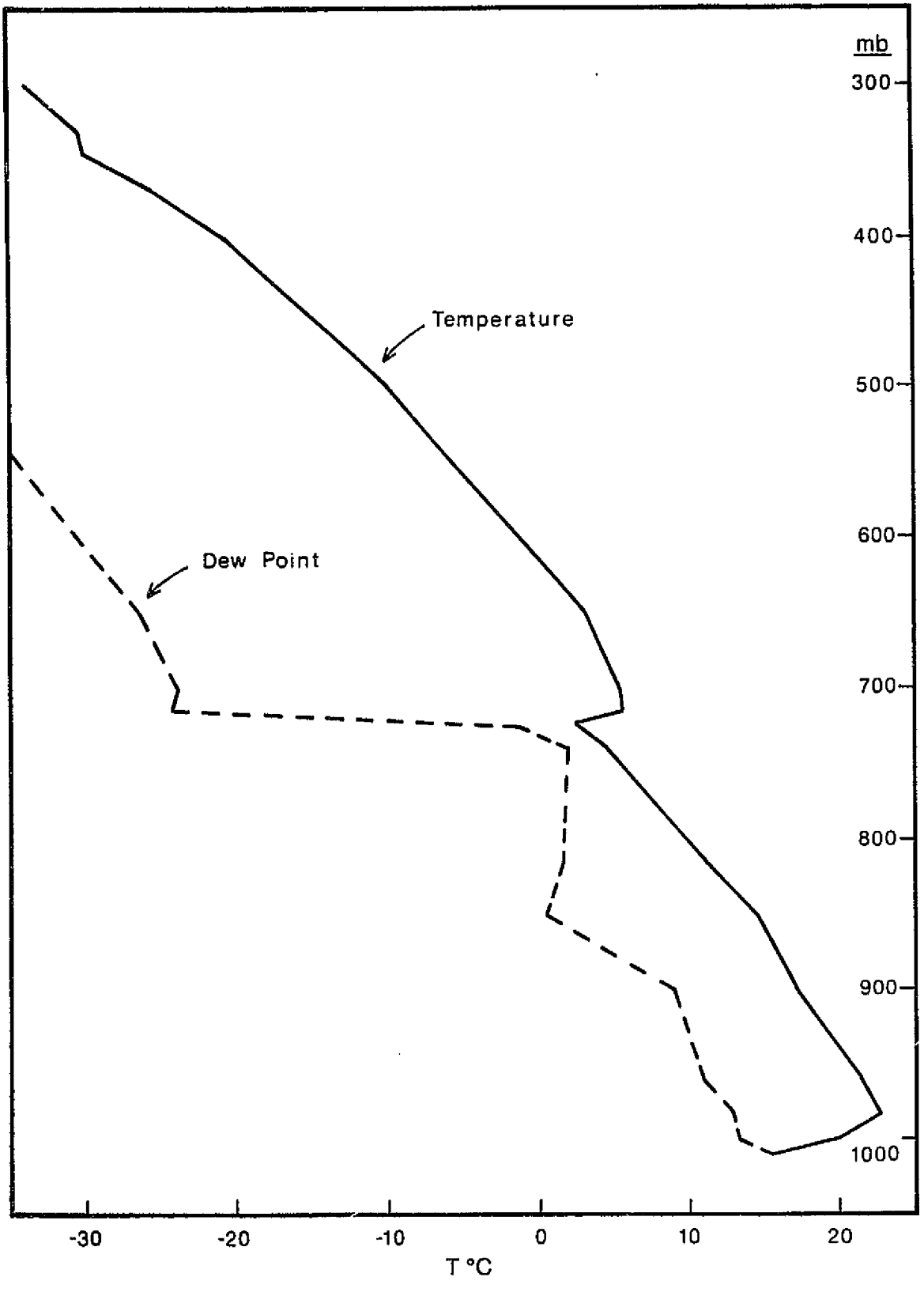


Figure 3.2--Rawinsonde profile for 7:15 a.m. EST, August 5, 1973, Washington, D.C.

of layers, particularly when more than one modifying element must be combined at each level. The water vapor and temperature profile is tabulated in table 3.5 in five layers below the inversion but a single layer above since the subsiding air has low water vapor and turbidity content and thus is relatively inactive as a modifying element. Layer 1, that closest to the surface, is at the top of the table.

Before obtaining the sounding, a moderately successful attempt was made to reconstruct the profile from synoptic data alone. Because of the lack of cloud buildup, the inversion, indicated by the presence of the high pressure cell, could be estimated as little more than 300 m above the cloud base or level of cloud formation. The inversion height could be estimated by extrapolating the surface dew point upward, with an allowance made for a lapse in value, to the point where the dew point profile intersected an estimated temperature profile constructed to a lapse of 7.5 °C/km. This placed the inversion at about 2 km rather than the 2.45 km indicated by the sounding.

Calculation of the overall thermal IR transmissivity (T) of the profile is made by multiplying all discrete layer transmissivities together. For the simple water vapor model indicated by the table, the value of T is 0.823. Upward radiance (R↑a) is calcualted by multiplying the radiance of layer 1 by the transmissivity of layer 2 to which is added the radiance of layer 2. This accumulated value is processed through layer 3 in the same manner and is repeated through all layers and into space. The process is shown by the following relationship:

$$R\uparrow a = ((((R\uparrow_1 T_2 + R\uparrow_2) T_3 + R\uparrow_3) T_4 + R\uparrow_4) T_5 + R\uparrow_5) T_6 + R\uparrow_6 \qquad (3.10)$$

$$= 1.3534 \text{ ex-4} \quad W/cm^2/\mu m/sr$$

Table 3.5--Temperature/water vapor profile from rawinsonde data
Washington, D.C., 11:15 a.m. GMT, August 5, 1973

| Layer | Depth | $\bar{t}$ °C | $\bar{DP}$ °C | $\bar{m}$ | u | $T_{wv,t}$ | E | R↑ |
|---|---|---|---|---|---|---|---|---|
| 1. 1000-950 | 50 mb | 21.64° | 12.64° | 9.3 | 0.474 | 0.945 | 0.046 | 3.9563 ex-5 |
| 2. 950-900 | 50 mb | 19.28° | 9.6° | 8.2 | .418 | .959 | .041 | 3.4057 ex-5 |
| 3. 900-850 | 50 mb | 15.56° | 5.0° | 6.2 | .316 | .969 | .031 | 2.4350 ex-5 |
| 4. 850-800 | 50 mb | 11.90° | 1.3° | 5.1 | .260 | .974 | .026 | 1.9302 ex-5 |
| 5. 800-740 | 60 mb | 7.15° | 1.8° | 5.7 | .349 | .966 | .034 | 2.3409 ex-5 |
| Inversion - 740 mb (2.45 km) | | | | | | | | |
| 6. 740-365 | 375 mb | -12.0° | -36.0° | 0.35 | .134 | .987 | .013 | 0.6429 ex-5 |

Depth = pressure depth of layer in millibars
$\bar{t}$ °C = mean temperature of layer in °C
$\bar{DP}$ C = mean dew point of layer in °C
$\bar{m}$ = mean mixing ratio of layer in grams/kilogram
u = water vapor in layer measured as precipitable centimeters ($gm/cm^2$)
$T_{wv,t}$ = transmissivity of layer due to water vapor
E = emissivity of layer
R↑ = layer radiance emitted to layer above in $W/cm^2/\mu m/sr$

Note: Values for $T_{wv,t}$, E, and R↑ apply to the spectral band of the sensing window only, 10.2-12.5 μm

The subscripts indicate the layer numbers. A calibration model which considers only water vapor modifications is then,

$$R_o = \frac{R_z - 1.3534\ ex{-}4}{.823} \tag{3.11}$$

Data Correction Factor

When the 149 PCM count is made to match the 27°C radiation temperature of Chesapeake Bay, no choice of transmissivity for the atmosphere will yield an up-radiance (R↑a) sufficiently large to match the radiance calculated from the atmospherics of the optical path. This is not simply a matter of incorrect choice of values because when water vapor alone is considered the up-radiance must be a function of the transmissivity of the column ($\varepsilon = 1 - T$) and the temperature of the active air layer. To satisfy this transmissivity-emissivity relationship, the temperature of the bay must be close to 21°C when the NASA-supplied radiances are used without a correction factor. No attempt is made here to designate whether this is an error in satellite measurements or is an artifact of the present gray-window atmospheric model. For the purposes of the calibration of satellite data to the surface, the correction factor can be considered simply a matching factor of convenience.

The factor is obtained by calculating an $R_o$ value that matches 27°C (300°K) using equation 3.6 and with the gray-window model in the form of equation 3.2, calculating a corresponding value for $R_z$, the radiance received aloft. The factor is then,

$$\frac{R_z \text{ (per model)}}{R_z \text{ (NASA)}} \tag{3.12}$$

and for the values of equation 3.11 above is 1.0698.

A case might be made that the presence of aerosols will reduce this apparent discrepancy. Aerosols are of sufficient size that they absorb and scatter about equally at the sensing wavelengths. Scattering helps attenuate or extinguish the surface signal and helps lower the transmissivity of the optical path but does not add to the emission. Only the absorption by the aerosols can equal emission. This would seem to permit a deviation from the assumption that emissivity of the optical path must be the perfect unity complement of the transmissivity. Such a deviation would reduce the discrepancy with satellite-measured values to about 2.5 percent. However, we must assume that atmospheric radiation being scattered by an aerosol in the optical path has about the same chance of being directed toward the sensor as radiation emitted by the aerosol, and thus for this project a perfect unity-complement relation between emissivity and transmissivity is assumed and an approximately 5 percent correction factor is used. This aspect of the calibration needs more study.

## Turbidity and other Active Air Components

Initial work with the gray-window calibration model considered water vapor as the only atmospheric element acting to modify the surface radiance. In both the preceding Barbados (BOMEX) and Baltimore experiments, the air was nearly free of aerosols and gaseous pollution, but over the test site on August 5, 1973, the boundary layer below 2.45 km appears to have been moderately turbid and in all probability contained gases now common to urban pollution when air is stagnant. Previous work in atmospheric optics (McClatchey and others, 1972) as well as an ongoing inquiry[2/] in the eastern

2/An inquiry into the transmissivity and radiance of typical combinations of moisture haze and pollution has developed from the S-192 calibration problem. It is being conducted by the University of California in conjunction with the USGS by Robert Pease of the Riverside campus. Measurements are made with a Barnes PRT-5 radiometer with a 10-12 μm bandpass in conjunction with rawinsonde soundings made by the Forest Fire Laboratory of the U.S. Forest Service. The inquiry is not complete.

Los Angeles Basin indicate that these elements in the scanner optical path both absorb and radiate between 10.2 and 12.5 μm and therefore must be considered in a calibration model, particularly for urban areas.

Since turbidity measurements per se are not routinely reported, other means have been employed to estimate the effects of aerosols on atmospheric optics in the thermal spectral regions from turbidity in the short-wave spectral bands. The best available indicator for the time of the Skylab pass is meteorological visibility ($V_m$) recorded on the daily weather map as 10 miles or 16.07 km for 7 a.m. EST, some 3 h before imaging. Meteorological visibility was a horizontal surface measurement, but subsequent visual observation (August 1, 1975), from an aircraft climbing from Dulles Airport through a similar boundary layer capped with subsiding air, indicates that turbidity density holds constant with elevation and may actually increase at the level of cloud formation where the relative humidity is high. The visibility range can then be considered typical for the whole depth of the boundary layer.

Meteorological visibility can be transformed to a visible or short-wave transmissivity ($T_{vis}$) by the following two steps:

$$\text{(a)}\ \sigma/\text{km} = 3.912/V_m, \qquad \text{(b)}\ T_{vis}/\text{km} = e^{\sigma} \tag{3.13}$$

with $\sigma$ the shortwave scattering coefficient. A more direct conversion is

$$T_{vis}/\text{km} = (.02)^{\,1/V_m} \tag{3.14}$$

The one-step method depends upon three facts: (1) That by definition, the value (0.02) is the minimum contrast the eye can detect when a dark object is outlined against the skyline, (2) that a contrast under these terms is interchangeable with transmissivity, and (3) that sequential transmissivities

in a path are multiplicative. The 16.07 km visibility range becomes a shortwave transmissivity (0.551 μm wavelength) of 0.784 by either method.

The second step is to convert transmissivities in the short wavelength realm to longwave or thermal infrared. There is little in the literature to use as guide for the process. On the basis of Mie theory as expressed in McClatchey and others (1972), the ratio of extinction coefficients between short and longwave is 0.082 which could also be expressed as $(\tau_{vis})^{.082}$. Extinction coefficients for a wavelength of 10.591 μm are plotted against meteorological visibilities in figure 3.3 with data supplied by McClatchey for visibility ranges of 5 and 23 km. This would give a turbidity extinction coefficient for the test site of 0.980/km, or 0.952 for the entire boundary layer, and approximately 0.990 for the 0.45 km (50 mb) layers. A calibration model which incorporates both water vapor and turbidity according to the above Mie theory is:

$$R_o = \frac{R_z - 1.712\ ex{-}4}{.7884} \tag{3.15}$$

The ratios of $TIR_{(10 - 12\ \mu m)}$ to shortwave extinction coefficients $(\gamma_{10 - 12}/\gamma_{vis})$ obtained by the ongoing inquiry at Riverside are on the order of values obtained by Mie theory only when turbidity consists of moisture haze or evaporating fog.[3/] When these conditions exist, ratios of 0.05 to 0.10 have been ascertained. Under conditions where smog pollutants are prevalent, the ratio rises rapidly and in certain cases has approached unity. In other words, the pollution is transparent and the visible extinction coefficient may be no higher than that at a wavelength of 11 μm. Mixtures of haze and gaseous pollution have had empirically derived $\gamma_{tir}/\gamma_{vis}$ ratios that typically range from 0.20 to 0.50 with 0.30 a value for moisture

[3/] For the visible wavelengths, σ can be considered equal to $\gamma^-$.



REPRODUCIBILITY OF THE ORIGINAL PAGE IS POOR

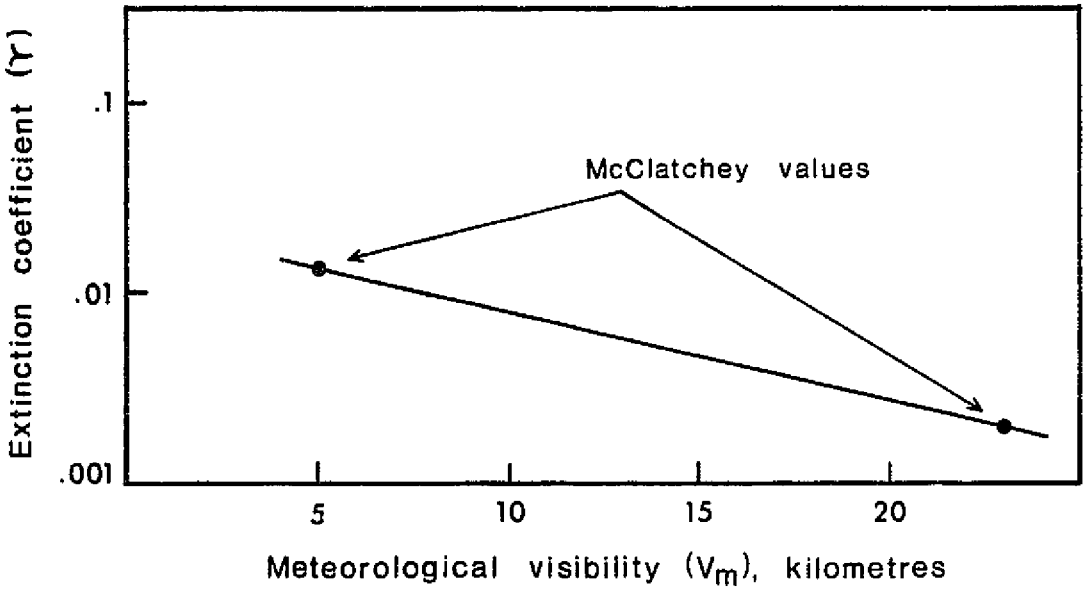


Figure 3.3--Extinction coefficients (γ) at a wavelength of 10.591 μm for various visibility ranges (McClatchey and others, 1972).

haze that contains a moderate amount of pollutants. This finding agrees with Yates and Taylor (1960) for summer measurements along horizontal paths over Chesapeake Bay for which a typical value is 0.30.

Spectrographic analysis of various common smog gases suggests a cause for the agreement. For the minor constituents, propylene and ethylene, there are absorption lines between 10 and 12 μm. Peroxyacetyl Nitrite (PAN), a persistent smog gas and one of the most prevalent where pollution is derived from automobile exhaust, has a strong absorption emission line that centers at 12.5 μm as well as several small bands between 10 and 12 μm which will affect the S-192 band 13 sensitivity (Scott and others, 1957) as shown on figure 3.4. For that portion of the spectrographic curve within the 10.2 - 12.5 μm spectral sensitivity of band 13 and for gas concentrations with which the curve was prepared, the transmission is only 0.74, which suggests a significant gray-window effect.

A meteorological visibility of 16.07 km has an extinction coefficient of $\gamma = 0.2434$. Changing this by a factor of 0.30 gives a $\gamma_{tir}$ of 0.0730/km and a $T_{tir} = 0.9295$/km or approximately 0.960 per 50-mb layer. Calculations for the atmospheric profile of the Washington-Baltimore test site are shown in table 3.6. These values, however, are for a vertical optical path. The slant path of the S-192 scanner is longer by a factor of 1.08, which increases somewhat the gray-window effect. Calibration models for both vertical and slant values, respectively, are

$$R_o = \frac{R_z - 2.4097\ ex\text{-}4}{.6925} \quad \text{and} \quad R_o = \frac{R_z - 2.4947\ ex\text{-}4}{.6835} \qquad (3.16)$$

[Vertical path] [Slant path]

Differences in calibration are very slight and either can be used for making the map of distribution of radiation temperatures. A procedure for converting

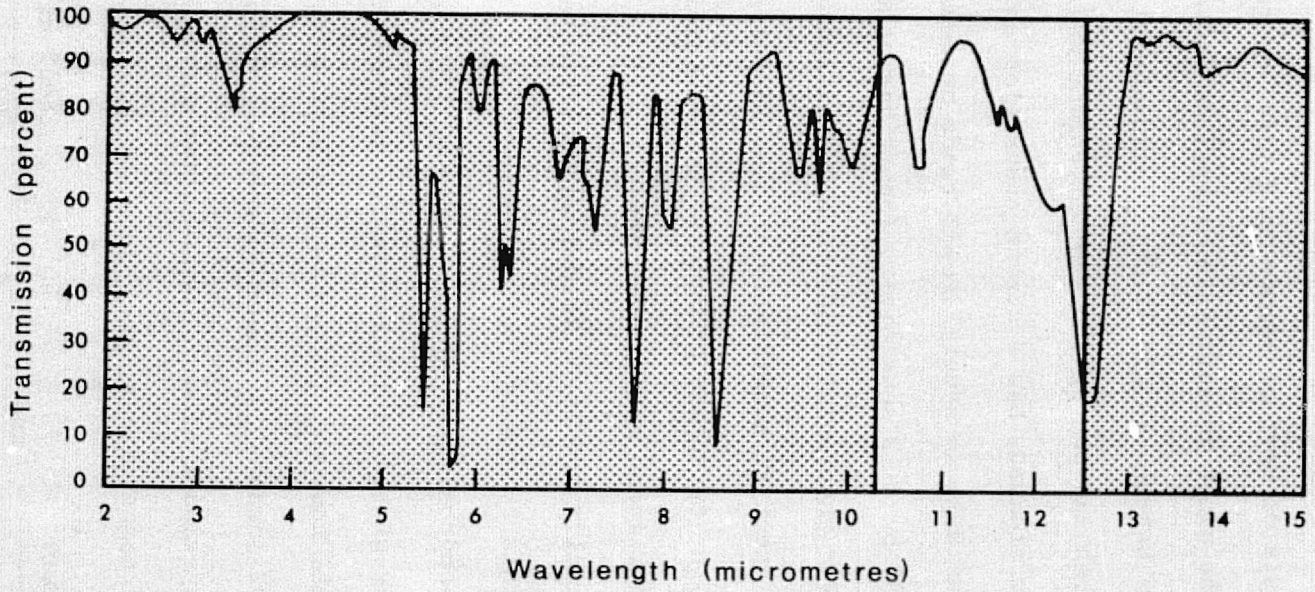


Figure 3.4--Absorption spectrum of Peroxyacetyl Nitrite (PAN). Nonshaded area is the 10.2 - 12.5 μm Sensing Window of Band 13 of the S-192 scanner (after Scott and others, 1957).

Table 3.6--Atmospheric profile for gray-window calibration of Skylab data including the effects of turbidity

| Layer | Depth | $\bar{t}^{o}C$ | $D\bar{P}^{o}C$ | $\bar{m}$ | u | $T_{wv,t}$ | E | R↑ |
|---|---|---|---|---|---|---|---|---|
| 1. 1000-950 | 50 mb | 21.64° | 12.64° | 9.3 | 0.474 | 0.954 | 0.046 | 3.9563 ex-5 |
| 0-.417km | .417km | | | | | .969 | .031 | 2.6659 ex-5 |
| | | | | | $T_1$ = | .924 | | 6.62218ex-5 |
| 2. 950-900 | 50 mb | 19.28° | 9.6° | 8.2 | .418 | .959 | .041 | 3.4057 ex-5 |
| -.85km | .441km | | | | | .966 | .034 | 2.8242 ex-5 |
| | | | | | $T_2$ = | .928 | | 6.2299 ex-5 |
| 3. 900-850 | 50 mb | 15.56° | 5.0° | 6.2 | .316 | .969 | .031 | 2.4350 ex-5 |
| -1.32km | .465km | | | | | .966 | .034 | 2.6706 ex-5 |
| | | | | | $T_3$ = | .936 | | 5.1056 ex-5 |
| 4. 850-800 | 50 mb | 11.9° | 1.3° | 5.1 | .260 | .974 | .026 | 1.9302 ex-5 |
| -1.82km | .479km | | | | | .963 | .036 | 2.6726 ex-5 |
| | | | | | $T_4$ = | .939 | | 4.6028 ex-5 |
| 5. 800-740 | 60 mb | 7.15° | 1.8° | 5.7 | .349 | .966 | .034 | 2.3409 ex-5 |
| -2.45 | .732km | | | | | .963 | .037 | 2.5474 ex-5 |
| | | | | | $T_5$ = | .931 | | 4.8883 ex-5 |
| Inversion - 740 mb, 2.45 km | | | | | | | | |
| 6. 740-365 | 375 mb | -12.0° | -36° | 0.35 | .134 | .987 | .013 | 0.6429 ex-5 |
| -8.21km | (no turbidity considered) | | | | $T_6$ | = .987 | | |

Notes: Definitions of terms in column headings are the same as those in table 3.5.

Layer transmissivities = $(T_{wv}T_t)$. $T_t$ = turbidity transmissivity.

$R\uparrow a = (((((R\uparrow_1 T_2) + R\uparrow_2) T_3 + R\uparrow_3) T_4 + R\uparrow_4) T_5 + R\uparrow_5) T_6 + R\uparrow_6$

$= 2.4097$ ex-4 $W/cm^2/\mu m/sr$

$T_{atmos} = 0.6925$

PCM counts to radiation temperatures in degrees celsius, shown in table 3.7, includes as a correction factor for tape-supplied radiances the value of 1.0514 (1.0513 for the vertical path)--a correction close to 5 percent.

To corroborate this choice of model in which gaseous pollution has a significant part, a day was chosen in the eastern Los Angeles Basin which was considered to have a mixture of moisture haze and pollution (oxidant 0.22 ppm) in the turbid marine layer that would be representative of the mixture in the boundary layer through which the Skylab scanner imaged. The day was July 24, 1975, and the site was close to the city of San Bernardino where measurements could be made in conjunction with rawinsonde soundings made by the Forest Fire Laboratory of the U.S. Forest Service. The chief difference between this and the Skylab site are: (1) The turbid layer over San Bernardino was shallower, 4,000 ft. (1.30 km) as opposed to 7,300 ft. (2.38 km); (2) the mean temperature of the significantly emitting air layer was higher, 295°K as opposed to 288°K; and (3) the visibility range at the sample site was less, 6 km as opposed to 16 km.

Downwelling longwave radiance was measured at the sample site with the Barnes PRT-5 radiometer. A radiance for a path from the zenith of 1.9522 ex-4 $W/cm^2/\mu m/sr$ was obtained. This was then corrected to adjust for differences with Skylab test site conditions. From the rawinsonde profile, radiance originating from clear air above the turbid layer was ascertained and subtracted from the instrument measurement after attenuating it with the approximate transmissivity of the turbid layer. The remaining radiance balance was 1.5625 ex-4. Adjustment then was made for the difference in thickness of the two turbid layers by multiplying the residual radiance by the factor 7300/4000 or 1.835, which increases the above value to 2.8576 ex-4. To adjust for the temperature difference, the fourth powers of the

Table 3.7--Procedure for converting PCM counts to T°C

1. Convert PCM count to $R_z$.

$$R_z = 1.0513\ (A_o + C\ A_1)$$

where: $A_o$ = 1.3114 ex-4
$A_1$ = 4.7650 ex-6
C = PCM count
1.0514 = correction/matching factor

2. Convert $R_z$ to $R_o$.

$$R_o = \frac{R_z - 2.4947\ e\ -4}{.6835}$$

3. Convert $R_o$ to T°K.

$$T^oK = \frac{1251.12}{\ln\left|\frac{.05921}{R_o}+1\right|}$$

4. Convert T°K to T°C.

$$T^oC = T^oK - 273$$

Terms: $R_z$ = radiance received at scanner in $W/cm^2/um/sr$

$R_o$ = corresponding radiance at surface in same units

two means were proportioned to achieve a factor to reduce the west coast radiance to that of the Skylab site. This factor, 0.9084, was combined with a correction for turbidity difference of -0.1658 ex-4 $W/cm^2/\mu m/sr$ to achieve a final value of comparison as follows:

$$((2.8516 \text{ ex-4}) - .1658 \text{ ex-4}) (.9084) = 2.4397 \text{ ex-4 } W/cm^2/\mu m/sr, \qquad (3.17)$$

a value close to that used for the model. To obtain the correction for differences in turbidity, extinction coefficients for 6 km and 16 km visibility ranges were taken from figure 3.3 and converted to transmissivities, which were then converted to emissivities by the relationship ($\varepsilon = 1 - T$). The emissivities were applied to air with a mean temperature of 295°K and the difference in radiance values was used for the correction.

Because of the uncertainty of the correction for gaseous pollution and turbidity, it is perhaps appropriate to note the differences the various calibration models make in radiation temperatures obtained. If all models are set by manipulation of the correction factor so that a PCM count of 149 will equal a temperature of 27°C, then values for a PCM count of 176, a representative high value, will be

Equation 3.11: water vapor only = 39.18°C

Equation 3.15: water vapor + turbidity = 40.14°C

Equation 3.16: water vapor + turbidity + pollutants = 41.30°C [slant path]

## The Necessity of the Gray-Window Calibration

If the scanner band 13 radiances, provided by the S-192 tapes, are converted directly to temperatures by the Planck Equation, Chesapeake Bay would have a temperature of 20°C and the warmest urban centers only 30°C. Even after increasing the radiances by the correction factor, the bay would

be 23.55°C, some 3.45°C too low, and the high temperature for the 176 PCM count would be only 33.7°C. Nor can a simple correction factor suffice because the values of $R_o$ and $R_z$ converge to a radiance where they are equal. For the gray-window model used, this radiance will be 7.8826 ex-4 $W/cm^2/\mu m/sr$, which corresponds at a wavelength of 11.5 μm to a radiation temperature of 288.79°K or 15.79°C. It will be noted on table 3.6 that this temperature is close to the mean temperature (15.56°C) of the middle layer of the boundary layer, a fact that confirms gray-window theory (Pease and others, 1970) and suggests that calibration can be plotted graphically when the mean temperature of the active layer and one target value for $R_z$ are known.

A Map of the Thermal State - Distribution of Radiation Temperatures

A map showing the distribution of surface radiation temperatures for the Skylab flightpath over the Washington-Baltimore area on August 5, 1973, is shown in figure 3.6, following the location reference map, figure 3.5. In most respects it is self explanatory. The two urban centers show as distinct heat islands with generalized values some 10°C warmer than surrounding nonurban lands. Cause of the heat islands is to be found in the discussion of the simulation experiment. As has been noted, the map represents a generalization of pixels by using a 10 x 10 block filter as a smoothing technique. The value of each cell in the grid-cell plot is the average of the 100 pixels which make up the block.

A Map of Terrestrial Albedos

The method for making a map of terrestrial surface albedos (figure 3.7) is as follows. Since no gray-window model has been f. mulated for reflected light, a simple target calibration of the scanner has been used. One target

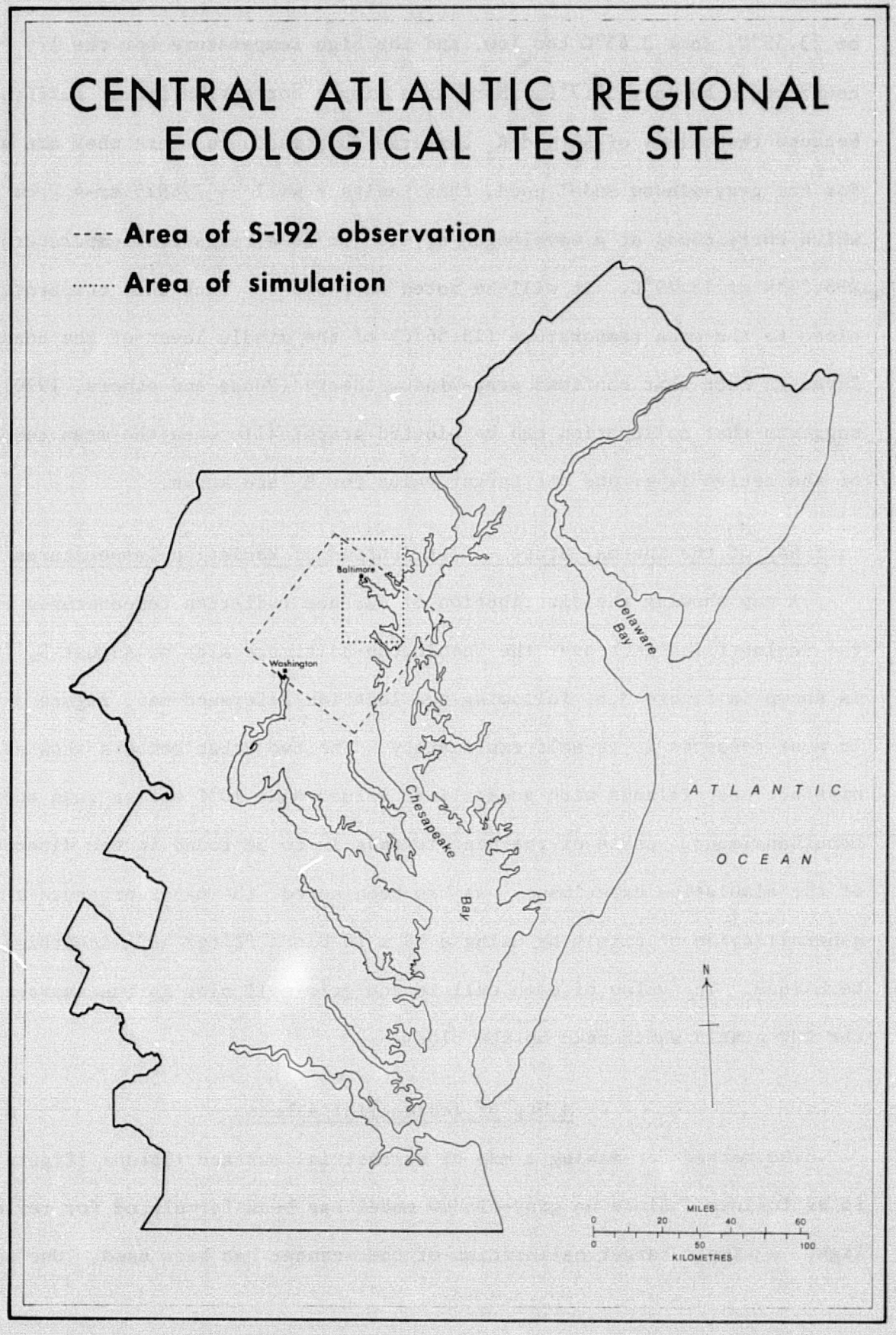


Figure 3.5--Location of mapped areas, thermal mapping experiment

Figure 3.6--Map showing distribution of surface radiation temperatures, Washington-Baltimore area, derived from band 13, S-192 (SDO channel 21), August 5, 1973. The map is made in a grid-cell form to facilitate combination with albedo map to generate a map of net radiation (not included in this report). Each cell represents an average of 100 pixels of line-straightened data (10.2 - 12.5 μm). The GEOPLOT program used for the grid-cell plot is the product of Ray Postma of the Environmental Systems Research Institute of Redlands, California. Unshaded cells near Baltimore and in the southern corner of the map are due to clouds, the temperatures of which are below 25°C.

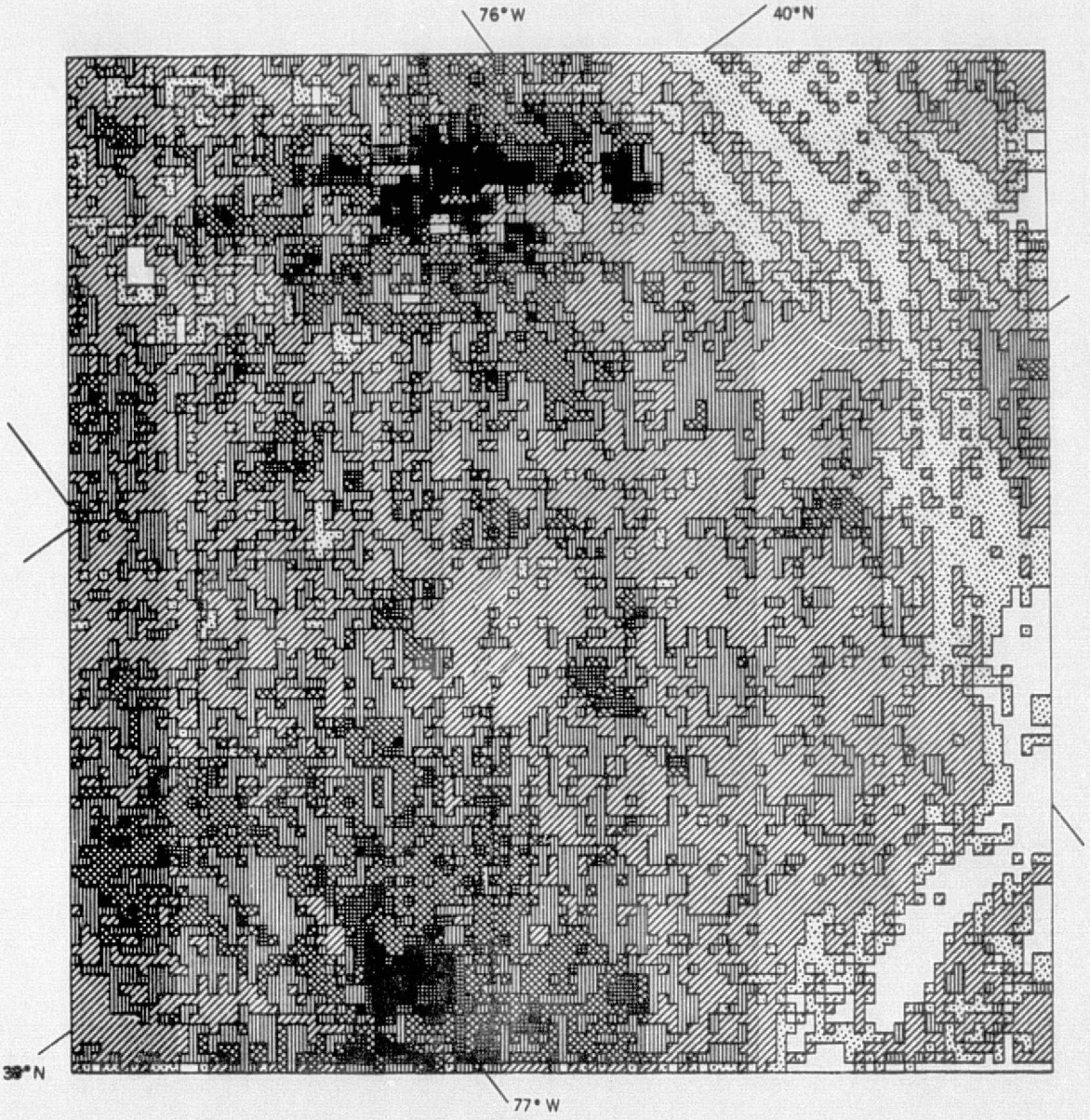


Figure 3.6

REPRODUCIBILITY OF THE
ORIGINAL PAGE IS POOR

Figure 3.7--Distribution of generalized surface albedos for the Washington-Baltimore area, derived from band 6, S-192 (SDO channel 7), August 5, 1973. Darkest grid-cell tones have the lowest albedos. Cell values are the average of 100 pixel blocks (10 pixels on 10 adjacent lines). Unshaded cells (albedos above .25) are clouds. Several small cumulus clouds occur west of Baltimore and are accompanied by low value cells that represent cloud shadows. This emphasizes the need for clear weather conditions when making energy-related observations from space. Map is made by the GEOPLOT program, which is the product of Ray Postma of the Environmental Systems Research Institute of Redlands, California.

Figure 3.7

REPRODUCIBILITY OF THE
ORIGINAL PAGE IS POOR

is Chesapeake Bay, which is assumed to have the 2 to 3 percent albedo typical of oceanic saltwater. A general lack of turbidity in the bay water is indicated by the very dark tone of the bay in the near-infrared bands as shown by the preview imagery made from the original tapes. Because the southern end of the bay appears lighter due to high cirrus clouds, a compromise value of 2.5 percent for the center of the northern end of the bay is therefore assumed. A high albedo target is a vegetated area on the image, grass but not woodland. Experience with the pre-Skylab Baltimore mission indicates a suitable value for this type of vegetated area to be about 22 percent, a value which, except for clouds, is representative of the brightest large targets on the image. An intermediate check is the average value for the Baltimore central business district where the above previous work indicates 8 to 10 percent to be rational values. Because PCM counts represent radiances, they are assumed to have a linear relationship for surface reflection of solar energy between target values and, therefore, a simple equation can be established that converts PCM counts directly to albedo values without computing actual reflected radiances. This bypasses the very knotty problem of trying to separate the attenuated reflection of the surface from the upscatter of the atmosphere, a procedure which at this state-of-the-art might yield less accurate results.

Either two spectral bands can be used as samples to ascertain values, one above and one below the rise in chlorophyll reflectance that centers at 0.725 μm, or a single band that straddles this rise can suffice. Two-band use requires calibration to the target in each discrete spectral interval. It also requires that a combination of reflectances be derived according to a weighting of 0.60 for the visual band to 0.40 in the near infrared. For this procedure, bands 4 and 8 are recommended.

The single band approach involves the use of band 6 (SDO channel 7 of tape output), which, although narrow, straddles the rise of vegetation reflectance quite nicely. Since the shortwave reflectance curves for most targets other than plants show relatively monotonic change, the albedo indicated by this band for plant targets is most critical. The use of band 6 results in an albedo calculation for chlorophyll of 0.22, which is the generally accepted value. The albedo map, therefore, was made from information collected in spectral band 6 (0.68 - 0.76 μm). The procedure used to construct the albedo map (figure 3.7) is condensed in table 3.8.

## Commentary about the Mapping Experiment

The mapping experiment provides insight into the distribution of radiation-related phenomena over an urbanized region in the Atlantic seaboard on one typical type of summer day. Previously hypothesized urban heat islands stand out well, and the relative coolness of nonurban lands is documented. Thermal patterns and absolute values therein are achieved that can be used both as inputs and tests of the simulation experiment. The project, therefore, can be considered more than just a simple determination of the utility of satellite-acquired data for making maps showing surface energy exchange phenomena. A significant amount of information is provided that has broader application than the technological problems of the experiment itself.

The above initial statement suggests, however, the degree to which the project is experimental. Although the technological problems have been surmounted with considerable success, data were for a single synoptic instance, which limits both broad use of results as well as the opportunity to further perfect this method of climatic map production. It is highly desirable,



ORIGINAL PAGE IS POOR

Table 3.8--Procedure for constructing albedo map

1. Create file of channel 7 (spectral band 6, 0.68-0.76 m)

2. Block filter this file into 10 x 10 blocks (10 lines of 10 pixels each) each block with an average PCM count value. This will create a matrix of values for the portion of the flightpath of concern of about 100 elements long and 130 elements wide.

3. Make histogram of block-filtered values by PCM counts. Use whole number counts only.

   This should be a pronounced bimodal distribution, a low set of values for Chesapeake Bay and a high set of values for land elements.

4. Select a PCM count in the lower mode to equal a 0.025 albedo value.

5. Select the highest significant value in the histogram (PCM count) to match a vegetation albedo of 0.22.

6. Write an equation for a linear curve that joins these values in a form that x(PCM count) = a (albedo value).

7. a. Create a plot tape to the centroid values of 10 x 10 blocks and plot isoline map. A problem here is that a strong gradient will occur along the edge of Chesapeake Bay due to the bimodal distribution of PCM count values. Or--

   b. Create a line-printed gray map with ordinal ranks for gray values which are not equal intervals. Or--

   c. Make an isoline plot with skewed intervals (non-linear) which show detail on the land but not on Chesapeake Bay. Or--

   d. Make a dasymetric thematic map cartographically that shows different albedo areas without intervaling or gradients.

then, to continue this line of inquiry with other satellites, or perhaps high-flying aircraft, which carry calibrated scanners with a thermal infrared capability such as the forthcoming Heat Capacity Mapping Mission (HCMM). Data obtained upon a regular schedule will permit analysis of the dynamics of surface energy exchanges and will give this area of climatic inquiry the element of spatial variability that has been lacking in past strictly surface investigations. Regularly acquired data will change what has been primarily a technological experiment into a source of data for the discipline, land use climatology.

The foregoing does not imply that there is no further need for technological advance in producing the maps. Prior to the experiment, most thought relating to the calibration model had been simply theory. Work with Skylab products has successfully applied the theory but at the same time has given rise to new questions to be answered. The ongoing inquiry at the University of California, Riverside attempts to assess more explicitly the role of gaseous pollution in the gray-window model. Better means than meteorological visibility are being explored to determine visual transmissivity of the atmosphere. For example, measurement of the attenuation of the solar beam may be useful. The solar beam can be measured with an occulted pyranometer (global less diffuse incoming solar radiation) and this value is then divided by a theoretically calculated beam that includes water vapor attenuation.[4/] Such a measurement should be made when the Sun has a relatively high altitude, but the problem of translating the visual transmissivity to its thermal infrared counterpart still remains.

---

[4/] A tentative suggested equation for the solar beam without turbidity is

$$\text{Beam } (Q) = [1.841(e^{-.066p \text{ s } Z}) - .21(1 - e^{-.23u \text{ s } Z}) - .1] \cos Z$$

where p is the pressure height of the observer in mb/1,000, Z is the zenith angle of the Sun, and u is the water vapor in a vertical or zenith profile in precipitable cm. The equation assumes pyranometric measurements are made on a horizontal plane. All radiation values are in 1 ly/min.

Another continuing investigation involves the use of a longwave radiometer with a sensitivity close to that of the thermal channel of the scanner to measure atmospheric radiance, and concomitantly transmissivity, as a ground truth activity at the time of a satellite or aircraft imaging flight. Such a measurement would combine all of the gray-window elements into one value with no need to treat them separately. Nor would an atmospheric sounding be necessary. Most radiometers are not sufficiently sensitive to measure sky temperatures in a vertical optical path but can be tilted until the slant path achieves a valid reading. A vertical value can be converted from the slant reading by using the cosine of the zenith angle of the slant path as a multiplicative factor.

Some comments are in order regarding the utility of the S-192 data as supplied by NASA. All data, both ancillary and PCM count for a single scan line, are in discrete blocks. This fact requires that the entire tape set be read to secure information for a single band, a rather expensive computer operation. Of course, all channels can be placed in separate files with this one reading. But this reading may well involve each user with up to $2,000 worth of computer time for the 4,000 scan lines contained in our data set. It would have been most helpful if NASA had separated the PCM counts into separate files that would have circumvented the necessity of each user making this initial reading expenditure.

An error in mapping results that must be considered is the occurrence of clouds over the site. Clouds show as relatively cool areas on the map of radiation temperatures and as very high albedo areas on the surface albedo map. Only because their values fall outside the spectrum of surface values can the existence of the clouds be recognized on the maps. Clouds therefore

produce areas of erroneous values, the existence of which must be recognized to achieve accurate interpretation of results. Cloud shadows on the surface also disrupt true energy-budget values.

On the two maps displayed in this project (figures 3.6 and 3.7), clouds covered a minor area, but small cumulus humilus clouds did obscure a portion of western Baltimore. Further, a light, high cloud veil in the southern corner of the image gave values somewhat too high for the albedo of Chesapeake Bay and tended to reduce radiation temperatures. Cloud cover is a constraint on the use of satellites as platforms for energy-budget studies that use outputs from electro-optical scanners.

The quality of band 13 data appears only slightly better than marginal for thermal mapping. The use of the 10 x 10 block filter has helped suppress unwanted system noise and made the mapping possible. The quality of the shortwave channels appears better, and they contain better defined information. How well data from multiple channels can be combined to make maps as sophisticated as net radiation still remains to be tested.

A decided commendation for the S-192 scanner system, however, relates to its conical scan pattern with an optical path of constant length. As a path lengthens, the gray-window effect becomes greater. Thus data from a straight scan line instrument should be treated with a model that changes as the optical path swings away from nadir. For space, where the swing is only in the order of 15 degress, the error would be slight, but for an airborne instrument the dampening of the signal from a longer path is readily discernible by a darkening toward image edges.

In summary, use of S-192 outputs has brought major advances in calibrating scanner data with minimal ground correlation, has proven the feasibility of

using satellite data for making maps of surface energy exchange phenomena on a regional scale, and has pointed the way toward desirable future inquiries into the impact of land use upon climate.

## THE SIMULATION EXPERIMENT

The basic premise underlying land use-based surface energy balance modeling is that each land use type has a particular mix of surface cover and building configuration associated with it. Thus, given a land use map with an appropriate classification scheme, it should be possible to use the distribution of land use classes as surrogate for information regarding the distribution of significant surface cover characteristics important in energy balance modeling. If the available land use breakdowns are not appropriate for the distinction of these terms, then other sources must be consulted or further land use subdivision must be made.

### Modeling the Spatial Pattern

For the purpose of modeling the temperature field of an urban area, a gridded land use information system is employed in this study. Other subdivisions such as census tracts or zoning divisions might be used for the areal breakdowns. A gridded array of information, however, provides a uniform density of sampled land use over the area as well as a convenient arrangement of input data for the model. The collection of information related to land use and other surface characteristics on a grid-square basis has been employed or discussed by several researchers in connection with urban climate applications. Myrup and Morgan (1972) have conducted

a detailed survey of surface characteristics of the Sacramento, California, metropolitan area using a gridded system. Marotz and Coiner (1973) have explored the nature of the distribution and spatial association of types of surface cover in various Kansas cities. Bornstein (1968) cites a survey of anthropogenic heat production carried out on a grid-square basis in the New York area.

The general approach taken in the modeling of the urban temperature field is based on the simulation of a set of temperatures associated with surface characteristics representative of particular land uses. To obtain an average temperature for a grid cell under a specified set of synoptic conditions, the land use associated temperatures are weighted according to the frequency of the occurrence of each of the land use types within that cell. Thus, within cell (i,j) the mean temperature $T_{i,j}$ is given by

$$T_{i,j} = \left(\sum_{k=1}^{m} f_{ijk} \; T_k\right) \; /n \qquad (3.18)$$

where k denotes land use type with a total of m land uses being considered, $T_k$ denotes the simulated temperature associated with land use type k, $f_{ijk}$ represents the frequency of land use type k within cell (i,j), and n is equal to the number of points sampled from each grid cell.

The rationale behind this method of treatment is that each land use type, with its characteristic mix of surface properties, generates an energy expenditure regime unique to that type. The average temperature of an area is the spatial average of these land use-generated thermal regimes.

The alternative is represented by the work of Myrup and Morgan (1972) where the individual surface characteristics are averaged over grid cells as if the simulation were to be based on averaged surface characteristics.

This alternative assumes a linearity in the behavior of the parameters within the model, a quality not discussed by Myrup and Morgan. In addition, a significantly larger amount of computational time is required using the Myrup and Morgan method because each grid cell must be modeled as a unique case.

Scale considerations

The urban climate can be examined on a variety of scales. On one hand, the microclimate of a particular blockfront within a city may be of interest as in the case of architectural considerations. At this scale thermal radiation, the effects of shadows, the different thermal properties of the street and wall faces and other phenomena may be examined in a relatively precise manner. On the other hand, when the simulation procedure is applied to an entire urban area, which contains thousands of such smaller scale environments, gathering and treating the surface characteristics in such detail becomes infeasible.

Since this application is dealing with a rather large area, block-to-block variations in temperature cannot realistically be considered. Indeed, the land use-based model is not intended to be applied to attempts at this scale. It is the mesoscale aspect of temperature variation over the urban area that is being modeled. A scale must be chosen to complement the degree of detail in the land use classification system being employed.

Sources of Land Use Information

Land use information for Baltimore and other cities exists in a variety of scales and for a variety of purposes. Probably the most detailed information regarding land use may be obtained from maps produced by the Sanborn Map Company. Intended for insurance purposes, these maps provide actual building

dimension. Scales are typically on the order of 1:2,400 or 1:1,200. Sanborn maps are published for most major cities. Their purpose is not to describe land use per se, but to describe only the particular building configurations which exist as the expression of the land use.

Next in line are the various land use maps used by local governments for zoning and planning purposes. Often, these maps utilize scales and classifications that are unique to a particular political jurisdiction. Typically, the classification scheme, though it may contain many categories, does not differentiate among characteristics significant for microclimatological purposes. Occasionally, an entire metropolitan area encompassing several counties will have comprehensive land use information mapped. Rarely does this happen when more than one State is involved in an urban area.

Finally, in connection with increased interest in statewide and national land use planning, attempts have been made to develop land use classification schemes suitable for use with remotely sensed data. An example of such an attempt is the land use classification system of Anderson and others (1972).

This classification has a hierarchical structure with two levels specified. An earlier version of this classification system was used for the basic land use mapping in the CARETS investigation. The CARETS classification is presented in table 3.9 (see also table 2.2). Since no single classification system will suit the needs of all potential users, it is suggested that further breakdowns in the form of third and fourth levels be developed by the user. Nicholas (1974) has made an effort to develop a third level for use in urban climatological applications.

Land use maps using modifications of the basic two-level system have been published for several large regional test sites in various parts of

Table 3.9--USGS land use classification system as presented in Circular 671

LAND USE CLASSIFICATION SYSTEM FOR USE
WITH REMOTELY SENSED DATA

| Level I | | Level II | |
|---|---|---|---|
| 01. | Urban and Built-up Land | 01. | Residential |
| | | 02. | Commercial and Services |
| | | 03. | Industrial |
| | | 04. | Extractive |
| | | 05. | Transportation, Communications, and Utilities |
| | | 06. | Institutional |
| | | 07. | Strip and Cluster Settlement |
| | | 08. | Mixed |
| | | 09. | Open and Other |
| 02. | Agricultural Land | 01. | Cropland and Pasture |
| | | 02. | Orchards, Groves, Bush Fruits, Vineyards, and Horticultural Areas |
| | | 03. | Feeding Operations |
| | | 04. | Other |
| 03. | Rangeland | 01. | Grass |
| | | 02. | Savannas (Palmetto Prairies) |
| | | 03. | Chaparral |
| | | 04. | Desert Shrub |
| 04. | Forest Land | 01. | Deciduous |
| | | 02. | Evergreen (Coniferous and Other) |
| | | 03. | Mixed |
| 05. | Water | 01. | Streams and Waterways |
| | | 02. | Lakes |
| | | 03. | Reservoirs |
| | | 04. | Bays and Estuaries |
| | | 05. | Other |
| 06. | Nonforested Wetland | 01. | Vegetated |
| | | 02. | Bare |
| 07. | Barren Land | 01. | Salt Flats |
| | | 02. | Beaches |
| | | 03. | Sand other than Beaches |
| | | 04. | Bare Exposed Rock |
| | | 05. | Other |
| 08. | Tundra | 01. | Tundra |
| 09. | Permanent Snow and Ice Fields | 01. | Permanent Snow and Ice Fields |

Source: Anderson and others, 1972.

the country. In addition, land use of the metropolitan area of Washington has been mapped at a scale of 1:100,000, and comparable classification systems and mapping scales will be used in other metropolitan areas. This classification is especially well suited for the determination of surface characteristics because land cover is actually used to distinguish land use types as mapped. For these reasons the USGS classification scheme is used as a basis for obtaining surface characteristics for input into the simulation model.

## Land Use Data Collection

The USGS land use map of the Baltimore area is available at a scale of 1:100,000. The map covers 2,500 $km^2$ and includes most of the Baltimore SMSA and the entire Census Bureau delineated metropolitan area. The location of the mapped area is shown in figure 3.5. The photomosaic base for the land use map is gridded into 1-$km^2$ cells, using the Universal Transverse Mercator system. Data could thus be collected conveniently in 1-$km^2$ units.

The land use polygon sizes vary considerably, with the smallest mapped units representing approximately 0.04 $km^2$. A portion of the map is shown in figure 3.8. Ideally, planimetered data or tabulations from digital maps should be used to obtain exact percentages of particular land use types within each sampling unit. These tabulations were not available at the time needed for this study. Therefore, a sampling scheme was used in collecting and aggregating land use information from the map. After testing three grid size areas of 1 $km^2$, 9 $km^2$, and 25 $km^2$ and two sampling densities of eight points per $km^2$ and four points per $km^2$ respectively, investigators found that the smallest grid size (1 $km^2$) and the sampling density of eight points per $km^2$ offered the best degree of spatial resolution.

Figure 3.8--Land use map of study area for simulation of surface temperatures.

Source: Central Atlantic Regional Ecological Test Site project, U.S. Geological Survey, land use categories derived from NASA high-altitude aerial photography, October, 1970. (See table 3.9 for category identification key.)

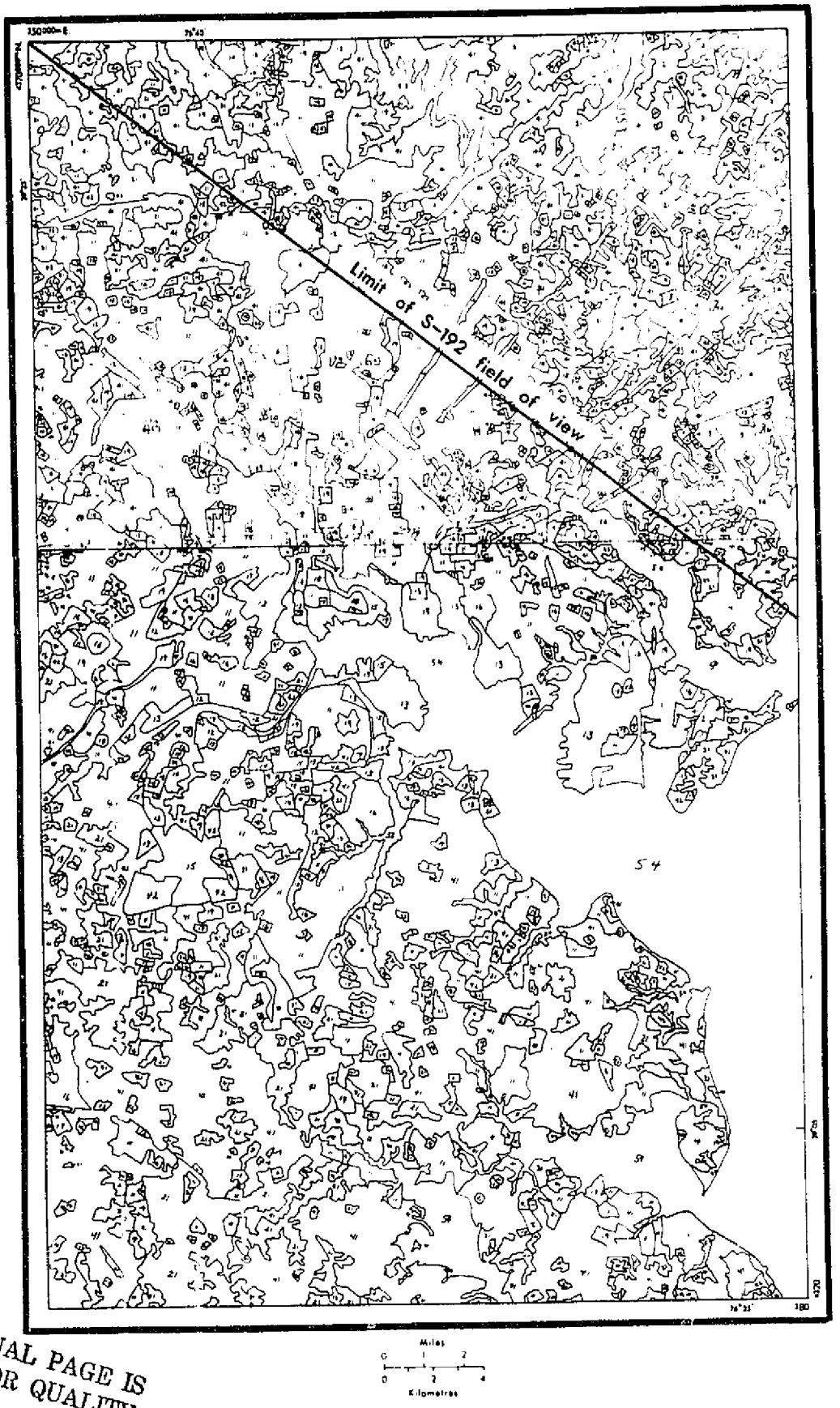


ORIGINAL PAGE IS
OF POOR QUALITY

Figure 3.8

The Universal Transverse Mercator grid system was used as the basis for the alignment of the sampled points. For each of the 1-$km^2$ cells an aligned sample was taken. The usual disadvantages cited with this method (Berry and Baker, 1968) are not applicable here. For example, the scale being dealt with is too coarse to pick up block-to-block periodicities in land use. In addition, land use tends to cluster and an unaligned sample might tend to accentuate a particular land use type.

## Surface Characteristics

The surface characteristics used as input for the energy balance model are: 1) Building configuration, which provides information related to the surface roughness length and to solar and thermal radiation calculations; 2) surface roughness for vegetation; 3) the wet fraction; 4) the substrate thermal diffusivity and conductivity; 5) surface albedo; and 6) surface emissivity. A discussion of the parameterization of each of these follows.

### Building Configuration

For land use classes that contain structures (i.e., industrial, commercial, and residential) a knowledge of building dimensions and spacing is important. From these values the surface roughness length ($Z_o$) and the silhouette ratio may be calculated. These values are shown in table 3.10.

In terms of surface roughness, the important surface characteristics are building density and height. Nicholas (1974) has developed a third level for the USGS land use classification system which distinguishes land use types based on these characteristics. A one-to-one correspondence in land use types between his three-level classification and the modified USGS system used for the Baltimore area does not exist. However, there is

Table 3.10--Values of surface characteristics used as input for each land use category

| | Albedo (%) | Surface roughness ($Z_0$) | Wet fraction (%) | Silhouette ratio |
|---|---|---|---|---|
| Residential | | | | |
| Low-density | 18 | 73 | 60 | 0.13 |
| High-density | 14 | 151 | 5 | .19 |
| Commercial | 15 | 78 | 5 | .02 |
| Industrial | 15 | 90 | 10 | .10 |
| Extractive | 12 | 3 | 10 | .01 |
| Transportation | 15 | 6 | 15 | .02 |
| Open | 22 | 80 | 90 | .71 |
| Cropland | 20 | 25 | 95 | .01 |
| Orchard | 20 | 115 | 90 | .25 |
| Forest | | | | |
| Heavy (40% & over) | 22 | 127 | 95 | .25 |
| Light (10-40%) | 22 | 25 | 90 | .25 |
| Nonforested Wetland | 18 | 10 | 95 | .05 |
| Beaches | 10 | 2 | 15 | 0 |

REPRODUCIBILITY OF
ORIGINAL PAGE IS POOR

close agreement, and typical land use associated values of surface roughness found by Nicholas have been used as a check for those derived from building dimensions and spacing shown above.

Surface Roughness for Vegetation

For areas dominated by vegetation, such as woodland and agricultural areas, the following formula developed by Kung (1961) is applied:

$$\log Z_o = -1.24 + 1.19 \log h, \tag{3.19}$$

where h = height of vegetation. To distinguish between totally wooded area and open park-like situations, a weighting scheme as used by Nicholas (1974) was employed. The result is an equation

$$\log Z_o = (-1.24 + 1.19 \log h) \cdot K \tag{3.20}$$

where K is a coefficient equal to the proportion of the surface which is tree covered.

Surface Wet Fraction

Values of surface wet fraction are based upon samples taken from high-altitude aircraft imagery of the study area. A detailed study has not been undertaken. Land use associated values are shown in table 3.11.

Substrate Thermal Diffusivity and Conductivity

Soil heat capacity is held constant at a value of 0.5 cal $cm^{-3}$ $°C^{-1}$ and thermal diffusivity is made a function of the wet fraction as given by

$$K = [(WF)\ (.005) + (1\text{-}WF)\ (.020)]\ cm^2\ s^{-1} \tag{3.21}$$

Typical diffusivity values for soil are 0.005 $cm^2$ $s^{-1}$ and for artificial surfaces 0.020 $cm^2$ $s^{-1}$.

Surface Albedo

Studies of the albedos of urban surfaces indicate that there is a variation in this term over the city. Variations may be due not only to

Table 3.11--Land use associated values of surface wet fraction

| Land use | Wet fraction |
|---|---|
| Industrial | 0.10 |
| Extractive Industry | .10 |
| Transportation | .15 |
| Commerical | .05 |
| Multi-Family Residential (high-density) | .05 |
| Single-Family Residential (low-density) | .60 |
| Park (Open and Woodland) | .90 |
| Wooded | .95 |
| Agricultural | .95 |
| Water | 1.00 |

surface materials but also to building geometry. However, the effects of building geometry could work either to increase or decrease the effective albedo. Values of urban albedo found in aircraft studies of the spatial character of this term are generally in the range of 0.11 to 0.25 (Kung and others, 1964; Barry and Chambers, 1966). Values taken at particular points at the surface typically exhibit less range and are centered around 0.15 (e.g., Bach and Patterson, 1969). Since the effects of building geometry are being considered in the model in connection with the shadow ratio and vertical wall calculations, a single value of albedo equal to 0.15 was used in the model for all built-up areas. For forested and agricultural areas, values of 0.20 (Sellers, 1965) were used.

Emissivity

An emissivity value of 0.9 is assumed for all surfaces. This is close to values cited by Sellers (1965) for almost all natural and manmade surfaces. Inaccuracies may arise in areas with certain metal surfaces where actual emissivity may be considerably less.

## Data Input into Simulated Surface Radiant Temperature Map

Table 3.12 shows the meteorological inputs on August 5, 1973, and table 3.10 displays the geographical surface characteristics used in the simulation experiment that are associated with each land use.

A subdivision of residential land use into low density and high density was made to portray urban conditions more realistically. High-density residential was defined as multi-family dwellings. Institutional land use temperature was obtained by weighting commercial and open land use category

Table 3.12--Meteorological conditions for August 5, 1973

| | |
|---|---|
| Mean Station Pressure | 1015.0 mb |
| Precipitable Water | 40 mm |
| Dust Content | 3 particles/cc |
| Mean Air Temperature | 24.0°C |
| Mean Air Relative Humidity | 61% |
| Mean Wind Velocity | 270 cm/s |

temperatures on a 1/3 and 2/3 basis respectively. Open land use was considered as park area, and strip and mixed land use were consolidated into commercial land use for the simulation experiment.

Table 3.13 lists temperatures produced by the simulation model as a function of land use. The simulated temperature map is shown in figure 3.9.

## COMPARISON OF SIMULATED AND OBSERVED SURFACE TEMPERATURES

Both the simulated and observed maps (figures 3.9 and 3.10) show the general heat island structure within the city of Baltimore and some of the satellite heat islands of outlying residential and commercial areas. Both maps show the same generalized patterns of temperature distribution. Differences occur, however, in shapes of individual features. The shapes on the observed map are much more complex and intricate in pattern than those on the simulated map. Furthermore, in the simulated map, temperatures in the higher values are as much as 6° to 8°C lower than those observed in the center of the city heat island. In the outlying agricultural and forest areas the differences in temperature between observed and simulated maps are not so great, usually on the order of 3° to 4°C.

We feel that the general approach of combining simulated and observed temperatures in a single effort has sufficient merit to be utilized for future remote sensing applications. Although absolute values are consistently low, the range of values is approximately correct, and spatial patterns of observed and simulated temperatures are sufficiently alike to merit further refinement of the techniques. First we would want to investigate the details of where the simulated map failed to provide the detail and/or accuracy of

Table 3.13--Simulated surface temperatures of each land use

| | Temperature °C |
|---|---|
| Residential | |
| Low-density | 24.9 |
| High-density | 30.9 |
| Commercial | 30.8 |
| Industrial | 30.1 |
| Extractive | 35.0 |
| Transportation and Utilities | 36.9 |
| Institutional | 27.2 |
| Strip | 30.8 |
| Mixed | 30.8 |
| Open | 25.4 |
| Cropland | 24.2 |
| Orchard | 22.7 |
| Forest | |
| Heavy (40% & over) | 22.3 |
| Light (10-40%) | 26.6 |
| Water | 24.0 |
| Nonforested Wetlands | 26.3 |
| Beaches & Sand | 34.9 |

Figure 3.9--Map of surface radiation temperatures for the Baltimore area made by simulation procedure described in the text. Area shown corresponds to that of figure 3.8.

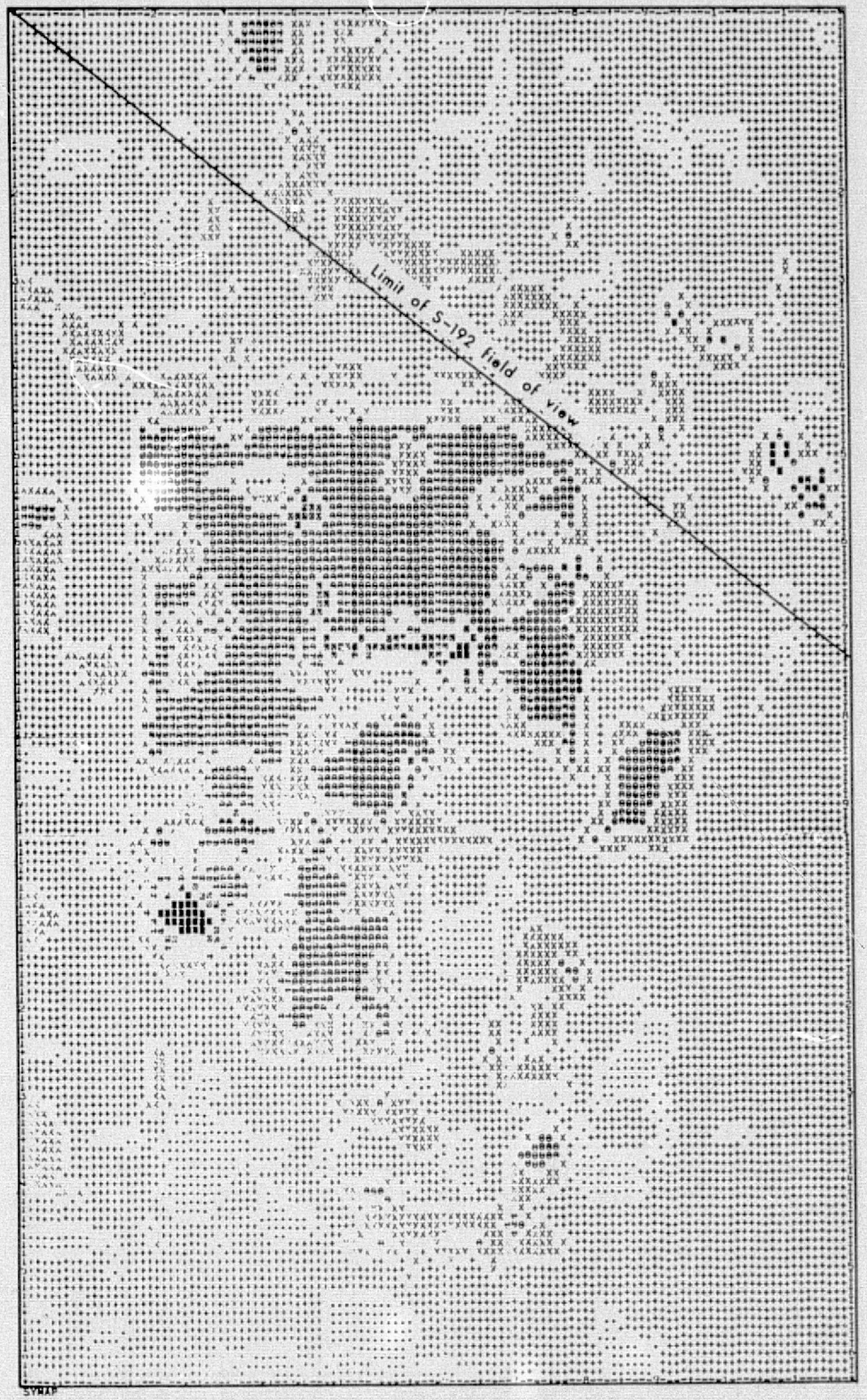


Figure 3.9



REPRODUCIBILITY OF THE
ORIGINAL PAGE IS POOR

Figure 3.10--Map of surface radiation temperatures for the Baltimore area made from Skylab S-192 data, band 13, as calibrated by procedure described in text. Area shown corresponds to that of figure 3.8.

ORIGINAL PAGE IS
OF POOR QUALITY

Figure 3.10

the observed map. Previous work with temperature simulations using the Outcalt model had given similar conservative results, i.e., simulations of temperatures were consistently lower than temperatures observed either in the field or on scanner data from the aircraft mission flown over Baltimore in 1972. Further improvements in the model could be achieved by including some additional function that would modify the height of the damping depth through a 24-h period in a more realistic simulation of conditions in the atmosphere. The damping depth produced gradients in temperature which are too steep during the daylight hours and cause convection or removal of too much sensible energy from the surface.

In addition, the input from the land use and land cover map constructed from the USGS remote sensing classification system appears to lack sufficient detail in the phenomena that affect surface temperature. The land use classes as mapped generalize features of the terrain, including a variety of phenomena such as houses, streets, lawns, forests, and fields. Such categories may not be a realistic enough representation of the distribution of features that actually affect the surface temperature regime or the surface energy-exchange phenomena. Therefore, we suggest that further research be conducted in refining and making more detailed a classification for land use and land cover to be used for urban climatological purposes, based upon the results obtained in this comparison. For example, we suggest the need for more detailed sampling within categories that have heterogeneous features but are classified as a single use category (such as urban residential). In general we feel that more attention needs to be paid to the types of spatial sampling and smoothing operations that are performed on the data. In the future we would like to be able to run quantitative comparisons of observed and simulated maps using, for example, such techniques as two-dimensional spectral analysis (Rayner, 1971).

This project's research, requiring quantitative manipulations and correlations of map data, would be greatly facilitated if the remote sensor data supplied by NASA were in a more readily accessible and readable form than were the S-192 tapes. The format presented required extensive reading and reformatting operations before the investigators were able to begin the analysis. Therefore, a disproportionately large amount of effort went into preliminary processing and mechanical separation of the signals representing a block of terrain on the ground. The investigators should have been able to devote a larger effort to the actual analysis, using the results in conjunction with the climatological model governing data collection and guiding the simulation effort which was run in parallel with the remote sensing effort.

We feel that there was sufficient similarity in the two maps and that the overall approach is sound and needs only the refining of data processing, sampling, and manipulation capabilities. These capabilities should be carried much further in future research than the investigators were able to do in this project. We recommend further efforts at refining these procedures for handling the remote sensor data from multispectral scanners in future spacecraft as well as for improving the handling and manipulation of processes in the simulation model. Work should be directed toward the improvement of the replication of actual environmental processes in that simulation effort by plugging in more realistic terms from both the atmospheric processes and the geographical distributions of terrain features in the urban areas that affect the energy balance at the surface.

REPRODUCIBILITY OF THE
ORIGINAL PAGE IS POOR

# CHAPTER 4

## SUMMARY AND RECOMMENDATIONS

The Skylab investigation in the Central Atlantic Regional Ecological Test Site encompassed two separate but related tasks: (1) Land use analysis, the evaluation of photographic sensors S-190A and S-190B as sources of land use information required for planning and managing the land resources in a major metropolitan region, and (2) land use climatology, the evaluation of the multispectral scanner S-192, when used in conjunction with associated data and analytical techniques, as a source of information on the components of the energy balance at the Earth's surface in an urbanized area. The investigation was conducted as an integral portion of a larger multidisciplinary demonstration project (CARETS) which sought to establish operational guidelines for future USGS program developments in land use information and analysis. The CARETS project aim is to strengthen linkages among remote sensing systems, land use mapping programs, environmental problem-solving strategies, and the decisions that affect future land use and environmental quality.

## LAND USE ANALYSIS

### Summary

The CARETS Skylab land use analysis experiment utilized data obtained on August 5, 1973, from the Skylab 3 mission over a portion of the test region. Data obtained included photographs from the multispectral cameras (S-190A) and the Earth Terrain Camera (S-190B). Of most interest to the

investigators and the users of CARETS land use information were photographs from the S-190B experiment, which were of sufficient spatial resolution to allow the identification of most of the Level II categories and some Level III categories of the multilevel land use classification system employed. The S-190B photography approached in its capability to discriminate land use types the capability of the high-altitude aerial photography that was used to derive the original CARETS land use information base.

To assess the value of Skylab photographic data as a land use mapping source, CARETS investigators compiled land use maps of the City of Fairfax, Virginia, utilizing high-altitude aerial photographs, S-190B photography, and S-190A photography. Researchers field checked and corrected the map derived from aircraft data to enable the measurement of the relative accuracy of the Skylab maps by direct comparison. Using a systematic aligned sample, the investigators found Skylab map accuracies to be S-190A, 74 percent; S-190B, 83 percent. The S-190B photography was of sufficiently high resolution to provide valuable inputs to land use mapping in urban as well as nonurban areas. Experience with various remote sensor data users, including planning agencies, indicates that photography of the caliber of S-190B could be of considerable value in the work of planning agencies at the State or regional level. This photography falls short, however, of being able to supply many of the detailed information needs of local or county-level planning agencies and many of the requirements for environmental impact applications.

Improved results in deriving valid land use categories could have been obtained if the superior spatial resolution of the S-190B system could have been combined with the multispectral capability of the S-190A system.



REPRODUCIBILITY OF THE
ORIGINAL PAGE IS POOR

The only data supplied to this investigation from the S-190B system were those employing high-resolution color film. The experience of USGS photo-interpreters indicates that the false-color or color-infrared format, such as that available in one of the cameras of the S-190A system, would have enhanced and improved the quality of the results. Furthermore, a slight improvement in the resolution of the S-190B system, through increase of the focal length, would have enabled that system to approach the ability of the high-altitude aircraft photography in distinguishing certain important land use measurements in this test region. For example, the S-190B system fell just short of the ability to distinguish single-family from multi-family residential land use, an important requirement of many of the local users. Also, the S-190B fell short of the ability to make dwelling unit counts, an ability of the high-altitude aerial photography in most areas of single-family residential land use.

Despite the above-mentioned limitations, the investigators feel that the S-190B system, when used with appropriate film and filter combinations, could provide the necessary data inputs to the operational land use mapping system in the USGS. The use of such data in an operational system, however, would require complete coverage of large geographic areas, obtained within required time intervals. The mode of operation of the Skylab sensors did not facilitate obtaining complete area coverage but rather was geared to the requirements of many separate investigators.

In general, we found that the USGS two-level land use classification scheme was suitable for use with enlargements of photographs from the Skylab S-190B system, with the land use data being extracted by manual photo-interpretation procedures. For such applications, photography of the caliber

of the S-190B could be utilized immediately in many operational land use mapping and analysis efforts, with a minimum of retooling or retraining of present personnel who have skills in the interpretation of small-scale aerial photography.

## Recommendations

One of the primary user requirements in this metropolitan region is for high-quality photographic imagery of the type obtained from high-altitude aircraft photography. The color-infrared film presentation is the favored one. Therefore, we recommend that an operational system be established as soon as possible for providing this high-quality photographic imagery to users.

Such imagery could be provided by high-altitude aircraft or by high-resolution cameras carried in orbiting satellites, as exemplified by imagery of the quality of the S-190B photographic system or preferably imagery of slightly higher ground resolving power. For image quality and use, whether the imagery is provided from Earth-orbiting platforms or high-altitude aircraft platforms is immaterial. The experience of this investigation indicates that the high-altitude aircraft system provides more flexibility for user requirements than a camera system aboard a spacecraft such as Skylab. If managed for operational purposes, however, a spaceborne system might be quite suitable for the provision of this high-quality photographic imagery.

We recommend that the Geography Program of the U.S. Geological Survey make use of unclassified high-resolution photography of the type mentioned above as its primary data source in land use/land cover mapping. The use of such photography as could be supplied by the NASA Earth

Observation Program would be preferable to the use of classified source materials that now constitute a major data source for the Geography Program. The reason for this recommendation is that the imagery itself is a high value user product and that much more information is available in the high-altitude photographic imagery than is utilized in extracting the Level II land use information. Furthermore, the availability of such imagery would enable user groups to cooperate and participate in mapping and updating programs, which is not possible if the basic imagery remains classified.

The above recommendations concerning photographic systems are made at this time because technology is now available and many user groups and Government agencies now have the capability of utilizing such data immediately. In the longer run, however, it will be important to develop more versatile and flexible information sources for land use information, such as computer compatible tapes. The examples available from other investigations which have made use of Landsat and Skylab S-192 multispectral scanner data are pertinent to this longer range consideration. Therefore, we recommend that research be continued with the aim of improving and making more efficient the use of computer compatible tape sources for obtaining basic land use information.

Beneficial combinations of the photographic systems and the multispectral systems might be devised in the near future. For example, one of the needs in using multispectral scanner data is a geographic location system for each picture element (pixel) in the data set. One approach to providing this location reference information is to accumulate a library of precisely located points on the Earth's surface that are also readily identifiable on the imagery produced by the scanners. Ideally such points

can be located by determining latitutde and longitude on a large-scale topographic map such as the USGS 1:24,000-scale map series. In portions of the country or in areas outside the United States not covered by such maps, it may be beneficial to use Skylab S-190B and possibly S-190A photography already obtained to extend locational control for further expanding and developing such a library of carefully located image points. This information could then be made available to all users, and it would greatly facilitate the use of multispectral scanner data where precise location and/or mapping reference are required.

For the kind of operational use of high-resolution airborne or spaceborne photography envisioned in these recommendations, a satisfactory user-delivered product must be obtainable without resorting to highly specialized photographic processing of the type required to bring out the finest detail in the NASA Skylab images. Although these highly processed images make beautiful illustrations and are of high value for use by photointerpreters, they should not be considered as part of a normal data delivery system if they cannot be produced operationally at such high quality. The need for fine detail is another reason for attempting to improve the resolution of future systems over that of the S-190B system, especially for operational uses in metropolitan area analysis such as that performed in the CARETS investigation.

Finally, we want to repeat, with increased emphasis, recommendations th were made in an earlier progress report under this investigation. Highest priority user requirements in metropolitan area land use planning and management are for data of at least as high resolution as that obtainable in the best high-altitude aircraft photography. Therefore any operational

remote sensing system, even if it be simply an extension of the present use of Department of Agriculture photographs, supplemented by work of private contractors, must provide for that basic high-resolution data need. This is the type of data needed at the level at which most decisions on land use change are made. Other users who have less detailed data requirements may benefit from lower resolution photographic systems such as the S-190B or even the S-190A. Therefore a two-level or multilevel imaging system is called for, with tradeoffs among different levels being determined by the least cost solution of providing the lower resolution data (whether from generalization from higher resolution data or from direct imaging at lower resolutions).

The answers to questions of how operational urban data user needs should be met depend no longer upon the results of spaceborne sensor experiments of the Skylab type. The NASA-funded programs of the past several years involving aircraft and satellite sensor tests, culminating now in the magnificient photographs produced by S-190B, have demonstrated amply the technical capability of the sensors. Rather, the remaining questions to be answered are in the areas of developing suitable data delivery systems for users, based upon an operationally assured source of high-quality remote sensor data. Such delivery systems would be a cost-effective mix of manual and automatic data-extraction methods. Immediate attention needs to be given to the selection of the cost-effective (and also politically effective) level or levels of the Federal-State-local governmental hierarchy where the data-gathering, interpretation, and analysis capabilities might best be located.

Tradeoffs between aircraft and spacecraft platforms should be matters of engineering considerations; these are not important to the users.

Operational needs for high-resolution data for urban and metropolitan area analysis are urgent, however, and would seem to justify an approach that combines early delivery of some useful data to priority users, with a longer range effort to improve system capabilities and prepare a capability that will most likely be required by users 5 to 10 years in the future.

## LAND USE CLIMATOLOGY

### Summary

The land use climatology portion of the Skylab experiment was the major CARETS project effort in studying the environmental impact of land use patterns and changes. The research that led to this part of the Skylab experiment began prior to Skylab as a NASA-funded investigation in the USGS, a study of the surface energy balance and consequent climatological effects of man's local modification of the land surface, as measured with the assistance of remote sensors. Although the concentration of effort has been the study of the urban heat island and other aspects of the climates of cities, the results have application as well to other types of land use, and the project has been given the generalized name of land use climatology. An integral part of this research effort has been the development and testing of an urban climate simulation model based upon the energy conservation equation. Each of the terms in this equation, net radiation, soil heat flux, sensible heat flux, and latent flux, is a complex function of certain environmental variables. Several of these variables (albedo, soil thermal properties, wet fraction, and aerodynamic roughness) are amenable to measurement and spatial analysis using remote sensing data.

In this light, the CARETS Skylab investigation and its precursor aircraft mission have employed analysis of calibrated multispectral scanner data in constructing radiation maps of an urban area (the Baltimore test site) and in coupling this information with the operation of the urban climate simulator.

The precursor mission to the CARETS Skylab climatology investigation was flown in May 1972 over the Baltimore test site by the Environmental Research Institute of Michigan aircraft, under contract to NASA as support to this USGS project. Researchers produced isarithmic maps of radiation temperatures derived from multispectral scanner data which successfully showed the development of the urban heat island from sunrise to early afternoon. Also, this research produced net radiation maps based in part on albedos determined from the scanner data. These maps, reflecting a single set of synoptic conditions, provided a base of observed environmental information against which the simulator was compared to see how well it could predict the climatic conditions that occurred at that time. Results showed the simulator capable of providing approximations to the energy balance conditions for specific land uses.

In similar fashion, investigators analyzed data from the S-192 multispectral scanner from the Skylab 3 mission of August 5, 1973. One result was the production of a map representing approximate albedos, constructed from output of band 6 (0.68 - 0.76 μm). The albedo was found to be an important component of the energy balance equation in urban areas.

The main thrust of the investigation was toward the production of a map of surface temperature distributions derived from the thermal channel (band 13, 10.2 - 12.5 μm), combined with the production of a simulated

temperature map of the same area using the surface climate simulation model. The results of this effort show broad similarities between the observed and predicted temperature maps, although considerable variation in detail exists between the two mapped patterns.

Using a modified version of the gray-window model developed by R. W. Pease and applied during earlier NASA aircraft missions, researchers calibrated thermal data from the S-192 multispectral scanner. The gray-window model converts a radiant energy signal received at the scanner in space to its value when emitted by the Earth's surface by compensating for both atmospheric attenuation (turbidity and water vapor) and for upward emitted radiant energy from the atmosphere. Results from this experiment indicate that land use related components of urban climate can be measured and modeled with the aid of input data from spaceborne remote sensors. These results are expected to have applications to urban land use planning, by making available as input to future urban design information on the climatological consequences of the land use patterns in and around cities. With energy shortages looming, opportunities to conserve energy inputs to urban heating and cooling systems may receive increased attention.

## Evaluation by Review Panel

An evaluation of the entire CARETS project, including the land use climatology Skylab experiment, was conducted at a special interest group session at the annual meeting of the Association of American Geographers held in Milwaukee, April 21, 1975. The evaluation was conducted by a panel of outside specialists, chosen for their expertise in the various component disciplines encompassed within the CARETS multidisciplinary experiment.

Evaluators for the land use climatology project were Dr. John Arnfield and Dr. John N. Rayner of the Department of Geography, Ohio State University. The evaluators had received drafts of project reports and maps in advance of the meeting. They discussed these materials and presented their evaluations, after which members of the audience had opportunity for questions or additional comments. This procedure enabled the project scientists in the Geological Survey to have the benefit of expert criticism, prior to publication, on scientific research results in a field which had not previously been conducted as part of the Geological Survey's regular research program. The remainder of this section contains a synopsis of the evaluation comments of Drs. Arnfield and Rayner.

The reviewers were impressed by the investigators' combination of two techniques applied to urban climatology: remote sensing and computer simulation. The remote sensing data are used to provide verification for substages of the simulation model.

The results can have applications for providing surface parameters for atmospheric circulation models at mesoscale levels. This approach provides a useful addition to related research going on at present. With the approach of this project, for example, it is possible to run experiments with the various data sets, e.g., change land use and see what changes are produced in local climates. Such capability is important for those who must make policy recommendations concerning the urban heat island and how it might be affected by various proposed development plans. Applications of the techniques used here are not limited to the urban situation--results are applicable to the study of rural microclimates as well.

Strengths of the project include the way it has identified the scale problem in climatological studies, e.g., relationships of heights of various land use/land cover types to surface roughness, and effects of the dimensions of sample terrain blocks selected for analysis. It also demonstrates the use of more conventional remote sensing techniques to provide data at different scales, useful to climatological analysis. For example, these techniques make it possible to obtain the effective albedo of an urban surface, a measure of importance in climatological studies. The approach stresses, quite correctly, the importance of radiative processes in the development and maintenance of the urban heat island.

There are some problems, and some areas that can be improved. The evaluators did not feel that the model had been adequately coupled with the remotely sensed data.[5/] Perhaps better integration between model and data could be achieved by improving the data processing techniques, enabling both to be brought into register spatially. This effort needs to be expanded in order to fully justify the title of Chapter 3 of this report. Also, the limitation to cloud-free conditions, for viewing from above, seems to be a drawback to full application of the remote sensing techniques. Results would also have to be extended to account for diurnal and annual variations, which would be theoretically possible with the model employed, but which would require verification with remote sensing data taken at a wider variety of times than were used in this study. The investigation does not have adequate sensitivity to estimate short-term variations in radiation. The model is better able to measure surface parameters.

5/ Subsequent to their review, maps were made from both remotely sensed data and numerical simulation and compared favorably as has been previously noted.

Another problem is that spatial variation in incoming radiation is not incorporated into this type of model. Also, shortwave absorption may be very important. Surface absorption is handled in a rather crude way in this study. Further, multiple reflection from complex urban surfaces could increase surface reflection significantly, and it is not clear how this factor is allowed for. Another criticism concerns the assumption of uniform emissivity--it would be desirable to utilize the remote sensing capability to associate more previse emissivity measures with the different land surface types.[6/]

In sum, however, the approach and results demonstrated here have considerable merit and have important implications for future climatological research, especially in obtaining measured or simulated data that are difficult or impossible to obtain in other ways.

## Recommendations

Based on the promising preliminary results reported here, we recommend that further investigations be undertaken to improve the uses of multispectral scanner data such as the S-192 for direct observations of surface energy balance parameters. Further, we recommend that increased attention be paid to preliminary data processing of the scanner data. Users need easier access to the data, including locational references of each pixel, than was possible with the output format of the S-192.

The use of the simulation model in conjunction with analysis of thermal data from the multispectral scanner seems to be a beneficial and promising approach. However, that the model has consistently underestimated surface temperatures, as compared with observed temperatures, suggests that

---

6/ It would have been impractical to calculate the average emissivity of the many elements of a data cell in this experiment. Since emissivities of virtually all natural surfaces in the thermal infrared are above 0.9, the value used in this study, 0.95, appears to be a representative average emissivity.

further refinements be made in the urban climate simulation model. These refinements would attempt to make more realistic the input of environmental data concerning atmospheric and terrain surface properties. To further improve the applicability of the simulation approach, we recommend that an improved classification of land use/land cover be developed and applied. Such a classification would more realistically represent the distribution of features that actually affect the surface temperature regime. For example, we recommend more detailed sampling within land use categories (in the standard USGS classification system) that have a variety of heterogeneous components within them. A promising approach to this problem would be through the use of classifications derived directly from the computer compatible tapes of Landsat or S-192.

We further recommend that improved analytical techniques and computer programs be developed to enable investigators to make direct quantitative comparisons of map distributions, such as those derived from simulated and observed maps of surface temperatures. Such quantification is essential to further development and refinement of a combined modeling and observation approach, which it is believed holds most promise for future applications in energy budget and microclimatological applications.

Finally, we recommend that Government research administrators take special note of the new field of land use climatology as approached through the use of calibrated data from remote sensors. During the course of this research project, there has been a greatly increased interest in the need to conserve our energy resources and in finding more efficient ways to utilize solar energy. One way to make better use of solar energy is to improve the spatial design of landscape modifications in urban areas, so



REPRODUCIBILITY OF THE ORIGINAL PAGE IS POOR

as to capture as much of the Sun's radiation as we can before it is reflected or reradiated back into space. Conservation may be served by attending to thermal consequences of land use patterns. The urban heat island, for example, works against energy conservation in the summer when air conditioning is required, and favors energy conservation in the winter when less heating is required. Examination of these effects in different land use design situations seems called for. Techniques employed in this investigation should be evaluated and possibly extended and the results guided toward practical applications in urban planning and design. There is at present, however, no agency which has either the responsibility or the people with the requisite qualifications to perform the necessary research--combining skills in climatology, instrumentation, remote sensing, land use analysis, and computer analysis of geographic data. The new field of land use climatology should be provided with some appropriate agency location, together with support necessary to nurture it and to maintain a critical mass of research capability, and to coordinate it properly with other energy research and development efforts. This Skylab investigation has defined the new field of land use climatology and opened the way to its future development and potential applications.

## SELECTED REFERENCES


Ackerman, E. A., 1958, Geography as a fundamental research discipline: Univ. of Chicago, Dept. of Geography Research Paper no. 53.

Alexander, R. H., Fitzpatrick, K. A., Lins, H. L., and McGinty, H. K., 1975, Land use and environmental assessment in the central Atlantic region: Natl. Aeronautics and Space Admin., Earth Resources Survey Symposium, Houston, Tex., 1975, Proc., v. I-C, p. 1683-1727.

Anderson, J. R., 1971, Land use classification schemes used in selected recent geographic applications of remote sensing: Photogramm. Eng., v. 37, no. 4, p. 379-387.

Anderson, J. R., Hardy, E. E., and Roach, J. T., 1972, A land-use classification system for use with remote-sensor data: U.S. Geol. Survey Circ. 671, 16 p.

Anderson, J. R., Hardy, E. E., Roach, J. T., and Witmer, R. E., 1976, A land use and land cover classification for use with remote sensor data: U.S. Geol. Survey Prof. Paper 964, 28 p.

Bach, Wilfrid, and Patterson, William, 1968, Heat budget studies in greater Cincinnati: Assoc. Am. Geographers Proc., v. 1, p. 7-11.

Barry, R. G., and Chambers, R. E., 1966, A preliminary map of summer albedo over England and Wales: Royal Meteorological Soc. Quart. Jour., v. 92, p. 543-548.

Berry, B. J. L., and Baker, A. M., 1968, Geographic sampling in Berry, B. J. L., and Marble, D. F., eds., Spatial analysis: Englewood Cliffs, N.J., Prentice Hall, p. 91-100.

Berry, B. J. L., and Marble, D. F., eds., 1968, Spatial analysis: a reader in statistical geography: Englewood Cliffs, N.J., Prentice Hall, 512 p.

Bornstein, R. D., 1968, Observations of the urban heat island effect in New York City: Jour. Appl. Meteorology, v. 7, p. 575-582.

Ellefsen, Richard, 1963, ADP pattern recognition of urban land uses from satellite-borne multispectral scanner: Ann. Conf. on Remote Sensing in Arid Lands, 4th, Tucson, Ariz., 1973, Proc., p. 71-81.

Estoque, M. A., 1963, A numerical model of the atmospheric boundary layer: Jour. Geophysical Research, v. 68, 1103-1113.

Fitzpatrick, K. A., 1975, Cost-accuracy-consistency comparisons of land use maps made from high-altitude photography and ERTS imagery: Natl. Aeronautics and Space Admin. Goddard Space Flight Center, Type III Final Rept. for ERTS-1 Investigation SR-125, v. 6.

Garrison, W. L., and Marble, D. G., eds., Quantitative geography - Part I: Economic and cultural topics and Part II: Physical and cartographic topics: Evanston, Ill., Northwestern Univ., Dept. of Geography.

Geiger, Rudolf, 1965, The climate near the ground: Cambridge, Mass., Harvard Univ. Press, 611 p.

Gottmann, Jean, 1961, Megalopolis: the urbanized northeastern seaboard of the United States: New York, Twentieth Century Fund.

Goddard, W. B., 1973, Exploring man's possible effects on Arctic pack ice and their paleoclimatological significance: AAS-AMS Alaskan Science Conf., 24th, Fairbanks, Ak., Aug. 1973, Paper.

Halstead, M. H., Richman, R. L., Covey, Winton, and Merryman, J. D., 1957, A preliminary report on the design of a computer for micrometeorology: Jour. Meteorology, v. 14, p. 308-325.

Hare, F. K., 1973, Energy-based climatology and its frontier with ecology, in Chorley, R. J., ed., Directions in geography: London, Methuen and Co.

Hudson, R. D., 1969, Infrared system engineering: New York, John Wiley and Sons, 642 p.

Klemas, V., Bartlett, D., and Rogers, R., 1975, Coastal zone classification from satellite imagery: Photogramm. Eng. and Remote Sensing, v. 41, no. 4, p. 499-513.

Kondratyev, K. Ya, 1969, Radiation in the atmosphere: New York, Academic Press, 912 p.

Kung, E. C., 1961, Derivation of roughness parameters from wind profile data above tall vegetation in studies of the three-dimensional structure of the planetary boundary layer: Madison, Dept. of Meteorology, Univ. Wisconsin Ann. Rept. 1961, p. 27-36.

Kung, E. C., Bryson, R. A., and Lenschow, D. H., 1964, Study of a continental surface albedo on the basis of flight measurements and structure of the Earth's surface cover over North America: Monthly Weather Rev., v. 92, p. 543-564.

Landsberg, H. E., 1956, The climate of towns, in Thomas, W. L., ed., Man's role in changing the face of the Earth: Chicago, Univ. of Chicago Press, p. 584-606.

Letteau, H. H., 1969, Note on aerodynamic roughness parameter estimation on the basis of roughness element description: Jour. Appl. Meteorology, v. 8, p. 828-832.

Lins, H. F., Jr., 1975, Land-use mapping from Skylab S-190B photography: Photogramm. Eng. and Remote Sensing, v. 42, no. 3, p. 301-307.

Lowry, W. P., 1967, Weather and life - an introduction to biometeorology: New York, Academic Press. 305 p.

Marotz, G. A., and Coiner, J. D., 1973, Acquisition and characterization of surface material data for urban climatological studies: Jour. Appl. Meteorology, v. 12, p. 919-923.

McClatchey, R. A., Fenn, R. W., Selby, J. E. A., Volz, F. E. and Garing, J. S., 1972, Optical properties of the atmosphere: Air Force Cambridge Research Laboratories, Environmental Research Paper 411, 108 p. Available from Natl. Tech. Inf. Service, Springfield, Va. 22151 as AD 753 075.

Miller, D. H., 1965, The heat and water budget of the Earth's surface, in Advances in geographics 11, p. 175-302.

Miller, E. L., Johnston, R. F., and Lowry, W. P., 1972, The case of the muddled metromodel, in Am. Meteorological Soc., Conf. on Urban Environment and Second Conf. on Biometeorology, Philadelphia, 1972, Preprints, p. 185-190.

Monteith, J. L., 1973, Principles of environmental physics: London, Edward Arnold, 241 p.

Myrup, Leonard, 1969, A numerical model of the urban heat island: Jour. Appl. Meteorology, v. 8, p. 908-918.

Myrup, L. O., and Morgan, D. L., 1972, Numerical model of the urban atmosphere, in v. 1 of the city-surface interface: Davis, Univ. of California, Contributions in Atmospheric Sciences no. 4, 237 p.

National Academy of Sciences-National Research Council, 1966, Spacecraft in geographic research: Washington, D.C., 107 p.

Nicholas, F. W., 1974, Parameterization of the urban fabric - a study of surface roughness with application to Baltimore, Maryland: Univ. of Maryland Ph.D. thesis. Available from University Microfilms.

Outcalt, S. I., 1971, A numerical surface climate simulator: Geographic Analysis, v. 3, p. 379-393.

_____1972a, A reconnaissance experiment in mapping and modeling the effect of land use on urban thermal regimes: Jour. Appl. Meteorology, v. 11, p. 1369-1373.

_____1972b, The development and application of a simple digital surface climate simulation: Jour. Appl. Meteorology, v. 11, p. 629-636.

Outcalt, S. I., 1972c, A synthetic analysis of seasonal influences in the effects of land use on the urban thermal regime: Arch. Met. Geoph. Biokl., ser. B, v. 20, p. 253-260.

_____1973, The simulation of diurnal surface thermal contrast on sea ice and tundra terrain: Arch. Met. Geoph. Biokl., ser. B, v. 21, p. 147-156.

Pease, R. W., Alexander, R. H., and Pease, S. R., 1970, Mapping terrestrial radiation emission with the RS-14 scanner: Tech. Rept. 4, USGS Contract no. 14-08-0001-11914.

Rayner, J. N., 1971, An introduction to spectral analysis: London, Pion, Ltd., 174 p.

Reed, S. E., and Lewis, J. E., 1975, Land use information and air quality planning: an example of environmental analysis using a pilot national land use information system: Natl. Aeronautics and Space Admin. Goddard Space Flight Center, Type III Final Rept. for ERTS-1 Investigation SR-125, v. 7.

Reifsnyder, W. E., and Lull, H. W., 1965, Radiant energy in relation to forests: U.S. Dept. of Agriculture Tech. Bull no. 1344, 111 p.

Scott, W. E., Stephens, E. R., Harst, P. L., and Doerr, R. D., 1957, Further developments in the chemistry of the atmosphere: Am. Petroleum Inst. Proc., v. 37 [III], p. 171-183.

Sellers, W. D., 1965, Physical climatology: Chicago, Univ. of Chicago Press, 272 p.

Steiner, Dieter, and Salerno, Anthony, 1975, Remote sensing data systems, processing, and management, in Manual of remote sensing: Falls Church, Va., Am. Soc. Photogramm., p. 611-803.

Taaffe, E. J., 1970, Geography: Englewood Cliffs, N.J., Prentice Hall, 143 p.

Terzaghi, Karl, 1952, Permafrost: Boston Soc. Civil Engineering Jour., v. 39, p. 319-368.

Yates, H. W., and Taylor, J. H., 1960, Infrared transmission of the atmosphere: Washington, D.C., U.S. Naval Research Laboratory, NRL Rept. 5453.

Yuill, R. S., 1970, Technical notes on the measurement of census tracts and land use area, in Simpson, R. B., Production of a high-altitude land use map and data base for Boston: U.S. Geol. Survey Phase I Final Tech. Rept., Contract no. 14-08-0001-12640, p. 26-36.

APPENDIX A

# THE BALTIMORE AIRCRAFT MISSION, PRECURSOR TO SKYLAB LAND USE CLIMATOLOGY EXPERIMENT

Final Report, USGS Contract No. 14-08-0001-11914, Energy-Exchange Phenomena at the Earth-Air Interface, including Report of the Baltimore Mission, and Energy-Exchange Mapping Project

by Robert W. Pease, Principal Investigator, Department of Earth Sciences, University of California, Riverside

Riverside, California, February 10, 1975

## ABSTRACT

The advent of calibrated, constant gain, multispectral scanners caused the objective of this contract inquiry to be the relationship of scan imagery to surface energy-exchange phenomena. Models for calibration of scanners to the surface have been created, particularly for the modifying effects of air in the sensing path. Techniques are described for creating isarithmic maps of energy-related surface phenomena, such as the distributions of radiation temperature, surface energy emission, surface albedos, energy absorbed by the surface, and net radiation.

## EARLY ACTIVITIES

The first efforts of this contract were directed toward completing certain inquiries which had been started under USGS Contract No. 14-08-0001-10694. These dealt with color infrared film as a remote sensing system and produced three technical reports, abstracted as numbers 1 - 3 in Appendix 1 of this report.

The original thrust of this inquiry, as indicated by the project title, was an endeavor to correlate energy conditions at the terrestrial surface with their replication on thermal infrared scan images. When the contract was initiated, available thermal images were from RS-7 and RS-10 thermal imaging systems as flown by the NASA Aircraft Program -- systems based upon AC circuitry with automatic gain control which rendered impossible quantitative measurement of surface energy states by the scanner. The original contract inquiry was thus conceived as an endeavor to understand better qualitative image diversity on the basis of quantitative ground measurements of energy involved in exchanges at the earth-air interface, usually referred to in this report as the terrestrial surface or, simply, surface. To accomplish this purpose, an array of fairly standard radiation and other energy measuring instruments was assembled which included a pyranometer to measure shortwave incoming solar energy, two net radiometers to assess the energy balance at the surface, a Barnes PRT-5 Precision Radiation Thermometer with a custom 10 - 12 micrometer bandpass for measuring longwave or thermal energy and a portable recorder for the pyranometer and one net radiometer. Upon completion of the contract, this array was delivered to the Geography Program of the U.S. Geological Survey and is now in Reston, Virginia. Certain minor equipment items were fabricated by the University of California, Riverside, including thermistor soil probes with appropriate readout bridges and a field potentiometer furnished with the main array. An ISCO Spectroradiometer, used for measuring the spectral distribution of incoming solar energy, was furnished to the project by the Geological Survey on a temporary basis. The initial use of this array was that of familiarization with the energy phenomena to be studied, familiarization with the instruments, and the acquisition of certain information pertaining to the transmission of longwave energy in the atmosphere that was precursor to participation in the BOMEX experiment.

## THE BARBADOS (BOMEX) EXPERIMENT

Shortly after the project commenced, two things acted in concert to focus the direction of the inquiry and make it more relevant to needs of the Geography



REPRODUCIBILITY OF THE ORIGINAL PAGE IS POOR

Program. One of these was the chance to participate in the BOMEX experiment on the Island of Barbados and the other, in conjunction with the first, the opportunity to work with a calibrated electro-optical scanner. Flown by the NASA Aircraft Program, the Texas Instruments RS-14 is capable of not only constant gain but self-calibration as well. In effect, this meant that a scanner was available which, in addition to producing a thermal image, could be considered a scanning radiometer by which energy-exchange phenomena occurring at the terrestrial surface could be quantitatively measured remotely from above. Thus the inquiry was converted to studying this scanner potential with the instrument array used for ground calibration measurements. A short term goal became the production of synoptic isarithmic maps showing thermal emission by the surface and concomitant radiation temperatures as they existed for a flightpath across a portion of Barbados at the north edge of Bridgetown (see Technical Report 4, abstracted in Appendix I). The maps were to be generalized to give a better feel for the way the surface was affecting the air above it.

Participation in the BOMEX experiment proved to be especially fruitful. The RS-14 scanner, mounted and flown in the NASA NP3A aircraft, recorded a high quality thermal scan across the island of Barbados from the west coast eastward at 1030 hrs. local time on the morning of June 29, 1969, yielding a scan image along the flightpath which included ocean surface, the northern portion of the city of Bridgetown, and sugar cane fields in various stages of growth east of the city. The radiances of a number of ground targets, easily recognizable on the ensuing imagery, were obtained at the time of overflight which permitted calibration of the radiometric scan image since the gain of the scanner had been kept constant during the imaging period. Further, self-calibration of the instrument was subsequently achieved with the aid of Victor Whitehead of NASA/JSC (MSC in 1969) who calculated a compensation for the Irtran windows over the internal calibration sources in the scanner. The NP3A aircraft carried two downward-looking PRT-5 radiation thermometers which gave ancillary airborne measurements with which the calibration of the scanner could be compared.

To make generalized maps of the distribution of surface radiance and radiation temperatures from the scan image, a process of optical integration of data on an image transparency was used. A simple densitometer was devised, the wide aperture of which integrated an image area equal to .40 $km^2$ ground measure. In this manner the intricate patterns of radiance of the raw image were converted to values susceptible to isarithmic mapping. The methods and results of this successful initial attempt at mapping surface diversity of radiant emission from a calibrated scanner are reported in Technical report 4 of this contract entitled, Mapping Terrestrial Radiation Emission with the RS-14 Scanner (see Appendix I). This report was also reprinted for internal dissemination by Texas Instruments, Inc.

## The Gray-Window Model

A significant contribution of this initial effort was the development of a viable physical model for compensation of the modification of the surface emitted radiance by the air intervening between the surface and sensor. Whereas the simple calibration of the scan image to surface radiance values by means of multiple surface calibration targets automatically makes this adjustment, the

alternate use of the self-calibration potential of a scanner requires that an atmospheric adjustment be made. It was discovered that the heavily humid air of the tropics rapidly modifies the surface signal, even in the so-called "water vapor window" between 8 and 12 micron wavelengths. The transmissivity in this spectral band of the air in the 3,000-foot sensing path over Barbados during imaging was less than 0.60. A gray-window model based upon Schwarzchild's Equation was devised by which the signal received at the sensor could be converted to a surface value when the mean temperature of the intervening air column and the radiance of a single ground target were known. In its basic form, the equation for any intervening air column is:

$$\underset{\text{b.}}{} \qquad \underset{\text{a.}}{}$$

$$I_z = \varepsilon[E_{bb}(\bar{T})] + (1 - \varepsilon)\, I_o \qquad (1)$$

where $I_z$ is the radiance at the scanner, $I_o$ is the radiance leaving the surface, $[E_{bb}(\bar{T})]$ the blackbody equivalent of the mean temperature of the air column, $\varepsilon$ the emissivity of the air, and $(1 - \varepsilon)$ the transmissivity.

It was further conceived that the transmissivity $(1 - \varepsilon)$ could be ascertained by using Beer's Law in the form:

$$(1 - \varepsilon) = e^{-ku} \qquad (2)$$

where u is the optical depth of water vapor in precipitable centimeters and k a mass absorption coefficient for water vapor which would be as low as .117 for a 10-12 micron sensing band and .25 for an 8-14 micron window. These values are according to Kondratyev (1969). In the model, in essence the atmosphere is attenuating the surface signal according to the multiplicative factor, transmissivity (a in Equation 1), and adding its own emission in a temperature-dependent manner (b in Equation 1). When the air temperature mean is lower than the surface temperature, as is usually the case, the radiance is damped. This model was used and tested in later project experiments.

## THE BALTIMORE EXPERIMENT

The success of the Barbados effort led to the belief that the methods developed should be further applied to studying the heat-island effect in a city in the United States. It was also desired to expand the time-frame from a single flight to a multiple sampling of a diurnal period to produce eventually a study by remote means of seasonal change in terrestrial energy exchange phenomena. Houston, Texas was initially chosen as the urban target because (1) it was close to the base of operations of the NASA aircraft program; (2) it was essentially a city rising out of a flat plain which would simplify conclusions reached; and (3) it was adjacent to the Gulf of Mexico, the humid air of which would enable further improvement of the gray-window model which in turn would eliminate or reduce the need for calibration targets, an improvement particularly desirable for the calibration and use of possible satellite thermal data.

The extended experiment, however, was subsequently moved with Baltimore, Maryland as the new test site city. At the time Houston overflights were desired, the NASA NP3A aircraft, with the previously used calibrated scanner, was grounded by structural failure in its wings. Project delay caused by the many months that the aircraft and scanner were not available was compounded after repairs by backlogs of flight requests and the fact that the scanner itself suffered a series of malfunctions. In the meantime (1) the original term of this contract was approaching its end and (2) the Central Atlantic Regional Test Site (CARETS) had been created and placed under the supervision of the Geography Applications Program of the U.S. Geological Survey. It was mutually agreed by the Principal Investigator of this contract and the Chief Geographer of the Geological Survey that an extension of the project would be funded but that the test-site city would be in the CARETS area. Baltimore was chosen. It was further decided that the Baltimore experiment would be classed as a preliminary study to the forthcoming NASA/SKYLAB experiment.

The near impossibility of again obtaining use of the NASA NP3A aircraft plus the reported RS-14 scanner malfunctions led to a request that the M-7 scanner, operated by the Environmental Research Institute of Michigan (ERIM) and often termed the "Michigan Scanner," be used in its place. The first request was placed on a contingency basis with the monitoring of corn blight during the summer of 1971. Because of the rigors of corn blight monitoring, no Baltimore flights by the ERIM aircraft and scanner were possible until the following spring. The Baltimore mission was rescheduled for the spring of 1972 and consummated on May 11, 1972 with the Principal Investigator of this project supervising ground truth calibration at Baltimore. The wait for the imaging overflights had caused close to a two-year delay in completing the project.

Following the Barbados inquiry, and in consultation with Dr. Reid Bryson of the University of Wisconsin, the suggestion was made that phenomena other than surface radiances and radiation temperatures could be mapped from calibrated scanner data. In brief, it was felt that surface albedos could be ascertained and then, with a knowledge of incoming solar and atmospheric down-radiation, the absorption of solar energy by the surface could be determined. By properly adding the energy absorbed as a positive quantity to the energy emitted as a negative quantity, the distribution of net radiation could be plotted. Unlike strictly climatic studies that use data obtained over a prolonged period of time, the map plots obtained from scanner images would be synoptic in character, that is, show conditions as they existed for essentially a given moment in time. From such synoptic maps the dynamics of urban thermal systems could be studied.

Thus by May 1972, the Baltimore experiment had been expanded from a simple analysis of a diurnal surface temperature and radiant emittance study for an urban area to an attempt to ascertain from a scanning radiometer more complete pictures of the distribution of energy-related phenomena at the surface. An attempt would be made to create generalized maps showing not only radiation temperatures but also surface albedos, the diversity of energy absorbence, and net radiation or the radiation balance at the surface.

Following the Bryson conference, thought was given to ways of measuring surface albedos remotely from an imaging aircraft. The problem revolved around the fact that it would be difficult to measure the whole spectrum of reflection from a



REPRODUCIBILITY OF THE
ORIGINAL PAGE IS POOR

surface target since sensors with a spectrally flat response are too slow in response time to be used in a scanning radiometer. Because all sensors used have pronounced spectral selectivities, sampling techniques were deemed necessary. Consideration was given to photographic films and images as possible data sources if careful controls were exerted in taking and processing of film images. To aid in this additional inquiry, the Geological Survey provided an employee to work under the supervision of the project to ascertain not only potentials of photography for albedo determination, but the nature of spectral samples that would be representative for various natural reflectance curves involved in albedo determination as well. This study, reported as Technical Report 5 under the title Photographic Films as Remote Sensors for Measuring Albedos of Terrestrial Surfaces, is abstracted in Appendix I. It has served well as a guide for selecting the bands of the M-7 scanner for use in the energy absorbtance aspects of this experiment.

With the change of the test-site city to Baltimore, the project became more closely allied with "in-house" activities of the Geographic Applications Program and its work with the CARETS test site. Work of the contract was integrated with that of two Geological Survey employees, Drs. Samuel Outcalt and John Lewis, and in this way became a part of a three-way analysis tentatively labeled "land-use climatology." Outcalt's primary concern was numerical computer modeling of energy-exchange phenomena and Lewis's the effects of urban surface roughness. Outcalt's models were to be tested by the Baltimore mission data with inputs from Lewis. Lewis acted as coordinator for the combined in-house aspects of the project due to his proximity to Washington as a member of the geography staff at the University of Maryland. Both Lewis and Outcalt were active, along with the Principal Investigator of this project, in gathering data during the Baltimore mission.

## The Baltimore Mission

The Baltimore mission was flown on May 11, 1972. The day was cool and clear, a cold front having passed through the area the previous night. The air between the surface and sensor was virtually free of particulates and aerosols and the water vapor content was low. These conditions were confirmed by later calculations that indicated an overall air transmissivity for the 5,000-foot sensing column as above 0.90 for all flight times. The spatial homogeneity of the air mass in this regard was checked at noon by means of a circuit of the Baltimore Beltway with a silicon cell pyranometer attached to the auto roof. Recorded variations between 1.35 and 1.43 langleys/minute appeared to be due to instrument deviation from the horizontal. Even around Sparrows Point steel mill no increase in atmospheric turbidity could be noted.

The mission consisted of a sequence of flights at three flight times during the single day: one close to sunrise and listed as beginning at 0515 hrs. EDT, a mid-morning series at 1015 hrs. EDT, and a high sun series at 1345 hrs. EDT. For each flight time a pattern of three flights was flown: Path 1, a calibration run, extended from the fairgrounds of the northern Baltimore suburb of Timmonium eastward across large Loch Raven Reservoir with the fairgrounds parking lot and the reservoir surface prime calibration targets. Path 2 was in two parts: 2b extended southwest across the central business district (CBD) of the city, with an interrupted extension as Path 2a over the community of Columbia, Md. Path 3

extended southeast from city suburbs across the CBD and included the Sparrows Point steel mill complex. Paths 2 and 3 formed an "X" pattern with the crossing over the CBD. Path 3 proved to have the most interest for the study of the diversity of energy-related phenomena and was used for the experimental mapping of phenomena more complex than simple radiation temperatures. The 1345 hrs. images were used for the experimental mapping of this project since it was deemed that at this time both temperatures and shadows would remain most stable during the 30 minutes of the flight. A map of flightpaths is shown in Figure 8.

The following ground measurements were made for the calibration targets (the blacktop and reservoir) as close to the time of overflight as possible:

1. Radiation temperatures of the calibration surfaces were measured with the Barnes PRT-5 radiometer.

2. Albedos of target surfaces were measured with both thermopile and silicon cell pyranometers. The method used was to measure, with the instrument inverted, direct and diffuse solar radiation as values to be divided into the reflection from the surface in question. Two thermopile instruments, a Schenck (Austrian) and a temperature-compensated Eppley, were crosschecked and correlated. The silicon cell instrument was calibrated to these.

3. Downwelling solar radiation (shortwave) was measured with the pyranometer in its normal position only.

4. Downwelling atmospheric radiation (longwave) or "sky temperature" was ascertained with the Barnes radiometer with optics changed for this purpose so as to have a bandpass of 3-20 μm.

5. Kinetic temperatures of both the water surface and blacktop were measured with small (.050 inch diameter) thermistors.

6. Net radiation was monitored for the blacktop surface only.

7. The spectral distribution of solar energy input was measured with an ISCO Spectroradiometer in a band from .380 to 1.55 μm.

During processing of data, the albedos of certain concrete surfaces of unfinished stretches of freeway were used as calibration targets with values assumed from both documented values (Sellers, 1965) and from measurements of concrete made in Riverside, California (Tech. Report 5, App. 1).

Although all of the 12 spectral bands of the M-7 scanner recorded data during the imaging overflights, only four were stipulated to be made into image transparencies for this contract: the .58-.64 μm, .62-.70 μm, 1.0-1.4 μm, and 9.8-11.7 μm bands. Two of the shortwave bands were subsequently used for albedo determination while the longwave or thermal band was used to determine radiation temperatures and energy emitted by the surface.

## Processing the Baltimore Data

Processing of the data gathered during the Baltimore mission into radiation-related maps has followed two paths. That directly the responsibility of this contract was carried out by the optical scanning of transparencies prepared from the magnetic tapes upon which the data were initially recorded during flight. Transparencies for the four multispectral bands were furnished by ERIM as a part of this contract. Analysis of these transparencies is described in this report. Separate from this contract, but related to it, NASA funded ERIM to consummate a completely computerized analysis to attempt to eliminate the need for the optical scan of transparencies by taking information directly from digitized versions of the scanner magnetic tapes. The results of this inquiry have been reported by ERIM to both this contract and directly to the Geography Program in a report entitled, Baltimore, Maryland Radiation Balance Mapping by F. J. Thomson and R. D. Dillman (1973).

The basic plan followed by this contract for extracting and analyzing data supplied by the transparencies can be described briefly. The use of generalizing or averaging data cells set in a matrix in essence was followed as was done with BOMEX information. But because the cell size was to be only 6.75 $mm^2$ (1/4 $inch^2$), more than 18,000 separate measurements would be necessary to create the matrices for radiation temperatures at all flight times and for other energy-related phenomena at 1345 hrs. The size of the analysis suggested the use of at least quasi-automated methods which would enable computerized decision making and automated isarithmic map plotting. Pursuant to this, a wide-aperture densitometer was designed and fabricated to be used as a data read-in attachment on an H. Dell Foster x - y digitizer to make data compatible with an IBM 360-50 computer. Details of the densitometer are described in Appendix 3 and illustrated in figures 4 and 5. The desired degree of generalization or smoothing was determined by the size of the densitometer aperture, the 6.75 $mm^2$ (1/4 $inch^2$) chosen to give a ground resolution of approximately 1,250 feet. Integrity of cell locations, both in a single matrix and between matrices of multispectral images which had been imaged simultaneously, was maintained by the visual readouts of the quantizer of the digitizer system. Images were keyed to each other either by an end and side or by prominent features that appeared in the flightpath, the latter frequently being the most accurate.

To ascertain the distribution of surface albedos for the 1345 hrs. flight paths that were used for the longer sequence of energy-related maps, only two of the shortwave or "reflection" bands were chosen. From the work of Pease, et al. (Technical Report 5, 1970) it was decided that two spectral samples, one on either side of the rapid near infrared rise in vegetation reflectance that centers at a wavelength of .725 μm, would suffice to determine albedos. Thus it was not necessary to digitize one of the bands obtained, a considerable saving in effort. Also in accordance with the 1970 study, the weighting of the two reflectivities derived from the shortwave bands was set as 60 percent for the visual red (.62-.70 μm) and 40 percent for the near infrared (1.0-1.4 μm). This derives from the fact that 60 percent of the solar or daylight spectrum at the surface is comprised of wavelengths shorter than the .725 μm partition of the vegetation reflectance curve. This weighting renders vegetation albedos most accurate although for the monotonic reflectance curves of most surfaces such a weighting is less critical.

The transparency images were initially converted to matrices of averaged transmittance by the wide-aperture densitometer and so read into the automated system. It was therefore necessary to convert these transmittance values into appropriate energy-related values. This could be accomplished either by (1) considering the scanner to be recording absolute energy values which could be interpreted according to the internal calibration sources of the M-7 scanner system or (2) handling the calibration empirically by relating the scanner values, in our case in the form of transmittances, to multiple calibration targets. Unfortunately for this contract, the first method was not possible because image elements of the calibration sources were not included in the transparency printout received due to format changes in the scanner recording (correspondence with Phil Haseli of ERIM, May 1973). Calibration depended therefore upon the multiple calibration targets described. This type of calibration, however, did eliminate the need to compensate for the modification of the surface radiance by the air column intervening between the surface and sensor. The parallel ERIM analysis depended upon the instrument self-calibration potential and of necessity compensated for the gray-window effect. Had the transmissivity of the air not been so high, there is some question as to whether this self-calibration would have been accurate for the attenuation-scattering effects in the evaluation of reflected light for albedo determination.

To convert transmittances to energy-related values in the computer, appropriate conversion curves were necessary. To construct the curves, the transmittances of image elements of calibration targets were measured with a MacBeth T100 Quantalog densitometer, utilizing its smallest possible aperture (1 mm) in order to include no more than the target. Transmittances were then plotted graphically against the energy value of interest with consideration given for the sensitometry of the transparency duplicating film. Fortunately, the transparencies did include step-wedges made by applying equal increments of energy during printout and these gray scales could be used to ascertain the typical S-shaped sensitometric curve for the film (Fig. 3).

Two options were possible for entering conversion information into the computer to make the desired translation of transmittance values. The first utilized a mathematical equation but posed difficulties in obtaining a good fit for the S-shaped conversion curves. The second involved simply digitizing the desired curve into the computer in x and y coordinates. The computer treated each segment between digitized points as a series of very short linear equations. This by far the most successful method was utilized.

After all data had been read from the transparencies and punched onto cards, a master tape file was prepared. Now in machine-compatible form, the data were subjected to manipulation. For this purpose, two programs were written in FORTRAN IV for an IBM 360-50 computer. The first utilized conversion curves for the three flight times (one for each scanner calibration) to convert the film transmittances to radiation temperatures. The second program performed the following: To determine total energy absorbed it converted transmittances of the solar band images to reflectivities, combined the reflectivities of the two shortwave bands into albedos according to the weightings just described, by the factor (1 - albedo) converted downwelling solar energy to solar energy absorbed, to which was added the downwelling longwave atmospheric radiation modified by an average .95 surface emissivity. The atmospheric down-radiation had been measured as ground-truth information during overflight.

To determine net radiation, appropriate radiation temperatures were entered from the first program, converted to energy emitted in langleys/minute by the Stefan-Boltzmann Equation, and added as a negative quantity to energy absorbed as a positive quantity. This sequence of processing was performed for each smoothing cell in the series of multispectral matrices which emphasizes the importance of maintaining registry between the several multispectral images of a flightpath during initial data read-in. At different stages of processing, maps showing various energy-related phenomena were plotted by applying matrix data values to the centroids of their respective averaging cells and interpolating isarithmic lines. The flow of data involved in these computations is diagrammed in Figure 2 and is detailed as Appendix 2.

The maps generated in this project used the TOPO contouring program with a preprocessor linear interpolation which had the dual purpose of scaling the matrix size and smoothing the surface. All maps were plotted with an H. Dell Foster RSS-700 flat bed vector plotter.

The TOPO program was written by Mr. Raymond Postma as part of a land-planning tools software package for the Environmental Systems Research Institute of Redlands, California. Programming for the project was performed by David A. Nichols, Research Specialist for the Department of Earth Sciences, University of California, Riverside. The project also acknowledges the invaluable assistance of Mr. Claude Johnson, Senior Research Specialist in the same department.

## THE MAPS

A sequence of synoptic maps of energy-related values is shown as a sample of the product of the project. Copies of all maps are furnished separately, made to a scale of one inch = 2,500 feet. The sample is for flightpath 3, NW to SE across Baltimore and displays distributions as they existed at 1345 hrs. on the flight day. The image, Figure 1a, is that of the visual red band and provides geographical orientation for the maps. On the left-hand end is the CBD of Baltimore with downtown Patterson Park prominent. To the southeast, an industrial area with large-roofed structures, parking lots, rail yards, and tank farms separates the CBD from a residential area that extends to an arm of the estuary of the Patapsco River. Across the estuary at the southeast end of the flightpath is Sparrows Point steel mill. The image is only one of the three used to furnish data for the sequence of maps. A series of radiation temperature maps for the same flightpath, but for all three flight times, is shown as Figure 1f. These show well the morning buildup of the urban heat island.

The maps to be furnished separately from this report include:

For flight time 0515 hrs.: maps of radiation temperatures for all flightpaths. Radiation temperatures are in degrees Kelvin because the contouring program would not handle negative values.

For flight time 1015 hrs.: radiation temperatures for all flightlines in degrees Celsius.

For flight time 1345 hrs.: radiation temperatures for all flightlines in degrees Celsius, energy emitted by the surface in langleys/minute x 10, energy absorbed by the surface in langleys/minute x 10, net radiation diversity over the surface in langleys/minute x 10, and the generalized distribution of surface albedos.

In all, 28 maps are provided.

## COMMENTS REGARDING PROCEDURES

As indicated by the foregoing, determination of generalized patterns of solar energy absorbtance is more complex than for simple thermal emission. Measurements of absorbtance must be based upon (1) solar and atmospheric energy reaching the surface, (2) solar and atmospheric energy reflected by the surface, with (3) the fact that energy absorbed is that reaching the surface less the energy reflected. The scanner or scanning radiometer can measure only energy reflected by the surface as it has been modified by the intervening atmosphere. If the scanner is to be used in the self-calibrating mode, as occurred at ERIM, adjustment must be made for the upwelling energy reflected by the atmosphere as an addition to the surface signal attenuated by the same air column. This is indeed a gray-window model but more complex than for longwave energy where the emission by the column follows a more consistent set of natural rules. The problem arises from the diverse nature of light scattering in the atmosphere which provides the up-radiation to the scanner. For example, Rayleigh scattering by air molecules is close to omnidirectional and provides a general background of atmospheric luminance, particularly strong at the short visible wavelengths but still of some effect for longer wavelengths. Generally of greater significance in scanner sensing bands, Mie scattering by aerosols is mostly forward scatter and attenuates a surface signal but adds little up-radiation to the scanner. The surface signal can be Mie scattered in the direction of the scanner, but this luminance addition is of a low order of magnitude compared to the signal itself during most imaging. Large aerosols such as fog and thin clouds scatter the least but are good reflectors of solar energy and provide such an upward flood of general radiation that surface signals are small in relative intensity and thus difficult to distinguish. No gray-window model has as yet been created to account for all combinations of Rayleigh, Mie, and non-selective scattering as has been done for thermal energy, but, with knowledge of such synoptic conditions as type of aerosol (e.g. fog, haze, factory smoke, etc.) and meteorological visibility, this might well be accomplished. At the present state-of-the-art, calibration targets with known reflectivities in the spectral bands chosen for albedo determination appear the most feasible means for shortwave energy assessment.

The direct processing by ERIM appears to have neglected the shortwave gray-window effect of the atmosphere because of the great clarity of the air during the Baltimore imaging, but results were checked empirically against calibration targets.

## ALBEDO CHANGE WITH SUN ALTITUDE

A problem in the remote measurement of albedos suggested in Technical Report 5 concerns the effect of varying shadow fractions in the image on measured albedos.

A commonly observed phenomenon from the air is the bright "no-shadow" spot directly opposite the aircraft from the sun. As the angular distance away from this spot directly under the solar beam increases, the degree or fraction of shadow in the image increases for any roughness of the surface. Darkening of the surface, then, would appear to record a lower than true albedo. The only true albedo, when considered as a conservative property of the surface, would be that measured directly along the solar beam.

To test the reality of this as a problem in the use of scanner imagery, a study was carried out with the aid of Gerald O. Tapper to determine the change in albedo with different sun altitudes and differing surface types. A silicon cell photometer with an 11° angle of acceptance was fabricated and the reflectivities of various surfaces were measured including several where urban residential and CBD conditions were simulated with blocks (Fig. 6). From a long series of observations of the surfaces as illuminated by sun at differing altitudes and degrees of ratios of beam to diffuse radiation (Q/q), a series of factors for converting vertical to beam or "no-shadow" albedos was empirically derived. The curves for the factors for various surface-types coincided for sun altitudes above 30° and varied only moderately for different surfaces when the sun was nearer the horizon. The suggestion was strong that all surfaces are rough surfaces and at a macro-scale the magnitude of the roughness makes little difference to a generalized albedo.

The empirically derived conversion curves were then compared with one derived simply from Lambert's Cosine Law (Fig. 7). For sun altitudes above 45°, the curves coincided fairly well but below 45° the cosine curve increased in factor much more rapidly than the empirically derived curves. Since the "cosine" correction curve would represent the solar beam illumination only, it is logical to assume that the difference between it and those derived from observations represents the fill-in shadow areas by diffuse skylight. Because the diffuse addition is essentially omnidirectional and because the pyranometric readings for determining albedos were taken on a horizontal surface, it has been assumed for this experiment that no conversion of data to what might be termed the "beam albedo" is necessary. In other words, the solar beam is being distributed over the surface according to the cosine law as it is on the sensing surface of the pyranometer, while the diffuse skylight is not subject to the cosine law except through some possible correlation to Mie forward scattering which is a relatively small value. Assuming the surface is an isotropic reflector, the acceptance cone of the scanner receives an equal amount of energy (for a homogeneous surface) regardless of the angle it makes with the surface. The diffuse solar radiation is a consistent addition regardless of the scanner angle of view.

## ERIM PROCESSING OF THE BALTIMORE DATA

Although the parallel direct processing of data from computer tapes by ERIM has been submitted as a report separately, it is briefly described here. To keep the processing as parallel as possible, an outline of the processing steps to be followed in this project was supplied to Fred Thomson of ERIM by the Principal Investigator of this contract who also spent time at the ERIM facilities in Willow Run, Michigan, during the ERIM project.

Differences in the ERIM data flow from that described here involved (1) direct conversion to digital form of the analog tapes made during imaging, and (2) the use of direct energy values of reflected light as a negative addition to sola

energy inputs to achieve energy absorbed by the surface rather than the use of albedos for the same purpose by this project. Thus in the ERIM method, no determination of albedos is necessary and an albedo map is merely a spinoff from the appropriate stage of computer processing if desired. It is felt that there is a certain analytical loss here since albedos appear to be the real forcing factor for the diversity of energy absorbed by the surfaces.

Surface element shapes remain more intact in the ERIM line-printed graymaps than they do in the isarithmic displays of this project, even though ostensibly ERIM used a lower degree of ground resolution. This seems to be an intrinsic difference in the two smoothing methods. At ERIM the data was digitized to 320 points per scan line. To reduce the graymaps to a manageable size (8 inches wide) the data were subjected to a 4 x 4 block smoothing (4 pixels on 4 lines) which reduced resolution to approximately 100 feet ground measure. Since the image was still spatially noisy, 3 x 3 running gaussian filtering was applied three times which reduced noisy detail but left image shapes intact and did not reduce scale.

A comparison of the ERIM graymaps with the isarithmic products of this contract suggests that both have advantages and disadvantages according to intended use. The line-printed maps tend to be dasymetric, with value polygons that approximate major surface elements in shape even though smoothed as regards spatial noise. This is a positive factor in analyzing the relation of land use to energy-related phenomena. The utility here, however, depends upon the effectiveness of the order-intervaling of data when the graymap is made since continuous gradients cannot be assumed. The maps are large to handle, on the other hand, and do not make as suitable displays when reduced for publication as do the isarithmic maps where an assumption of continuous gradients allows interpolation of values between isolines. Accepting the format differences, the accuracy of both methods appears good.

## FIRST-LOOK OBSERVATIONS

As has been mentioned, there is a strong suggestion that surface albedos are the forcing factor for the diversity of energy absorption by the surface for spatially constant values of downwelling solar and atmospheric radiation. These conditions are typical for a given flightpath and for a scale like that used in the Baltimore mission. Since at midday the energy absorbed has about double the value range of energy emitted, albedo also becomes a dominant control for the distribution of net radiation.

The fact that albedos appear as strong controls of both energy absorption and the distribution of net radiation (net radiation is considered, with reservations, the injection of natural energy onto a terrestrial thermal system) suggests that deeper inquiry into the causes or controls of albedos would be worthwhile. Certain quick-look observations then should be noted. In a city business district, absorption of downwelling energy is close to 90 percent, but when in vegetative growth parks absorb only about 75 to 80 percent. This arises from the fact that absorption is (1-albedo) and the high near infrared reflectance of the plants is responsible for the increase in albedo and concomitantly the lowered absorption. Traditionally it has been considered that low radiation temperatures in a park are due to the latent energy sink provided by plant transpiration, but lower energy absorbence appears also as a factor. Indeed, because of the latter factor, parks such as Patterson Park in downtown Baltimore have approximately the same net radiation as the CBD. Highest albedos occur where reflectivities are high in both the visual and near infrared bands, such as for the tank farm surrounded by bare-earth safety sumps. Residential areas in the city also have high albedos during the vegetationally active season which are especially high when houses have light-colored roofs. The steel mill has low reflectivities in both albedo-sensing bands



C-3

and therefore is a good absorber, but, since it emits strongly, injects little more energy than the CBD. Water is the best absorber and has the highest net radiation by far (1.20 ly/min. as against .80 ly/min.) but due to the thermal inertia of the water and tidal exchange with Chesapeake Bay, probably acts only to ameliorate sunrise and midday temperatures in the vicinity of the water.

An obvious observation is the buildup of a thermal or "heat island" over the business district during the morning (Fig. 1f). At sunrise little difference exists between the CBD and suburbs, but water surfaces appear warm. By 1015 hrs. a thermal island over the city is beginning to form which reaches its best development by early afternoon. By then parks and water surfaces appear as temperature depressions while minor temperature peaks appear over the steel mill. Since the radiometric temperatures displayed correspond within a few degrees to the kinetic or sensible temperatures, this buildup has definite physiological significance to the city residents and daytime transient populations within the CBD. An obvious conclusion is that city-center temperatures in the warm season could be lowered by increasing overall albedos by such means as parks or the use of light-colored and low emissivity roofing materials.

## GENERAL EVALUATION OF RESULTS

Because the dual technologies of multispectral scanning and automated contour plotting are not entirely new, it is felt that the major contributions of this project are (1) the successful creation of synoptic energy-related isarithmic maps from calibrated scanner imagery other than simple displays of the thermal state of the surface and (2) the symbiotic integration of scanner and automated cartography techniques to achieve such maps.

As regards accuracy of the project maps, the following observations can be made. Radiation temperatures closely correspond to target ground measurements, a fact that may not be surprising since the targets were used to make the appropriate conversion curves. Less directly derived, albedo values appear to be rational. Those for vegetated surfaces such as parks appear to be 20 to 22 percent which match both measured values made after the mission and are in the generally accepted range. Unfortunately, measurements of park albedos were overlooked during the mission but other vegetated areas with comparable values were measured. Net radiation values, which required the most complex series of data manipulations and thus potentially were most prone to error, also appear reasonable. The ground-measured net radiation for the blacktop surface of the fairgrounds parking lot was .81 ly/min. at the time of the 1345 hrs. flight time overflight. On the generalized map, this location can be interpolated as .77 ly/min., a low order of error if indeed it can be considered an error since the latter values had been generalized. As would be expected, there is some difficulty in checking smoothed values with point measurements.

Regarding the utility of the maps, one purpose for them is to supply spatially comparable data to be used in modeling in such areas as urban planning and the field tentatively described as land-use climatology. In the annual meetings of the Association of American Geographers in Boston in 1971, a significant point was made for the spatial extrapolation of the traditional point energy budget studies. The maps herein described provide such a way. As has been noted, this

project has been intended to develop methods applicable to outputs from SKYLAB and other satellites with a multispectral scanner capacity. It has achieved a great deal of success in this regard. The "quick-look" facts regarding the importance of the diversity of albedos are but one example.

The future of energy-exchange mapping as described depends to a great extent upon availability of appropriately calibrated multispectral scanner data which includes a thermal band. At the time of this writing, initial SKYLAB thermal imagery for the CARETS area, including Baltimore, has just been calibrated and would seem to indicate the feasibility of such use where broad geographic perspectives are desired. Scanner systems in high flying, U-2-type aircraft might well be cheaper and provide more consistent results, since times of imaging can be controlled better than in a satellite. This certainly would be an improvement over the narrow flightpaths attainable at only 5,000 feet as was the case for Baltimore.

Although future instrument platforms at this point are not well defined, it can be assumed that if the information maps of the type here described are of sufficient value, the scanner data necessary to make them will be forthcoming.

## REFERENCES CITED OR USED

In addition to the technical reports of this contract, listed and abstracted in Appendix 1, the following works have either been cited or used considerably for the final report of the contract.


Fleagle, Robert G. and Joost A. Businger, An Introduction to Atmospheric Physics, Academic Press, New York, 1963, 346 pp.

Junge, Christian E., Air Chemistry and Radioactivity, Academic Press, New York, 1963, 382 pp.

Kondratyev, K. Ya., Radiation in the Atmosphere, Academic Press, New York, 1969, 912 pp.

Wolfe, William L. (ed.), Handbook of Military Infrared Technology, Office of Naval Research, Department of Navy, U. S. Govt. Printing Office, Washington, D. C., 1965, 906 pp.


Unpublished:


Thomson, F. J. and R. D. Dillman, Baltimore Maryland Radiation Balance Mapping, Environmental Research Institute of Michigan, Nov. 1973, 97 pp. (unpublished report to U. S. Geological Survey).

APPENDIX 1.

ABSTRACTS OF TECHNICAL REPORTS SUBMITTED BY USGS CONTRACT NO. 14-08-0001-11914

Technical Report 1
MULTISPECTRAL IMAGES FROM MULTILAYER FILM
Robert W. Pease

Black and white multispectral images have found use as inputs to various image analyzing instruments and for densitometrically determining spectral signatures. Due to redundancy of information, spectral bands sensed have been reduced in number to essentially the three layer sensitivities of color infrared film. Since a rather meager bank of true multispectral photography exists, it has been deemed cogent to investigate the practicality of deriving black and white multispectral images from multilayer color infrared film. Not only is the potential data bank increased, but problems of registration are reduced and camera systems are rendered simpler.

The technique of separation involves confining light by means of a separation filter to a very narrow spectral band which matches the maximum density wavelengths of a layer modulation being extracted and in which the dye densities of the unwanted layers are low.

Errors inherent in the technique are of a low order of magnitude and result not only from interlayer interference during the separation process but from overlap of dye-forming layer sensitivities characteristic of color infrared film as well. Silver masking techniques can compensate for them but the size of the error usually does not warrant this extra trouble.

When used as inputs to the IDECS image analyzing instrument, the black and white transparencies separated from a color infrared original performed as well or better than multispectral images originally exposed onto black and white film.

Technical Report 2
MORE INFORMATION RELATING TO THE HIGH ALTITUDE USE OF
COLOR INFRARED FILM
Robert W. Pease

Use of EA-4 processing for color infrared film and observed deviations from normal sensitometric characteristics modify the previously made recommendations for the use of auxiliary minus-visual filters with the film system. With this processing, the need to equalize dye-forming layer sensitivities to combat the color shift due to air luminance can be met with filters that attenuate less the visual wavelengths. Loss of cyan sensitivity due to aging, on the other hand, increases the attenuation need. Simple tests are suggested whereby the user can ascertain the sensitometric characteristics of his film.

Technical Report 3
COLOR INFRARED FILM AS A NEGATIVE MATERIAL
Robert W. Pease

Original problems encountered in endeavors to use color infrared film as a negative material have been overcome by a simple modification in processing. This makes more feasible the production of infrared color prints for field use and yields an infrared counterpart to Aero-Neg.

Technical Report 4
MAPPING TERRESTRIAL RADIATION EMISSION WITH AN RS-14 SCANNER
Robert W. Pease, Robert H. Alexander, Steven R. Pease

Terrestrial radiation emission has now been successfully mapped from the image of a thermal infrared scanning radiometer by using the model RS-14 instrument flown by the NASA Aircraft Program. Because of a capability for constant amplifier gain, this instrument can be calibrated to surface targets--a capability which earlier model scanning radiometers lacked due to the necessity for automatic gain control. Even though the RS-14 sensors utilized the 8-14 micron water vapor window, a significant damping of the surface emission was encountered which became more pronounced as surface temperatures diverged from the mean temperature of the air column intervening below the remote sensor. Although multiple ground control targets, the radiation temperatures of which were measured during the imaging overflight, were used for the primary calibration of the experiment, experience gained has permitted formulation of a "gray-window" model by which much simpler cross-calibration techniques can be used in future radiation mapping missions. Several types of radiation maps are presented for Bridgetown and adjacent rural areas of the Island of Barbados, made with data collected in June 1969 in conjunction with the BOMEX investigation.

Technical Report 5 of Contract No. 14-08-0001-11914
Also, Interagency Report USGS-225
PHOTOGRAPHIC FILMS AS REMOTE SENSORS FOR MEASURING ALBEDOS OF TERRESTRIAL SURFACES
Steven R. Pease, Robert W. Pease

To test the feasibility of remotely measuring the albedos of terrestrial surfaces from photographic images, an inquiry was carried out at ground level using several representative common surface targets. Problems of making such measurements with a spectrally selective sensor, such as photographic film, have been compared to previous work utilizing silicon cells. Two photographic approaches have been developed: a multispectral method which utilizes two or three photographic images made through conventional multispectral filters and a "single-shot" method which utilizes the broad spectral sensitivity of black and white infrared film. Sensitometry related to the methods substitutes a Log Albedo scale for the conventional Log Exposure for creating characteristic curves. An adjustable Log Albedo scale is suggested which permits rapid matching of sensitometric characteristics to images of ground calibration targets. Certain constraints caused by illumination geometry are discussed.

REPRODUCIBILITY OF THE
ORIGINAL PAGE IS POOR

APPENDIX 2.

AN OUTLINE FOR PROCESSING DATA

A. To radiation temperatures ($T_r$) and radiant emittance ($I\uparrow$).

1. Convert transmittance values to radiation temperatures according to empirically derived conversion curves.

   Products: matrices of radiation temperatures in °C (and °K for 0515 hrs.) and isarithmic maps of radiation temperatures

2. Convert $T_r$(°C) to $T_r$(°K) or $T_r$(°C) + 273 = $T_r$(°K).

3. Convert $T_r$(°K) to radiant emittance ($I\uparrow$) in ly/min. x 100 using the Stefan-Boltzmann equation.

$$I\uparrow = (T_r, °K)^4 \ (8.14 \times 10^{-11})$$

Combining 2 and 3 into one equation:

$$I\uparrow = (T_r, °C + 273)^4 \ (8.14 \times 10^{-11}) = \text{longwave energy emitted}$$

For surface emission, $I\uparrow = E\uparrow$ (total energy emitted)

Products: matrices of radiant emittance in ly/min. x 100 and isarithmic maps of generalized radiant emittance

B. To surface albedos and net radiation (1345 hrs. flight time only)

1. Convert the transmittances of two solar reflection bands (.62-.70 μm and 1.0-1.4 μm) to reflectances from empirically derived conversion curves.

2. Combine the reflectances with a weighting, .60 visual red (.62-.70 μm) and .40 for the near infrared (1.0-1.4 μm) to ascertain albedos of each matrix cell.

   Products: matrices of generalized surface albedos and isarithmic maps

3. For each cell for a given flight time and flightline multiply solar radiation (Q + q) supplied from ground truth by (1-albedo) to ascertain absorption of solar energy by surface. Solar energy value = 1.43 ly/min.

$$(1 - a)(Q + q) = (Q + q)\downarrow = 1.43 \ (Q + q)$$

4. Add downwelling atmospheric radiation ($I\downarrow$) to determine total energy absorbed ($E\downarrow$). Value added = .418 ly/min. x an average emissivity of .95 = .418 ly/min.

$$(Q + q) + I\downarrow = E\downarrow$$

Products: Matrices of surface absorbtance and isarithmic maps of (E↓)

5. Determine the synoptic net radiation (R) by subtracting energy emitted (E↑) from energy absorbed (E↓).

$$R = E\downarrow - E\uparrow$$

Products: matrices and isarithmic maps of net radiation

Combining all equations:

$$R = [(1 - a)(1.43) + .418] - (T_r, °C + 273)^4 (8.14 \times 10^{-11})$$

An emissivity factor has been omitted for the initial radiant emittance determination since radiation temperatures were the field measure of temperature during ground truthing and these values were used in making conversion curves. The radiation thermometer used automatically compensated for the emissivity factor since it assumes an emissivity of 1.00.

EXPLANATION OF SYMBOLS

| | | |
|---|---|---|
| $T_r$ | = | Radiation temperature |
| I↑ | = | Longwave (thermal) energy emitted by surface |
| °C | = | Degrees Celsius |
| °K | = | Degrees Kelvin or absolute temperature |
| ly/min. | = | Langleys/minute = 1 calorie/$cm^2$/minute |
| E↑ | = | Allwave energy emitted |
| E↓ | = | Allwave energy absorbed by the surface |
| I↓ | = | Longwave (thermal energy from atmosphere) |
| Q + q | = | Incoming solar energy, beam and diffuse respectively |
| (Q + q)↓ | = | Incoming solar energy absorbed by surface |
| (1 - a) | = | (1 - albedo) equal solar energy absorbed by surface = (Q + q)↓ |
| R | = | Net radiation |

APPENDIX 3.

THE WIDE-APERTURE DENSITOMETER

A densitometer that can be attached to the Dell Foster digitizer has been designed and fabricated for extracting the average transmittance of each generalizing cell. This consists of an auxiliary light table 10 inches wide which stands approximately 2 inches above the surface of the digitizer. In place of the usual cursor, a frame is attached to the digitizer arm which places the densitometer light under the auxiliary light table with a light sensor directly above it. The entire lightweight frame moves with the digitizer mechanism, thus recording the exact x - y locations of its position. The imagery is placed upon the auxiliary light table so that the light source of the densitometer will be under it and the light sensor above. As the densitometer sensor moves from one x - y location to the next, the light source exactly follows it to provide a constant illumination. The light source is a 6-volt microscope illumination bulb operated from a 12-volt transformer through a dropping resistor. The bareter action of the bulb in this configuration tends to regulate the current through the filament to provide an even intensity of illumination.

The light sensor is a silicon cell held approximately 5 mm above the imagery. The cell load resistor is of low value to increase output linearity. Because this yields output voltages of a low order, a 5 millivolt potentiometric recorder was adapted as a readout device. A suitable sensitivity control, a potentiometer across the load resistor, was provided for calibration purposes in use. The recorder scale was constructed to match a standard gray-wedge produced by the MacBeth Company, the same gray-wedge that was used to calibrate the densitometer for making the original transmittance conversion curves.

A sophistication of the densitometer would place a shaft encoder on the main-shaft of the recorder to eliminate manual read-in of transmittance values. Details of the densitometer are shown in figures 4 and 5.

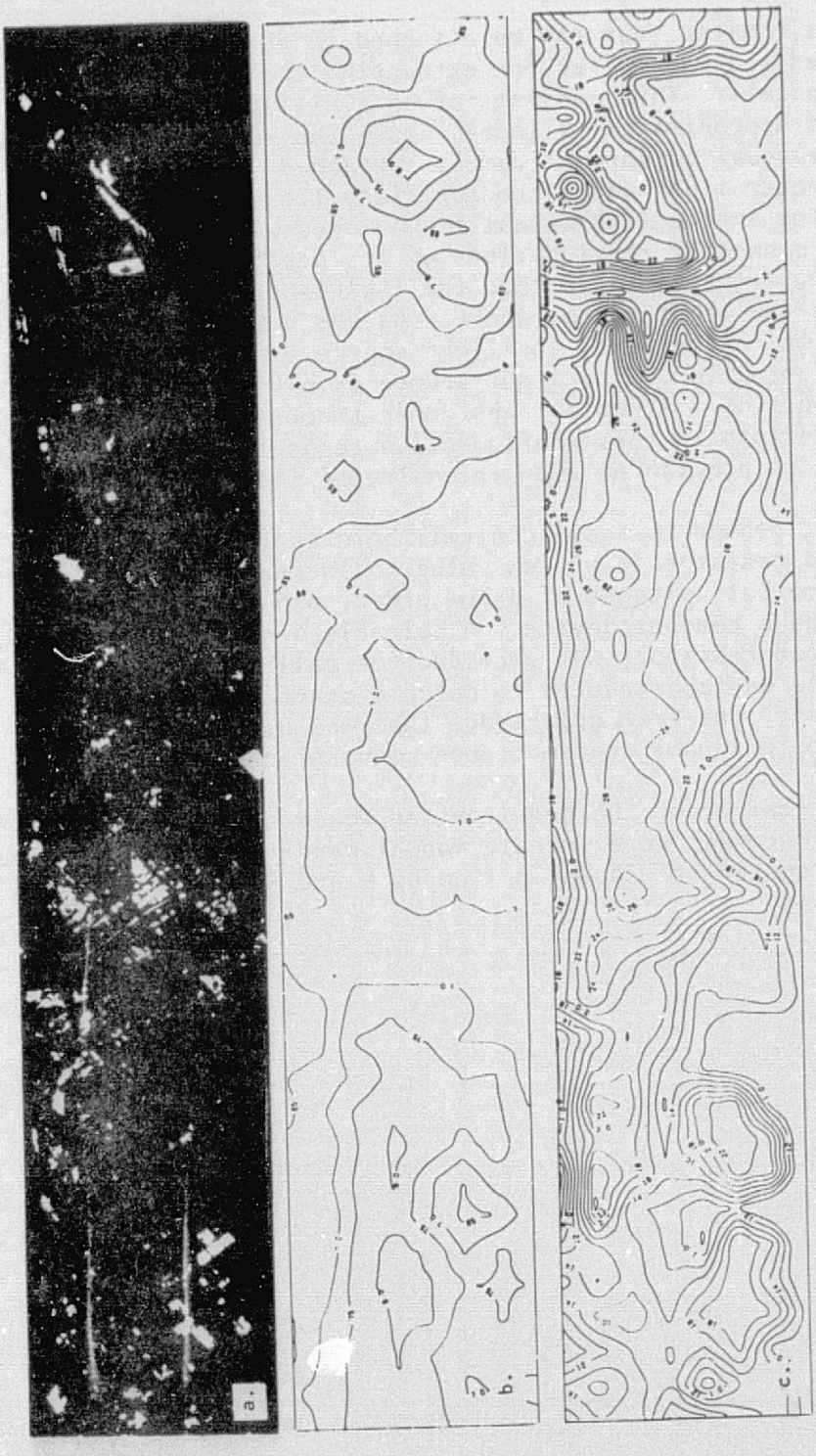


REPRODUCIBILITY OF THE
ORIGINAL PAGE IS POOR

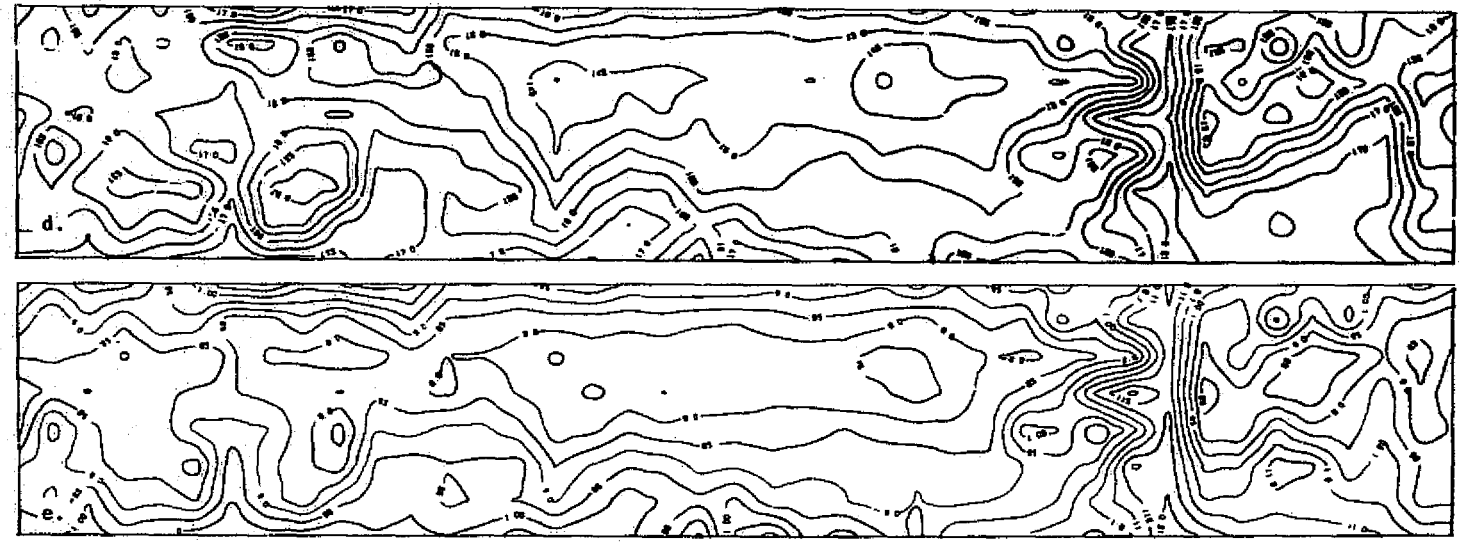


Fig. 1. A sequence of isarithmic maps showing various energy-related phenomena for a flightpath NW - SE across Baltimore, Maryland at 1345 hrs. on May 11, 1972. The image of the visual red band (a) shows the diversity of urban surfaces mapped. The maps generalize (b) the energy being emitted by the surface in (ly/minute) x 100, (c) surface albedos in percents, (d) the energy being absorbed by the surface in (ly/minute) x 100, and (e) the net radiation or balance of energy flows at the surface, also in (ly/minute) x 100.

Fig. 1f. The distribution of radiation temperatures at three flight times showing the buildup of the Baltimore heat island (left) and steel mill (right) during the morning. The temperatures for 0515 hrs. are in degrees Kelvin because the automated map system would not interpolate negative values. The flightpath is the same as for 1a.

ORIGINAL PAGE IS
OF POOR QUALITY




Fig. 2. A simplified diagram of the flow of data followed in making the maps.

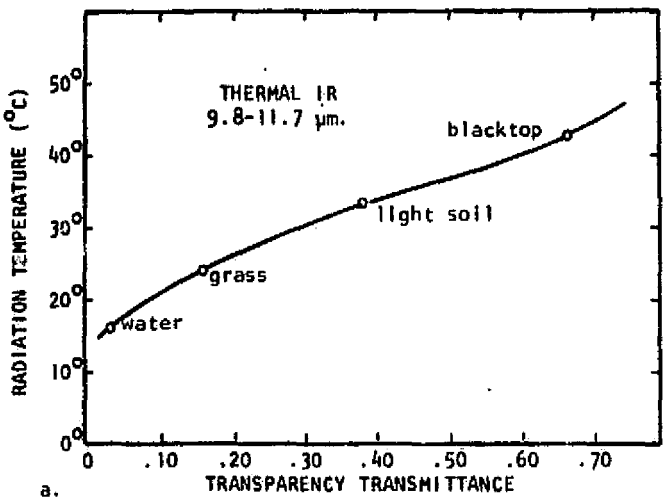


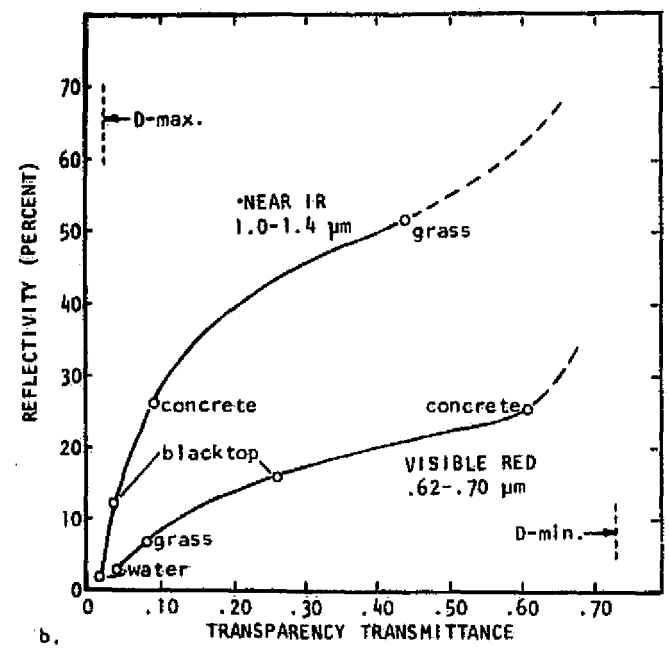


Fig. 3. Curves to convert the thermal infrared image to surface radiation temperatures (a) and two shortwave images to reflectivities (b) to determine albedos. Values for ground calibration targets are indicated. An S-shape is assumed to match film sensitometry.

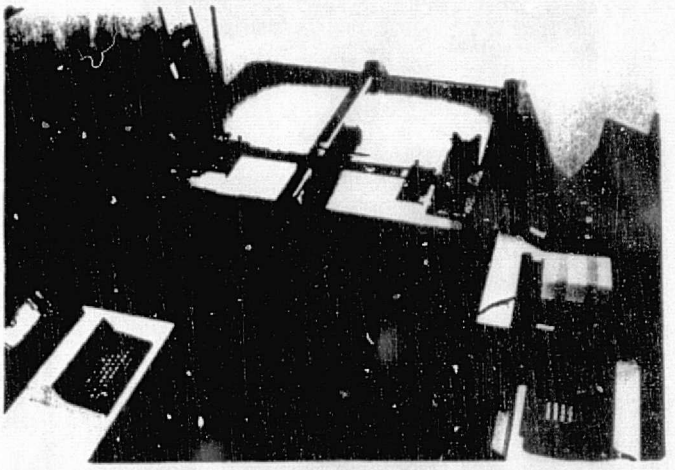

The H. Dell Foster x - y digitizer with the scanning wide-aperture densitometer attached to the cursor position. The quantizer and transmittance recorder are on the right.

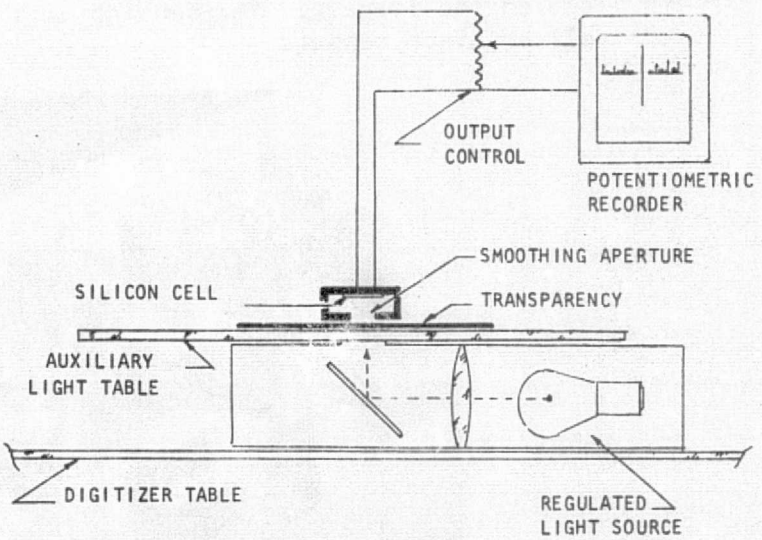


A simplified diagram of the wide-aperture densitometer. The transparency is attached to a stationary auxiliary light table with a moving light source below and light sensor above.

Fig. 4. Equipment for reading the transparency transmittances into the automated computer and map plotting system.

REPRODUCIBILITY OF THE
ORIGINAL PAGE IS POOR

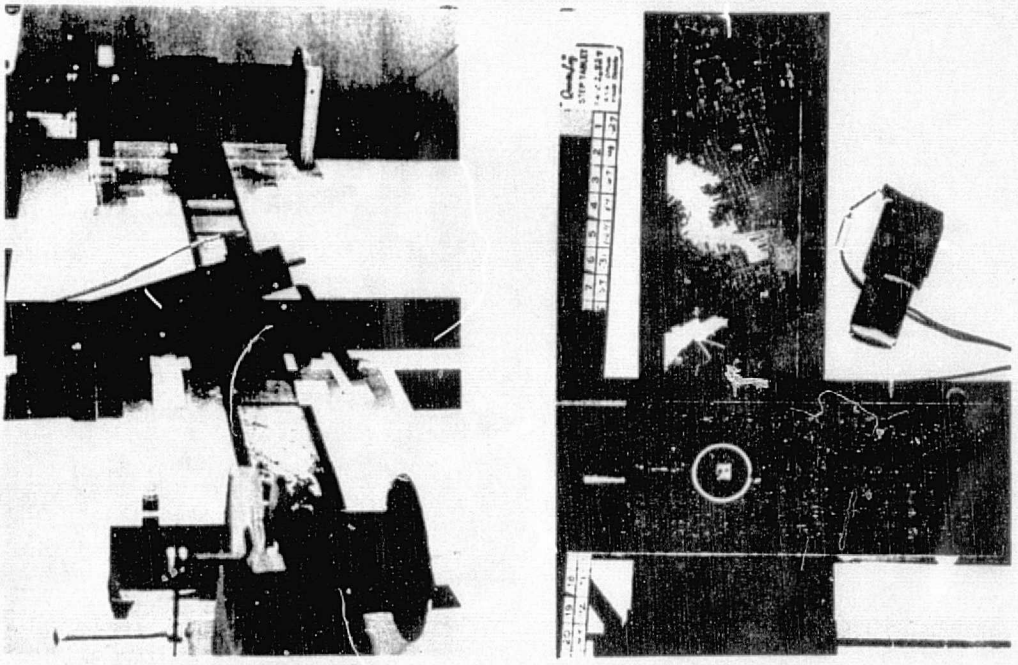

Fig. 5. Details of the wide-aperture densitometer. In the left hand view, the sensing head is lifted to show construction. In operation it nests in the channel. The vertical view on the right shows the smoothing aperture, which determines the matrix cell size, in place on the imagery. The sensing unit which contains the silicon cell has been removed.

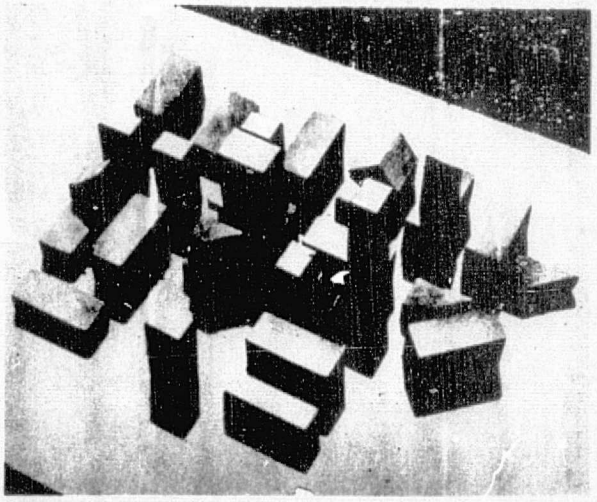

Fig. 6. A sample of a simulated urban CBD surface used to relate low sun to beam albedos. Residential areas were also simulated and naturally rough surfaces such as soil, gravel, a[illegible]grass were also tested.

REPRODUCIBILITY OF THE
ORIGINAL PAGE IS POOR

# APPENDIX B

## ENERGY BUDGET SIMULATION MODEL

by

Carol B. Jenner

and

John E. Lewis, Jr.

## ENERGY BUDGET SIMULATION MODEL

In recent years considerable success has been achieved in the use of surface energy balance modeling techniques for the simulation of micrometeorological processes in urban areas as well as in other applications including agriculture, permafrost, and pack ice behavior (e.g., Halstead and others, 1957; Myrup, 1969, Outcalt, 1973; Goddard, 1973). The surface energy balance approach is based on the surface energy conservation equation

$$R_{net} = H + LE + G,$$

where $R_{net}$ = net radiation receipt at the surface, H = sensible heat flux, LE = latent energy flux and G = soil heat flux. All four terms are in reality flux densities and are commonly expressed in units of cal $cm^{-2}$ $min^{-1}$. This energy conservation equation with occasional additional terms such as photosynthesis or snowmelt, if necessary, is thought to hold over varying time scales ranging upward from 1 second (Sellers, 1965). It is this equilibrium property of the surface energy expenditure system upon which the concept of surface energy balance simulation modeling is based.

The various surface energy balance models which exist vary in their parameterizations of particular terms, in input requirements, and in assumptions made. The general approach is identical, however. For each of the four components of the energy balance equation a combination of input boundary conditions and derived quantities serves

to express that component as a function of the surface temperature. There is one temperature, the equilibrium surface temperature, which balances this equation.

Halstead and others (1957) presented an early analog version using this approach. This model was applied exclusively to agricultural surfaces. Myrup (1969) developed a similar version, again in analog form, using different parameterizations. This model was originally designed for simulation of natural surface situations, but Myrup also pointed out the usefulness of such techniques in explaining urban-rural temperature differences. Outcalt (1971) carried this one step further and, using a digital version of the Myrup model with several specific urban processes built in, modeled various land use types occurring within a city.

Various other models similar in approach to, but using slightly different parameterizations of the energy balance terms than the Myrup-Outcalt model, also followed the work of Halstead and others (e.g. Miller and others, 1972; Estoque, 1963).

A digital version of the Myrup-Outcalt model serves as the basis for modeling efforts in this study. In previous efforts this model has been shown to be reasonably accurate in predicting surface temperatures for various land uses (Outcalt, 1972c).

## THE MYRUP-OUTCALT MODEL

As mentioned previously, this model is framed around the idea of energy conservation at the surface as expressed by the equation

$$R_{net} = H + LE + G \tag{1}$$

Through a series of parameterizations, each of the four fluxes is described as a function of input boundary conditions, derived quantities and the surface temperature. Since it is assumed that equilibrium energy conditions prevail at the surface at all times, an iterative algorithm is used to solve the set of equations for the one surface temperature which will balance the equation.

The assumptions made in determining the magnitudes of the various fluxes are critical in understanding the problems and inaccuracies in the model. Each of the four terms and their expression in the model will be discussed in the following sections.

### Net Radiation

Net radiation is best resolved into the solar and terrestrial components and may be described by the equation

$$R_{net} = R_{sw\downarrow} - R_{sw\uparrow} - R_{lw\uparrow} + R_{lw\downarrow} \tag{2}$$

where sw denotes short-wave (solar) components, lw denotes long-wave (terrestrial) components, and arrows indicate the direction of the radiation flux with respect to the surface.

Incoming solar radiation received on a horizontal plane at the edge of the atmosphere, $Q_o'$, is calculated from the set of geometrical relationships which follow. At a particular time,

$$Q_o' = Q_o \left(\frac{\bar{r}}{r}\right)^2 \cos Z \tag{3}$$

where $Q_o$ = the solar constant, taken to be 2 ly $min^{-1}$, $\bar{r}$ and r are the mean and instantaneous earth-sun distances, and Z is the solar zenith angle. At any time the zenith angle is given by

$$\cos Z = \sin\phi \cdot \sin\delta + \cos\phi \cdot \cos\delta \cdot \cos h \qquad (4)$$

where $\phi$ = latitude, $\delta$ = solar declination (north positive), and h = hour angle (morning negative). A negative value of cos Z indicates that the sun is below the horizon and that direct solar radiation equals zero.

Three major processes operating in the atmosphere account for the depletion of the solar beam between the edge of the atmosphere and the Earth's surface during clear-sky conditions. These are 1) scattering by air molecules; 2) scattering by atmospheric dust; and 3) absorption, chiefly by carbon dioxide, oxygen, and water. Brooks (1959) has found an empirical expression for each of these processes. Considering the sum of these expressions as a decay function, its combination with equation (3) yields

$$Q'_{sfc} = Q_o \left(\frac{\bar{r}}{r}\right)^2 \exp\left[-0.089\left(\frac{pm}{1013}\right)^{0.75} - 0.174\left(\frac{wm}{20}\right)^{0.6} - 0.083(dm)^{0.9}\right] \cos Z \qquad (5)$$

where $Q'_{sfc}$ = instantaneous direct solar radiation received at the surface, p = atmospheric pressure (mb), w = atmospherie precipitable water (mm), d = dust and haze particle concentration (particles per cubic centimeter), and m = optical air mass. The optical air mass m is calculated by

$$m = \left|\frac{1}{\cos Z}\right| \cdot \frac{P}{1013} \qquad (6)$$

In the case of sloping surfaces a corrected term, cos Z', must replace the cos Z value in equations (3) and (5). The general form is

$$\cos Z' = \cos i \cos Z + \sin Z \sin i \cos (a - a') \tag{7}$$

where a = solar azimuth angle, a' = aspect of the slope (with respect to true south; east negative), and i = slope. The solar azimuth angle is given by

$$\sin a = \frac{\cos \delta \cdot \sin h}{\sin Z} \tag{8}$$

Thus the complete equation for direct solar radiation receipt at the surface is

$$Q = Q_o \left(\frac{\bar{r}}{r}\right)^2 \exp \left[-0.089 \left(\frac{pm}{1013}\right)^{0.75} - 0.174 \left(\frac{wm}{20}\right)^{0.6} - 0.083 (dm)^{0.9}\right] \cdot \cos Z' \tag{9}$$

Formulae for diffuse radiation and corrections for sloping surfaces were taken from Kondratyev (1969) and adapted by Outcalt as follows. Diffuse radiation received on a horizontal plane is considered equal to one-half of the scattered component. Thus,

$$q' = 0.5 \left(\frac{Q_o}{r^2}\right) \cdot \cos Z \left\{1 - \exp \left[-0.083 (dm)^{0.9}\right]\right\} \cdot corr, \tag{10}$$

where r, d, Z, and m are previously defined and corr is a slope correction factor given by

$$corr = \left[\cos \left(\frac{I}{2}\right)\right]^2 \tag{11}$$

Backscattered solar radiation (B) is treated as a separate term and is given by

$$B = 0.5 (\alpha) (Q + q) \left\{1. - \exp \left[-0.083 (dm)^{0.9}\right]\right\} \cdot corr \tag{12}$$

where $\alpha$ = albedo.

So, total downward solar radiation (Q↓) is given by

$$Q\downarrow = Q + q' + B \tag{13}$$

Of this quantity a certain amount is reflected from the surface. Thus net shortwave radiation at the surface is expressed as

$$R_{sw\downarrow} - R_{sw\uparrow} = (1 - \alpha)\ Q\downarrow \tag{14}$$

where $\alpha$ = surface albedo.

In a city, the existence of buildings creates considerable shadowed area at the surface, so that the total downward solar flux is interrupted and only diffuse and backscattered radiation may reach the shadowed areas. The percentage of surface in shadow varies spatially depending on structure (and vegetation) height and density and also temporally depending upon sun angle. Outcalt's urban model attempts to calculate the "shadow fraction" based on an arbitrarily chosen function

$$S.F. = (1 - \cos Z)^3, \tag{15}$$

where S.F. represents the shadow fraction.

Accompanying the shadow effect, which causes a decrease in solar radiation at the surface, vertical faces of buildings interrupt the solar beam and add to the reflected load at the surface. Again this radiation component varies with sun angle as well as with building configuration. To deal with this term Outcalt considers the solar receipt for a vertical wall rotated through the day so that its exposure at all times is equal to the solar azimuth angle. The geometrical calculations involved here are identical to those discussed previously for the surface case. The total "upright" solar radiation receipt is given by

$$R_{uprt} = Q_{uprt} + 2.q_{uprt} \tag{16}$$

In this term it is considered that the shadowed wall receives only diffuse radiation. Both the shadow fraction calculation and the upright radiation determination will be evaluated at a later point.

Combination of the additional "urban radiation" terms with the previously developed net solar radiation equation produces

$$R_{sw} = [(1 - S.F.) \ (Q + q) + S.F. \ (q) + R_{uprt} \ (S1/S2)] \ (1-\alpha), \qquad (17)$$

where $q = q' + B$, S1 = building silhouette area and S2 = specific area = lot area / number of buildings per lot. The terms S1 and S2 are those defined by Lettau (1969) and will be used again in connection with surface roughness length determination.

Thermal radiation is calculated as a function of surface temperature and "effective sky temperature." The latter quantity is defined by Reifsnyder and Lull (1965) as the temperature "appropriate to" the total amount of long-wave emitted sky radiation, i.e., the atmosphere is treated as a blackbody radiating at the effective sky temperature. Outcalt uses a constant daily effective sky temperature equal to the daily shelter-level mean temperature depressed by 22° C. The basic equation is then

$$R_{nlong} = (\sigma T_{sky}^4 - \sigma T_{sfc}^4) \cdot \varepsilon \qquad (18)$$

where $\sigma$ = the Stefan-Boltzmann constant ($8.13 \times 10^{-11}$ ly $°K^{-4}$ $min^{-1}$), and blackbody emissivity for both surface and sky is assumed ($\varepsilon = 1$). In an urban area, however, there are obstacles to sky radiation and enhancement of ground radiation by the existence of building walls. Outcalt takes the approach of Reifsnyder and Lull (1965), who define the viewfactor for thermal radiation as "the fraction of the radiation leaving a surface in all directions that is intercepted by another surface." The viewfactor F is related to obstacle

height h and the spacing of the obstacles d as expressed by

$$F = \sin^2 (\arctan \frac{d}{2h}). \tag{19}$$

Outcalt considers that the viewfactor ( $F'$ ) is equivalent to 2 times the silhouette ratio (S1/S2) previously defined:

$$F' = 2 \cdot (S1/S2) \tag{20}$$

Thus,

$$R_{nlong} = [(1-F')\sigma T_{sky}^4 + (F' -1)\sigma T_{sfc}^4 ] \cdot \varepsilon \tag{21}$$

## Sensible Heat and Latent Energy Fluxes

The fluxes of sensible heat and latent energy are represented by the traditional equations

$$H = -\rho C_p K_h \frac{\partial \theta}{\partial z}, \tag{22}$$

and

$$LE = -\rho \quad LK_w \frac{\partial q}{\partial z}, \tag{23}$$

where $\rho$ is air density, $C_p$ is air specific heat at constant pressure, L = latent heat of vaporization, $K_h$ and $K_w$ are turbulent diffusivities for heat and water vapor, respectively, $\theta$ is potential temperature and q is specific humidity.

In the Myrup-Outcalt model the diffusivities for heat, water vapor, and momentum are assumed to be equal. By utilizing the logarithmic wind relationship and thereby determining $K_m$, the eddy diffusivity for momentum, $K_h$ and $K_w$ may be found.

In near neutral conditions, wind speed varies exponentially with height and may be expressed by the logarithmic wind profile equation (Sellers, 1965)

$$u = \frac{1}{k} u^* \quad \ln \left(\frac{z}{Z_o}\right), \tag{24}$$

where u = windspeed, u* = friction velocity, k = von Karman' constant = 0.4, z = height above the surface, and $Z_o$ = the surface roughness length, the height above the surface at which the wind speed is zero. Surface roughness is calculated by the formula

$$Z_o = (1/2) \cdot HO \cdot \left(\frac{S1}{S2}\right), \tag{25}$$

where HO is the mean height of objects at the surface. Differentiating equation (24) with respect to height gives

$$\frac{du}{dz} = \frac{1}{kz} u^*, \tag{26}$$

The flux of momentum near the surface ( $\tau$ ) is described by

$$\tau = \rho K_m \frac{\partial u}{\partial z} \tag{27}$$

Substituting equation (26) in this equation gives

$$\tau = \rho K_m \frac{1}{Kz} u^* \tag{28}$$

Thus,

$$K_m = \frac{\tau}{\rho} K Z \frac{1}{u^*} \tag{29}$$

and since, by definition

$$u^* = (\tau/\rho)^{1/2}, \tag{30}$$

then

$$K_m = u^* kz. \tag{31}$$

The substitution of equation (29) for u* yields

$$K_m = \frac{k^2 uz}{\ln (z/z_o)} \tag{32}$$

Since it is assumed that $K_h = K_w = K_m$, the flux density equations become

$$H = \frac{-\rho Cp k^2 u}{\ln (Z/Z_o)} \cdot \frac{\partial \theta}{\partial \ln z} \tag{33}$$

and,

$$LE = \frac{-\rho L K^2 u}{\ln(z/z_o)} \cdot \frac{\partial q}{\partial \ln z}, \tag{34}$$

where $\theta$ = potential temperature and q = specific humidity.

To improve upon the model, Outcalt added a stability correction term to the sensible heat equation so that in final form,

$$H = \frac{-\rho C p k^2 u}{\ln(z/z_o)} \frac{\partial \theta}{\partial \ln z} \cdot (|1-32Ri|)^{1/2} \tag{35}$$

Where Ri is the bulk Richardson number.

In finite difference form, equations (34 and (35) become

$$H = \frac{k^2 \rho C p u}{[\ln(Z_2/Z_o)]^2} \cdot (|1-32Ri|)^{1/2} \cdot (T_2 - TZ_2 - T_o), \tag{36}$$

and,

$$LE = \frac{k^2 \rho L u}{[\ln(Z_2/Z_o)]^2} \cdot (q_2 - qo), \tag{37}$$

where subscript 2 denotes values at the atmospheric "damping" depth $Z_d$. Outcalt and Myrup define this depth as that at which surface effects upon temperature and wind are almost completely damped out, i.e., the depth of the mixed layer. Myrup uses 300 m as a constant damping depth for urban applications. Outcalt modifies this approach and calculates $Z_d$ as the level in the atmosphere at which two particular expressions for diffusivity converge. These functions are

$$d_1 = \frac{k^2 u_2}{\ln (Z_d/Z_o)}, \tag{38}$$

a bulk diffusivity value, and

$$d_2 = \frac{Z_d^2}{5.184 \times 10^5} \tag{39}$$



REPRODUCIBILITY OF THE ORIGINAL PAGE IS POOR

a thermal diffusivity term defined by Terzaghi (1952) as the damping depth for a 12-hour temperature wave in a homogeneous medium. In the iterative procedure used to find $Z_d$, values of $Z_d$ are incremented at 1-cm steps from the surface roughness value and the final value for $Z_d$ is obtained as the point at which the two functions converge. This admittedly crude approach results in values for the mixing depth which vary spatially with surface roughness and from day to day depending on wind speed. The damping depth remains constant through the day, however.

## Soil Heat Flux

The soil heat flux term G is described by the equation

$$G = -\kappa \frac{\partial(\rho C_p T)}{\partial z} \tag{40}$$

where $\kappa$= thermal diffusivity of the soil and $\rho C_p$ represents the soil volumetric heat capacity (Sellers, 1965). The integrated form of the one-dimensional case is

$$G = -\rho C_p \frac{T_2 - T_1}{\int_{z_1}^{z_2} \frac{dz}{\kappa}} \tag{41}$$

where $T_2$ and $T_1$ denote soil temperature at depths $Z_2$ and $Z_1$, respectively. Diffusion here is considered to be purely a process of molecular conduction so that the thermal diffusivity can be considered independent of depth (Monteith, 1973).

Thus,

$$\int_{z_1}^{z_2} \frac{dz}{\kappa} = \frac{Z_2 - Z_1}{\kappa} \tag{42}$$

Substitution into equation (40) gives

$$G = -\rho\, C_p\, \kappa\, \frac{T_2 - T_1}{Z_2 - Z_1} \tag{43}$$

representing the soil heat flux term for a one-layer system. The Outcalt model treats a four-layer system using this same relationship, making possible the introduction of a realistic thermal lag into the diurnal soil temperature variations at various levels. The depth of penetration of the diurnal temperature wave into the soil is calculated by the Terzaghi (1952) relationship used previously (equation 39). The damping depth ZG is given by

$$ZG = (12 \cdot t \cdot k)^{1/2} \tag{44}$$

where $t = 4.32 \times 10^4$ sec (12 hrs).

Three additional depths (ZG/2, ZG/4, and ZG/8) in the soil are used as nodes for the calculation of the soil heat flux term. At any particular level the rate and direction of temperature change is expressed by

$$\frac{dT}{dt} = k \cdot \frac{\partial^2 T}{\partial Z^2} \tag{45}$$

In finite difference form then, the temperature at depth $Z_2$ in the soil at time increment I is given by

$$T_2\,(I) = T_2\,(I\text{-}1) + \kappa\, \frac{T_{sfc}\,(I\text{-}1) - 2 \cdot T_2\,(I\text{-}1) + T_3\,(I\text{-}1)}{Z_2^2} \tag{46}$$

where $T_3$ is the temperature at some depth $Z_3 > Z_2$. The use of a set of similar equations, each corresponding to one of the five nodal depths,

effectively introduces a lag in soil temperature change with depth. Figure 2-1 below illustrates the nature of this lag for the case of a soil with thermal diffusivity of .005 $cm^2$ $sec^{-1}$ for winter solstice, clear-sky conditions.

## GENERAL FLOW OF THE MODEL

The above discussion describes assumptions made and methods of parameterization of the four surface energy balance components as functions of surface temperature and various combinations of either input values or quantities derived from input values. Input boundary conditions required for the Outcalt model may be divided into three categories. These sets of inputs and their primary function in the simulation procedures are shown below.

I. Temporal Data

Solar declination
Radius vector of the sun

These are the only external variables required for the generation of diurnal values of extraterrestrial solar radiation.

II. Meteorological Data

Atmospheric dust content (particles/cc)
Air relative humidity (fraction)
Precipitable water (mm)
Station pressure (mb)

The above variables are used in calculation of the attenuation of the solar beam by atmospheric processes of scattering and absorption. Air relative humidity is also used in the determination of the latent energy flux term.

Air temperature
Wind velocity

These two variables, along with air relative humidity, serve as boundary conditions at the level of the atmospheric mixing height.

III. Surface Characteristics

Albedo

Albedo values are used in calculation of solar radiation terms.

Obstacle height
Silhouette ratio (S1/S2 in equation 17)

These terms are used in the calculation of the surface roughness length. The silhouette ratio is important in both solar and longwave radiation computations.

III. Surface Characteristics--Continued

Surface wet fraction

The specific humidity value at the surface is calculated based on this value

Computed boundary conditions include the depths of penetration of both the atmospheric and the substrate temperature waves (equations 39, 40, 44), the atmospheric exchange coefficient (equation 32), and the surface roughness length (equation 25). The general flow of the calculations is illustrated by the following flowchart.

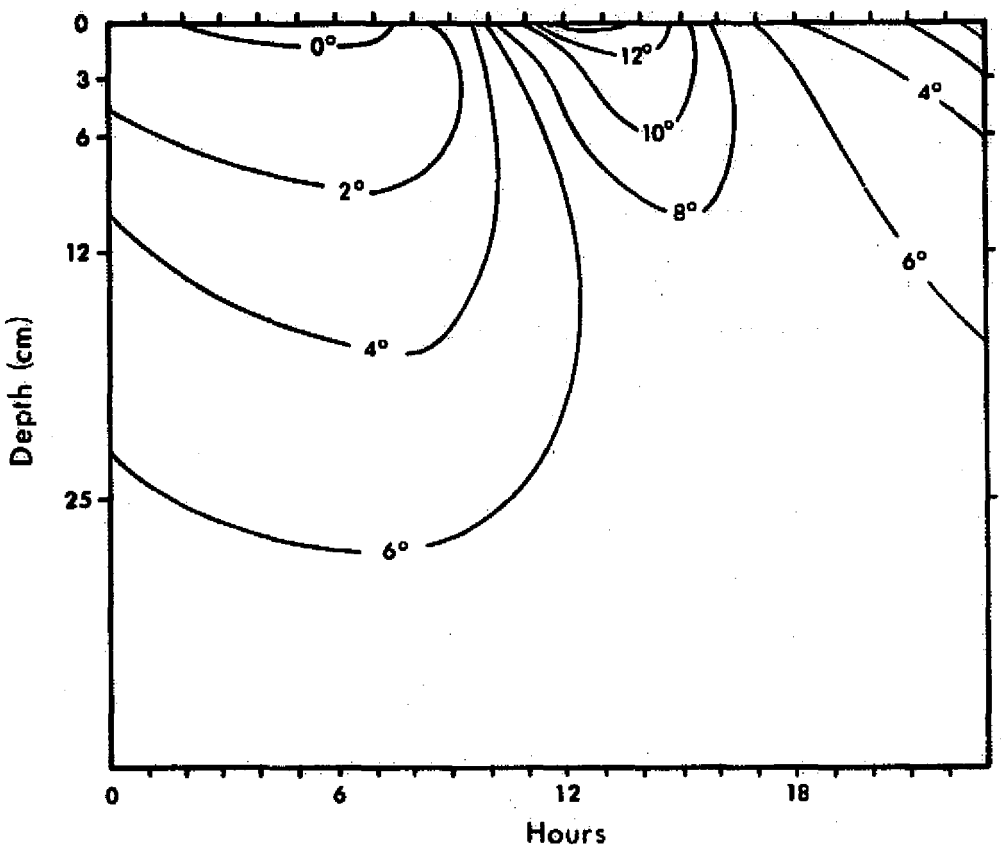


Isotherms in Degrees Celsius

**Figure 1--Simulated temperature variations in soil for a 24-hour period.**

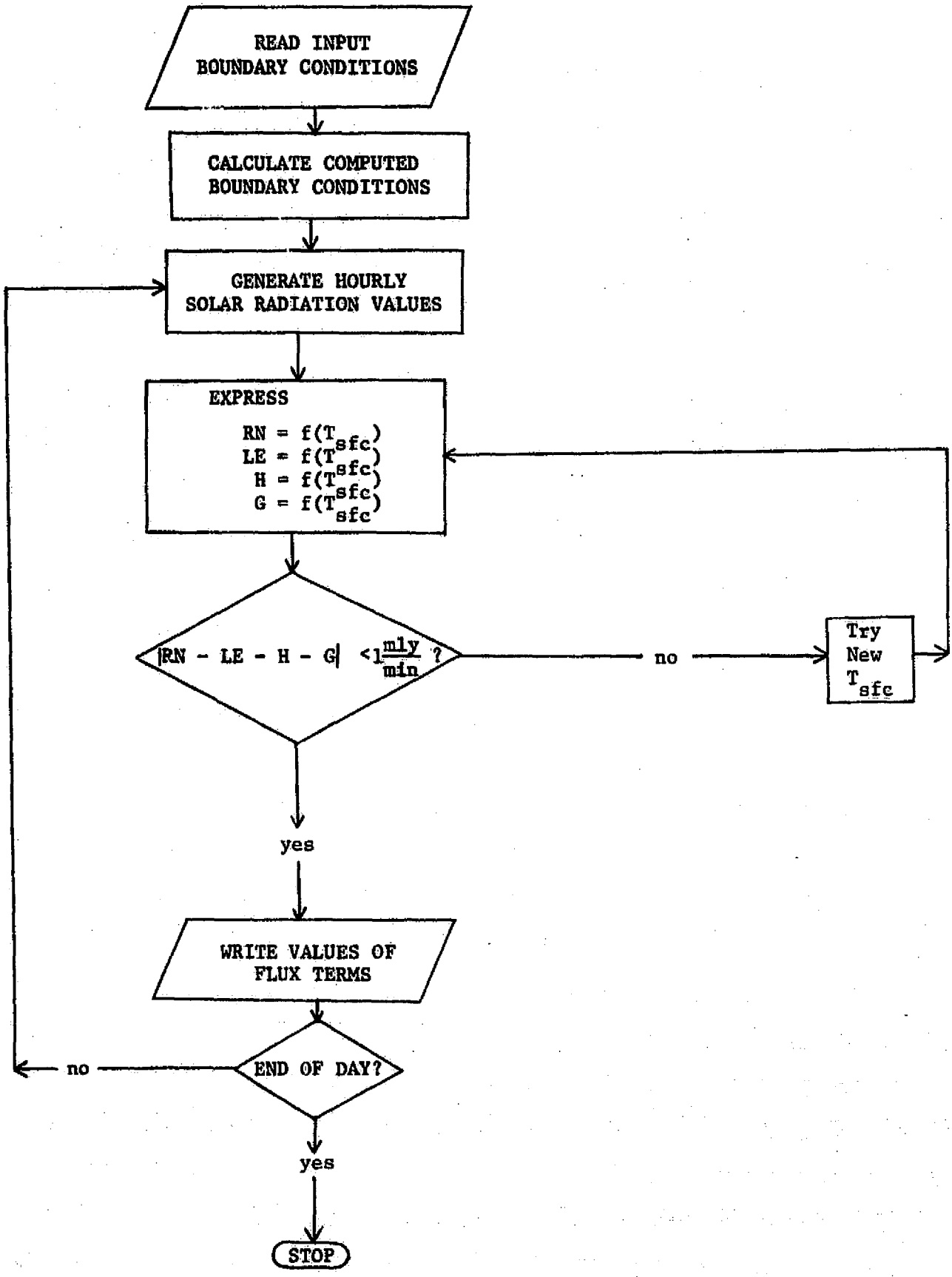


Figure 2--General flow chart for calculations of energy budget simulation model

## APPENDIX C

Reports, other than monthly progress reports, prepared with support of NASA/Skylab funding, and pre-Skylab NASA funding to USGS Geography Program climatology research.

Alexander, R. H., and Lins, H. F., Jr., 1974, Selected applications of Skylab high-resolution photography to urban area land use analysis: Internat. Soc. Photogramm., Comm. I, Symposium on Remote Sensing and Aerial Photography, Stockholm, 1974, Paper. Also an Interim Rept. under Skylab/EREP Investigation no. 469.

Lins, H. F., Jr., 1974, Interim report on the results of urban area land use analysis using Skylab S-190A and S-190B photography: Interim Rept. under Skylab/EREP Investigation no. 469, NASA Order no. T-5290B.

Alexander, R. H., Fitzpatrick, K. A., Lins, H. F., Jr., and McGinty, H. K. III, 1975, Land use and environmental assessment in the Central Atlantic region: NASA Earth Resources Survey Symposium, Houston, Tex., 1975, Proc., v. I-C, p. 1683-1727.

Pease, R. W., and Nichols, D., 1975, Energy balance maps from remotely sensed imagery: Photogramm. Eng. and Remote Sensing, v. 42, no. 11, p. 1367-1373.

Green, G., 1976, Sensitivity testing with energy-budget climate simulation: [Manuscript in preparation].

Jenner, C. B., 1976, Land use effects on the urban temperature field: a simulation experiment: [Manuscript in preparation].

Lins, H. F., Jr., 1976, Land-use mapping from Skylab S-190B photography: Photogramm. Eng., v. 42, no. 3, p. 301-307.

Nicholas, Francis, and Lewis, John, 1976, Relationships between aerodynamic roughness and land use in Baltimore, Maryland: [Manuscript in preparation].

Pease, R. W., Lewis, J. E., and Outcalt, S. I., 1976, Urban terrain climatology and remote sensing: Assoc. Am. Geographers, Annals, v. 26, no. 4, p. 557-569.

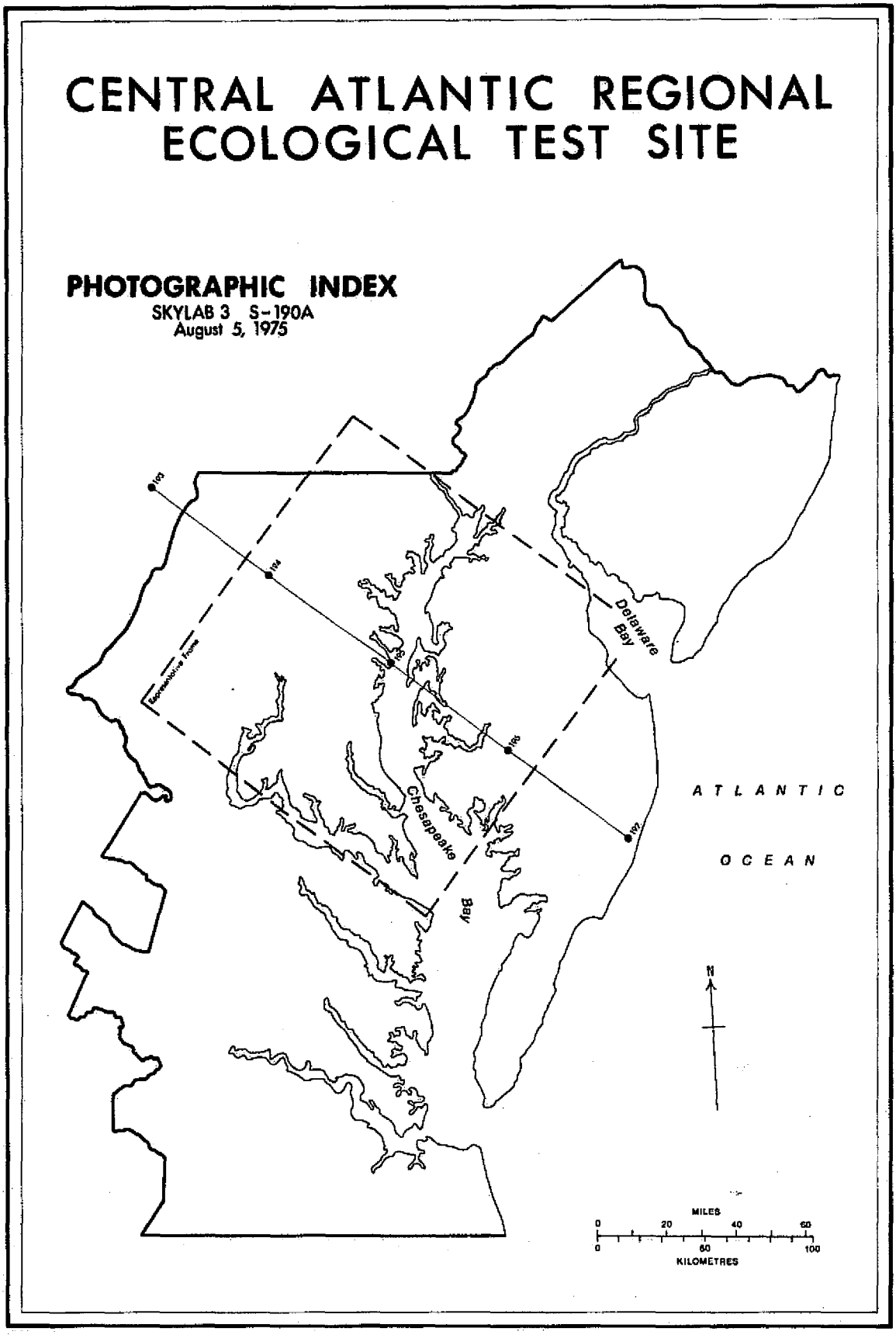


Figure 2.1--Index map showing location of ground trace, S-190A camera system, Skylab 3 pass over CARETS, August 5, 1973.

REPRODUCIBILITY OF TH
ORIGINAL PAGE IS POOR

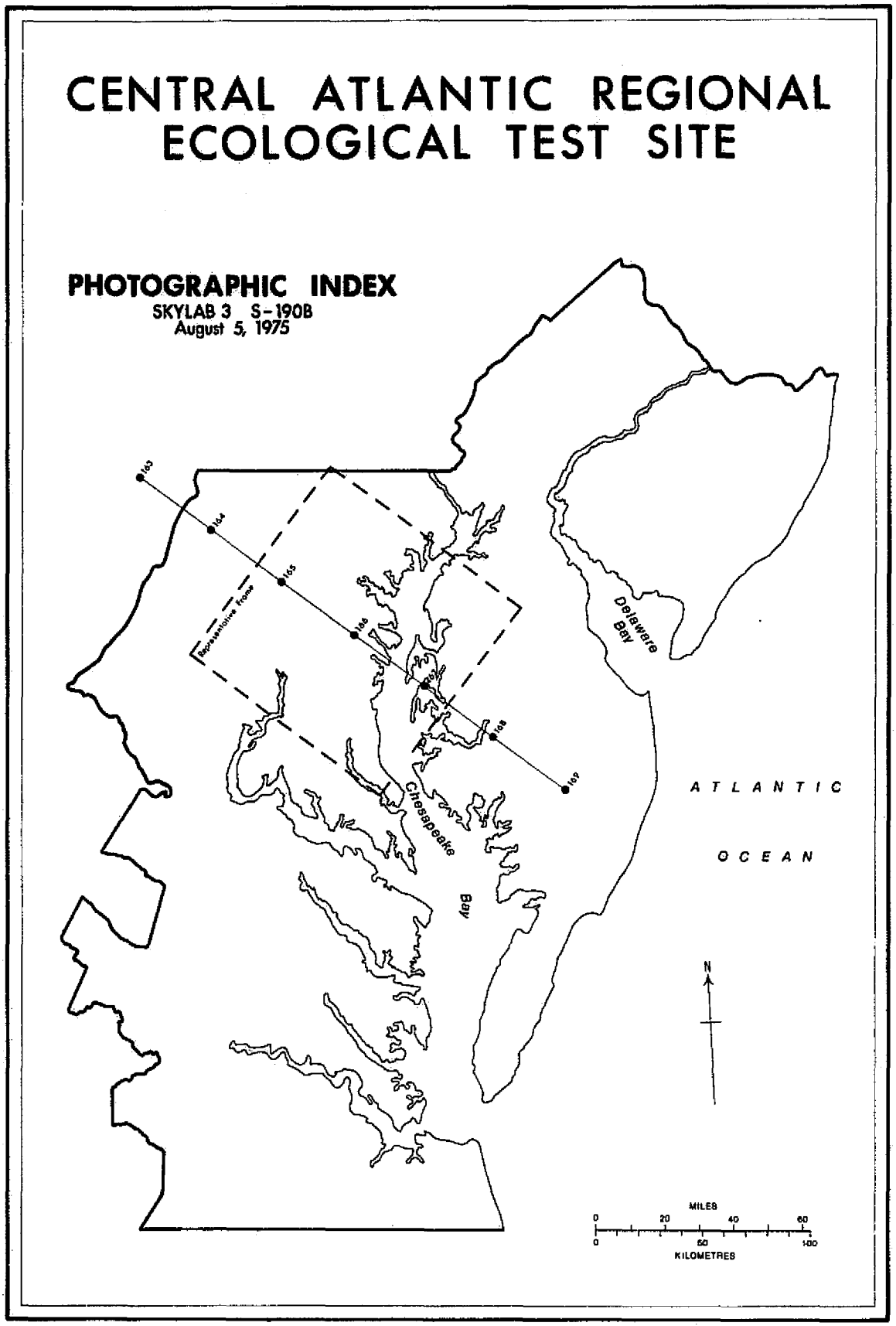


Figure 2.2--Index map showing location of ground trace, S-190B camera system, Skylab 3 pass over CARETS, August 5, 1973.

REPRODUCIBILITY OF TH-
ORIGINAL PAGE IS POOR

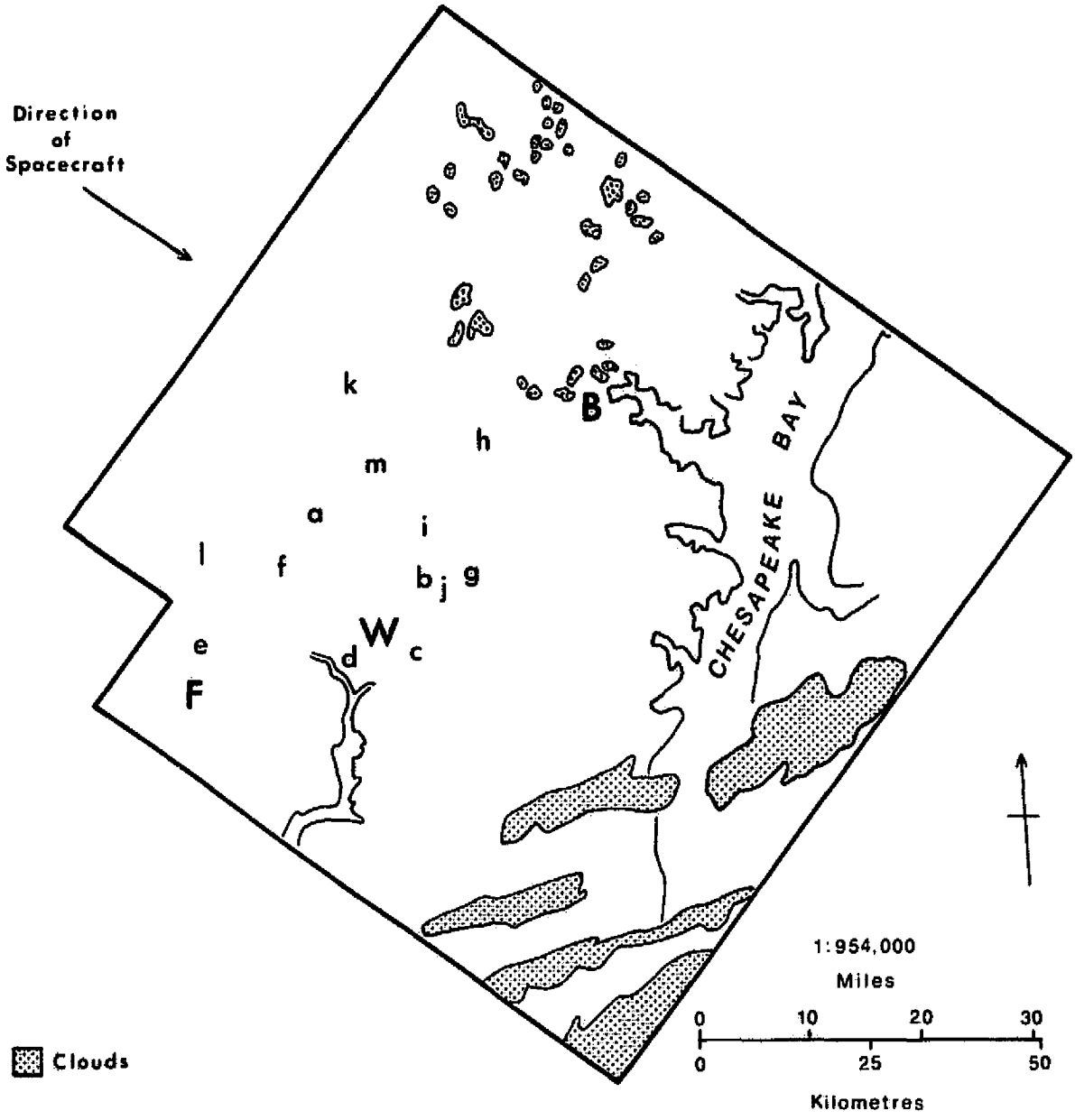


Figure 2.3--Index map to S-190B frame 83-166, Skylab 3 pass over CARETS, August 5, 1973; F = Fairfax, Va.; W = Washington, D.C.; B = Baltimore, Md.; a through m = locations of land use illustrations contained in figures 2.10a through 2.10m.

REPRODUCIBILITY OF THE
ORIGINAL PAGE IS POOR

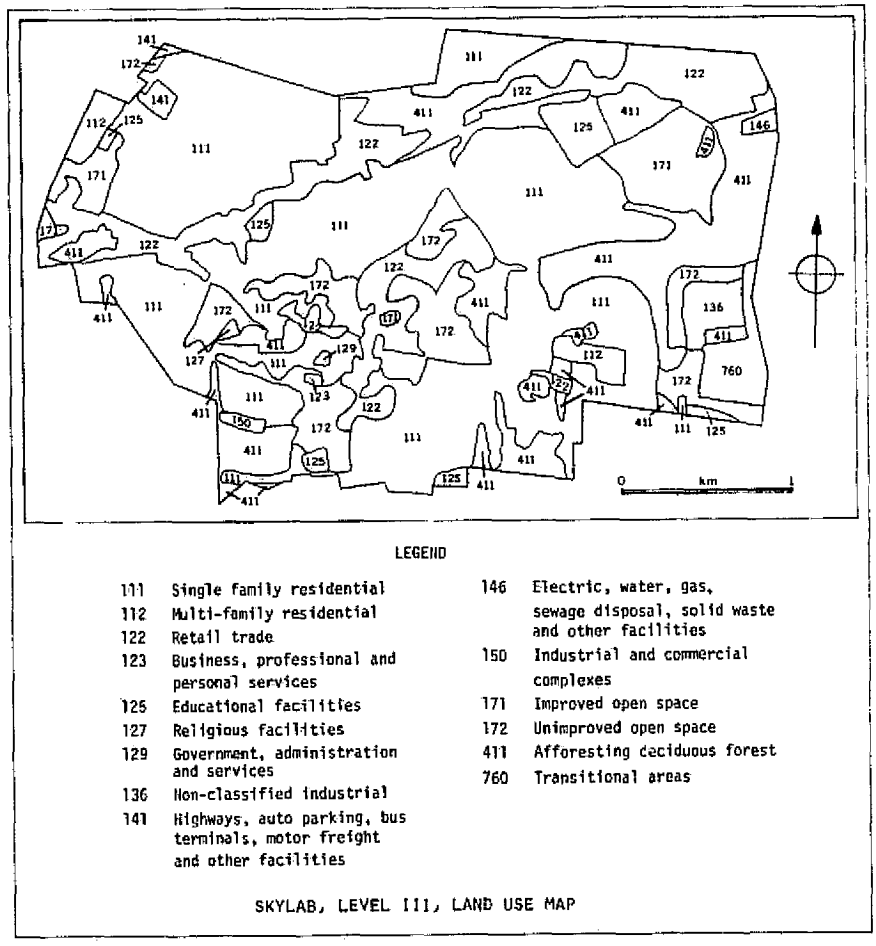


Figure 2.7--Level III land use map, based on interpretation of Skylab S-190B photography, Fairfax, Virginia.

REPRODUCIBILITY OF TH...
ORIGINAL PAGE IS POOR

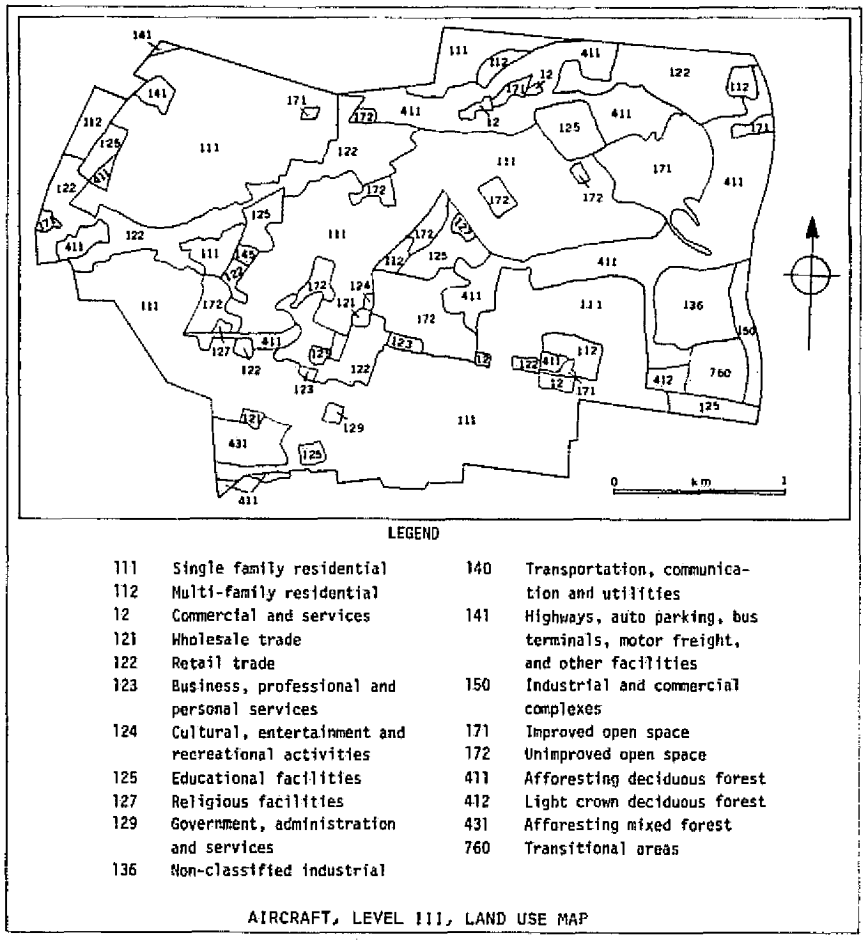


Figure 2.8--Level III land use map, based on interpretation of high-altitude aircraft photography, Fairfax, Virginia.

Primary source: U-2 flight 73-181, RC-10 color infrared photograph, frame 5296, 27 October 1973.

Supplementary source: U.S. Geological Survey, 7½-minute topographic map of Fairfax, Virginia, 1971 photorevised edition.

REPRODUCIBILITY OF
ORIGINAL PAGE IS POOR

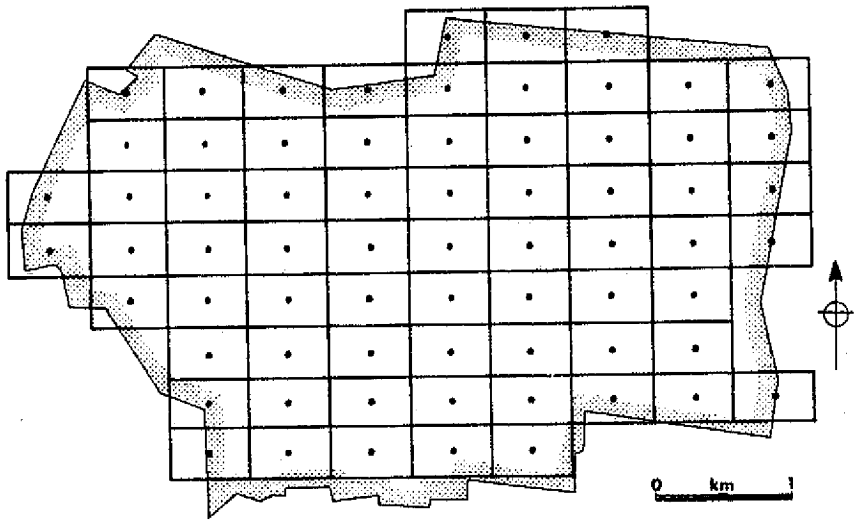


Figure 2.9--Location of points for comparing Skylab and aircraft-derived land use data, Fairfax, Virginia.

REPRODUCIBILITY OF THE
ORIGINAL PAGE IS POOR

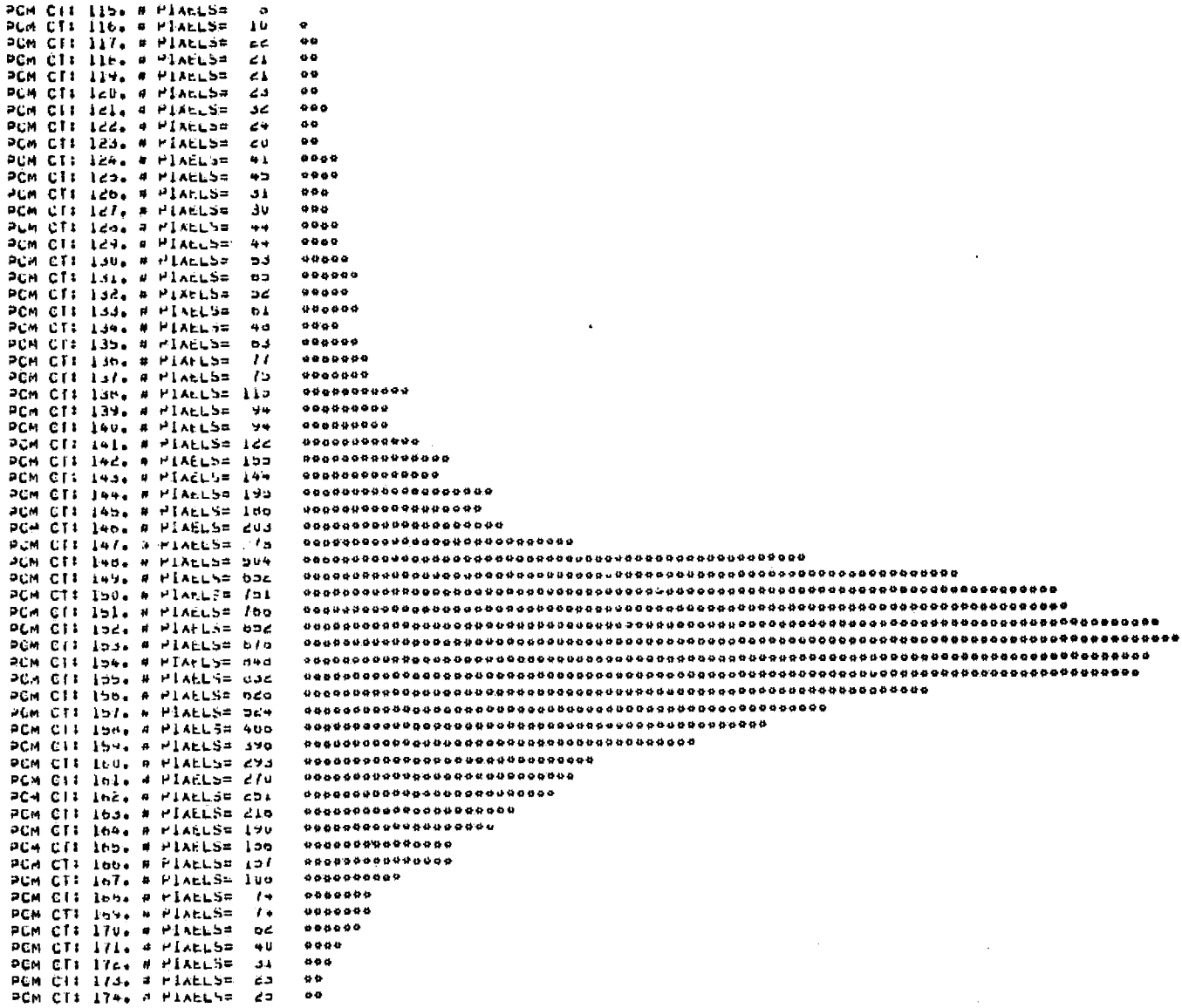


Figure 3.1--Distribution of PCM counts from S-192 output - Band 13

REPRODUCIBILITY OF THE
ORIGINAL PAGE IS POOR

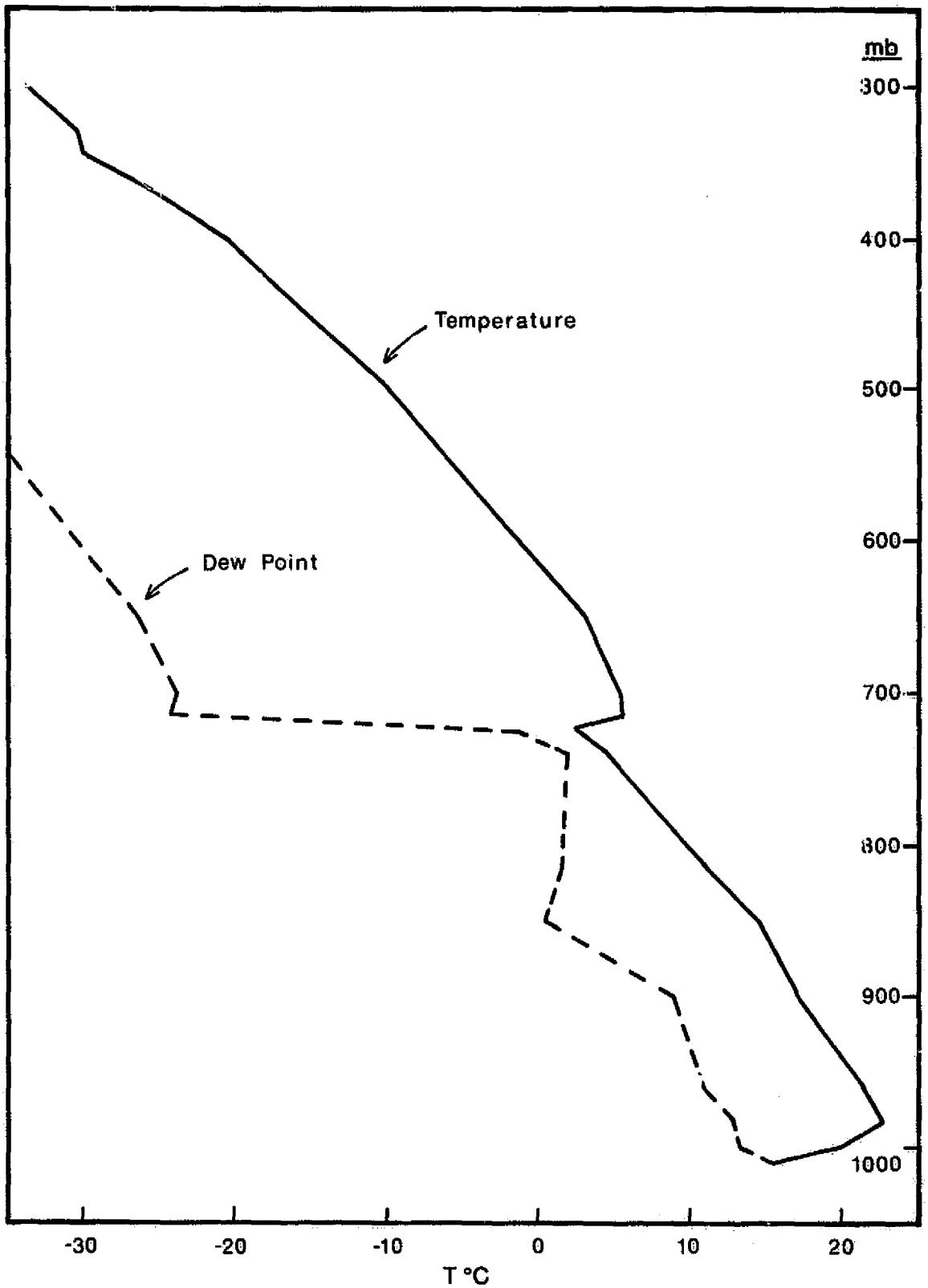


Figure 3.2--Rawinsonde profile for 7:15 a.m. EST, August 5, 1973, Washington, D.C.

REPRODUCIBILITY OF THE
ORIGINAL PAGE IS POOR

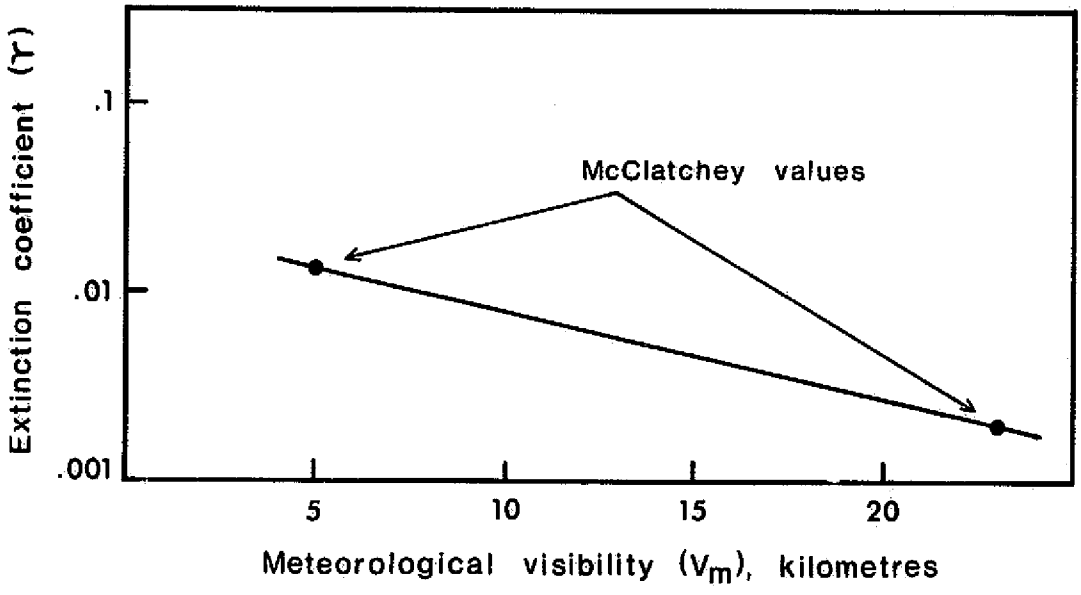


Figure 3.3--Extinction coefficients ($\gamma$) at a wavelength of 10.591 μm for various visibility ranges (McClatchey and others, 1972a).

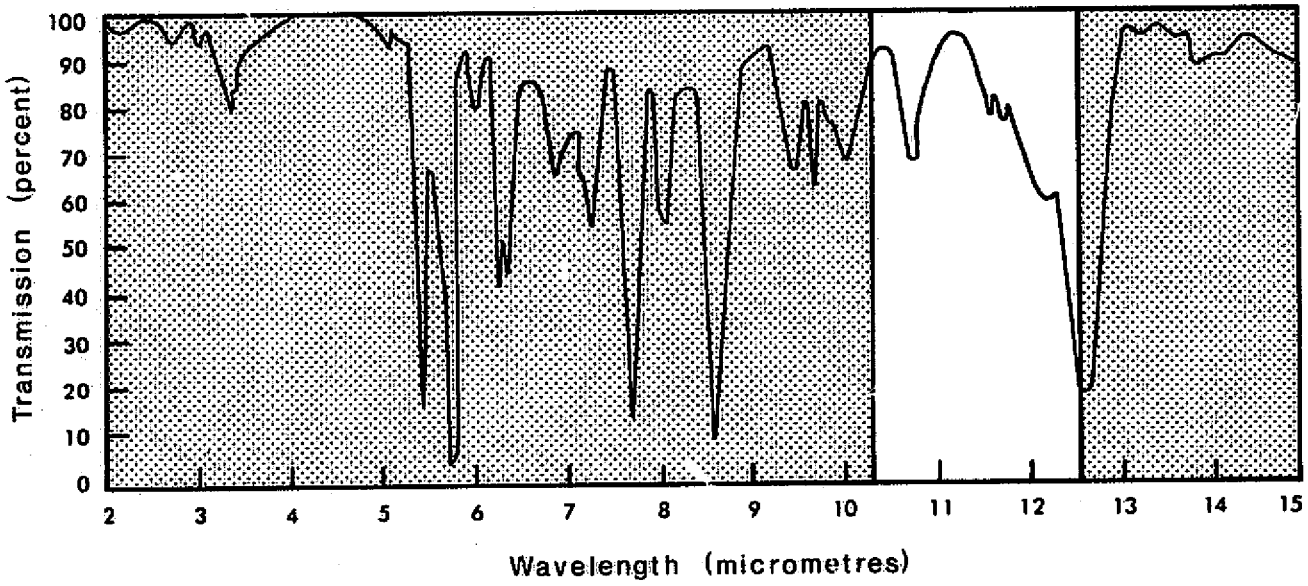


Figure 3.4--Absorption spectrum of Peroxyactyl Nitrite (PAN). Nonshaded area is the 10.2 - 12.5 μm Sensing Window of Band 13 of the S-192 scanner (after Scott and others, 1957).

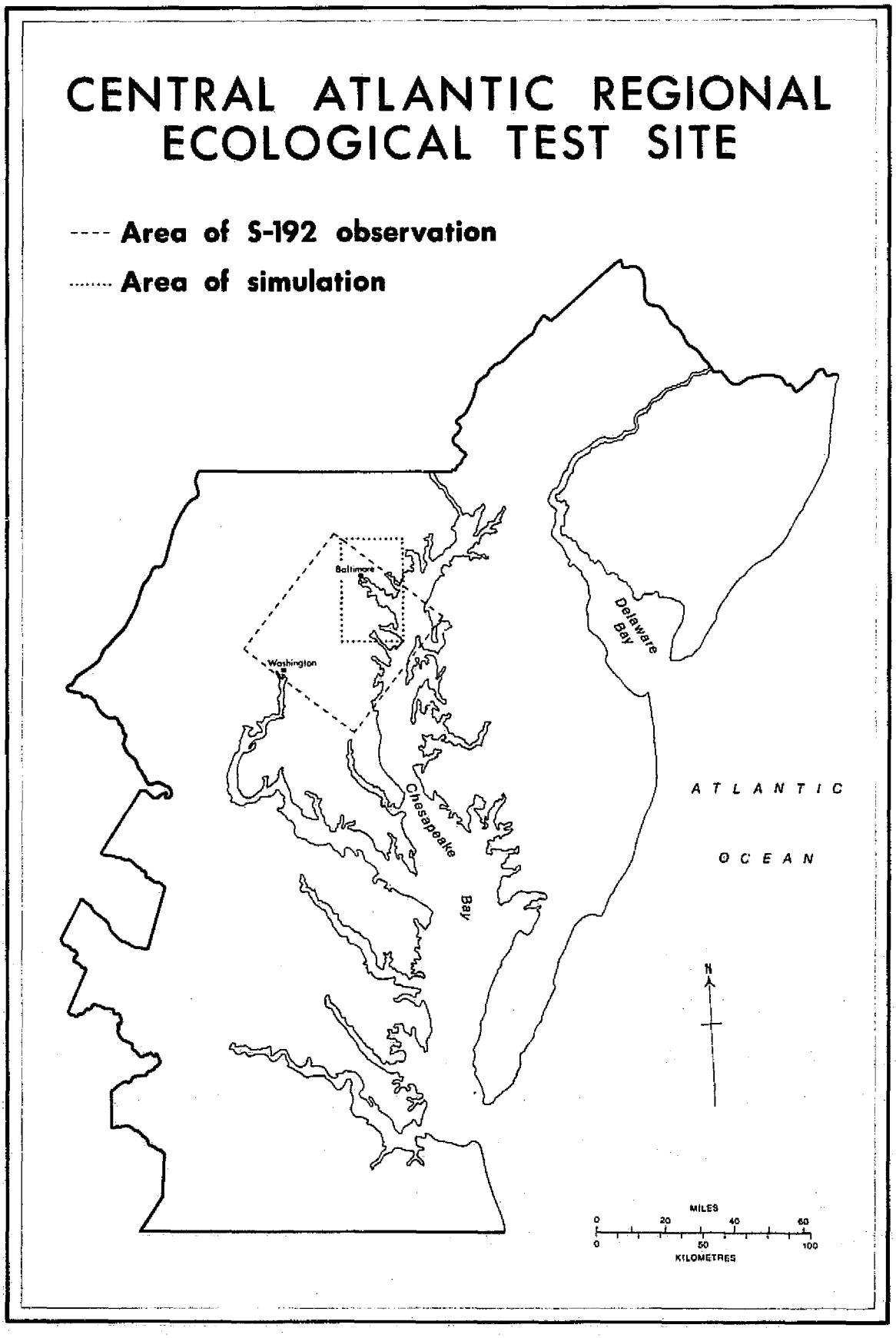


Figure 3.5--Location of mapped areas, thermal mapping experiment

REPRODUCIBILITY OF THE
ORIGINAL PAGE IS POOR

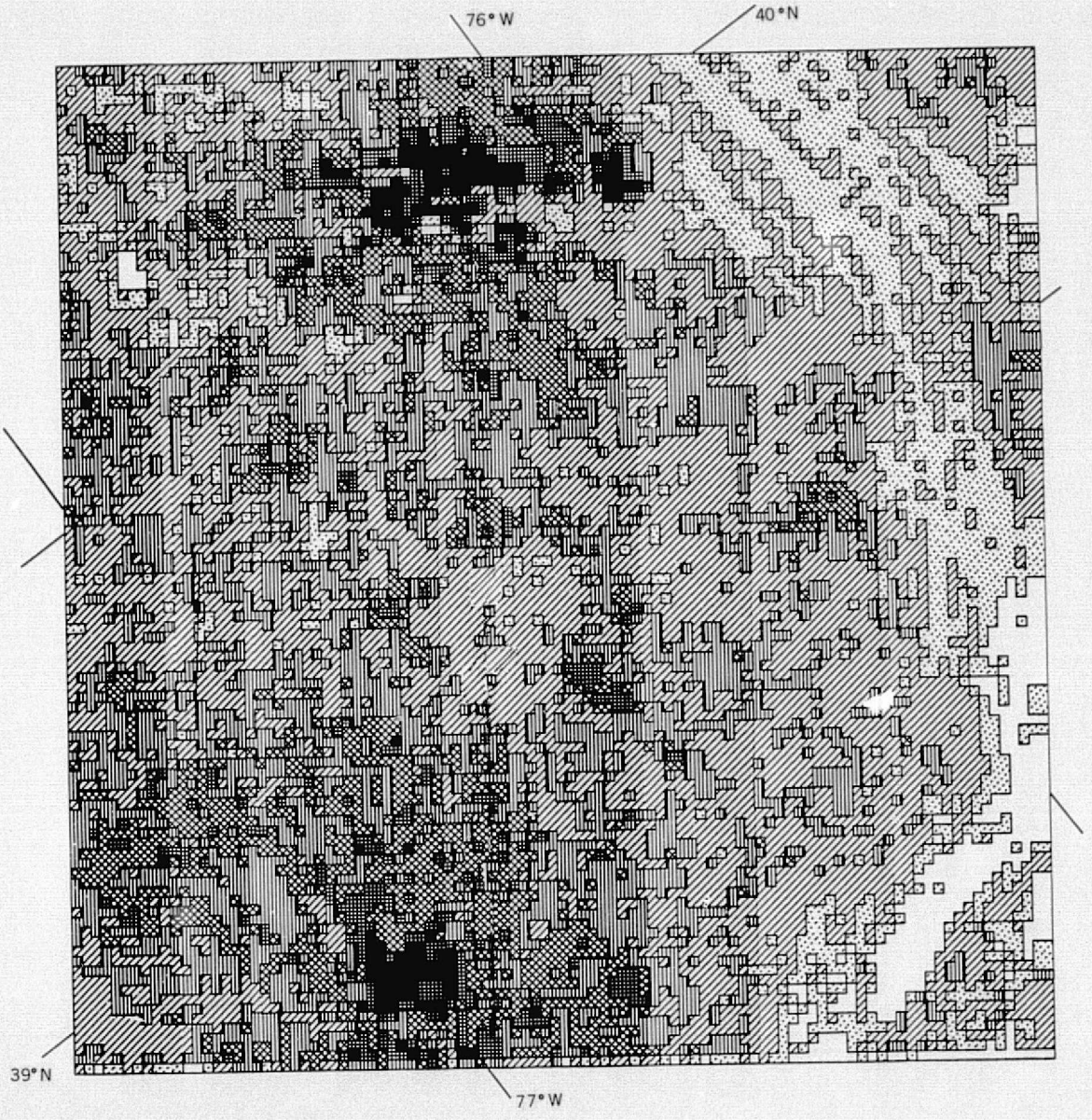


Figure 3.6

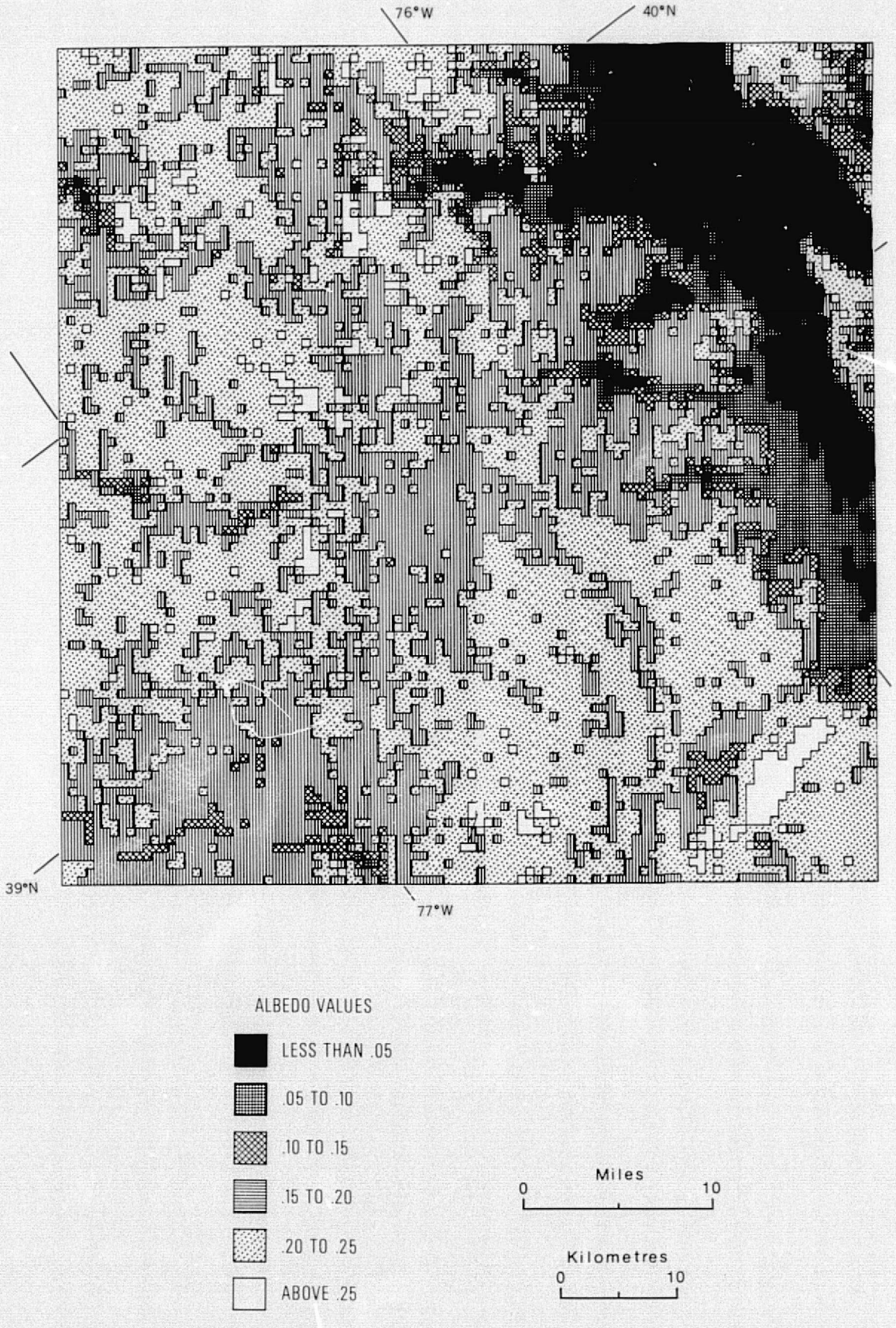
76°W
40°N
39°N
77°W
ALBEDO VALUES
LESS THAN .05
.05 TO .10
.10 TO .15
.15 TO .20
.20 TO .25
ABOVE .25
Miles
0
10
Kilometres
0
10

Figure 3.7

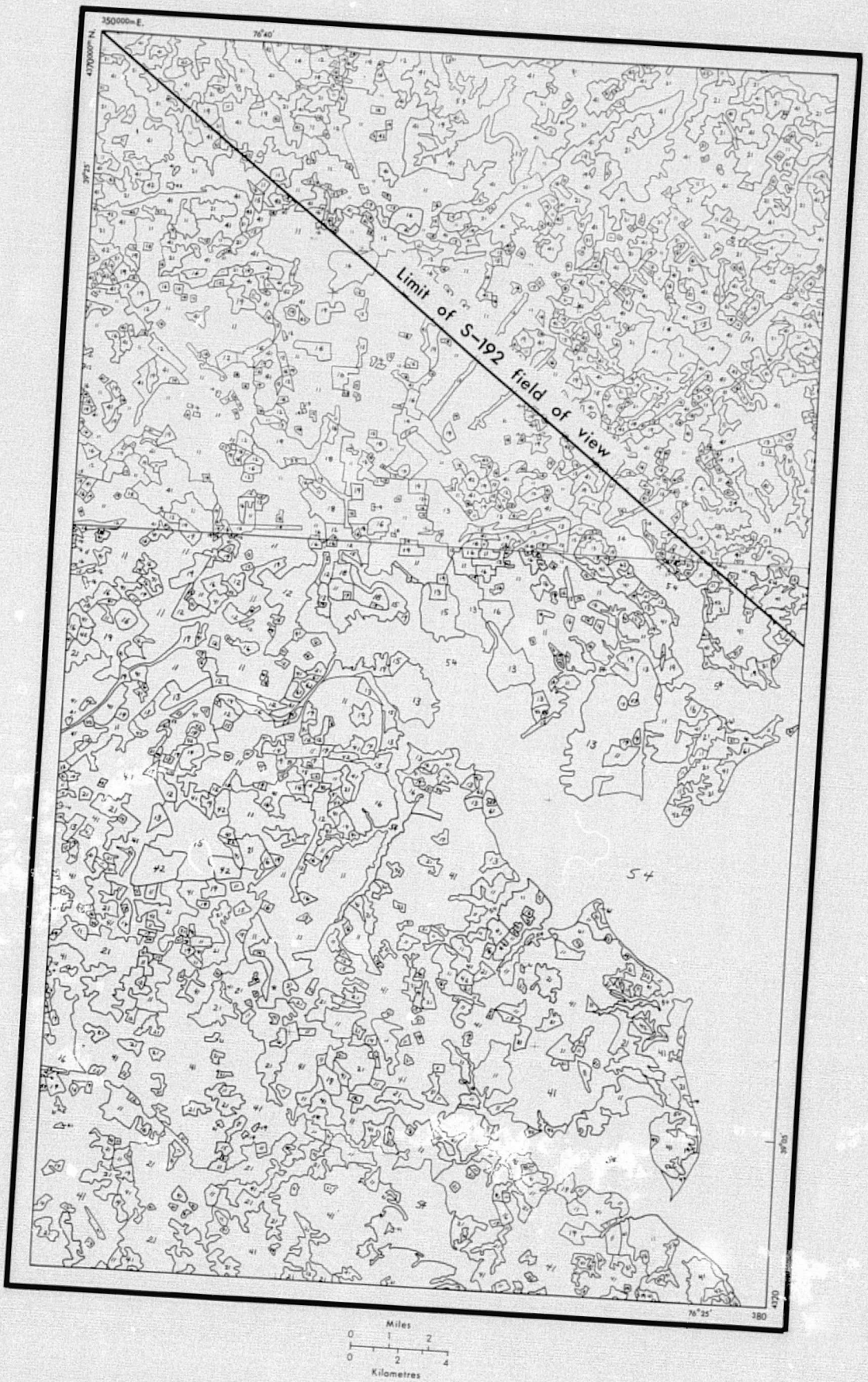
350000m E.
76°40'
4070000m N.
39°25'
Limit of S-192 field of view
54
76°25'
380
4020
39°20'
Miles
0 1 2
0 2 4
Kilometres

Figure 3.8

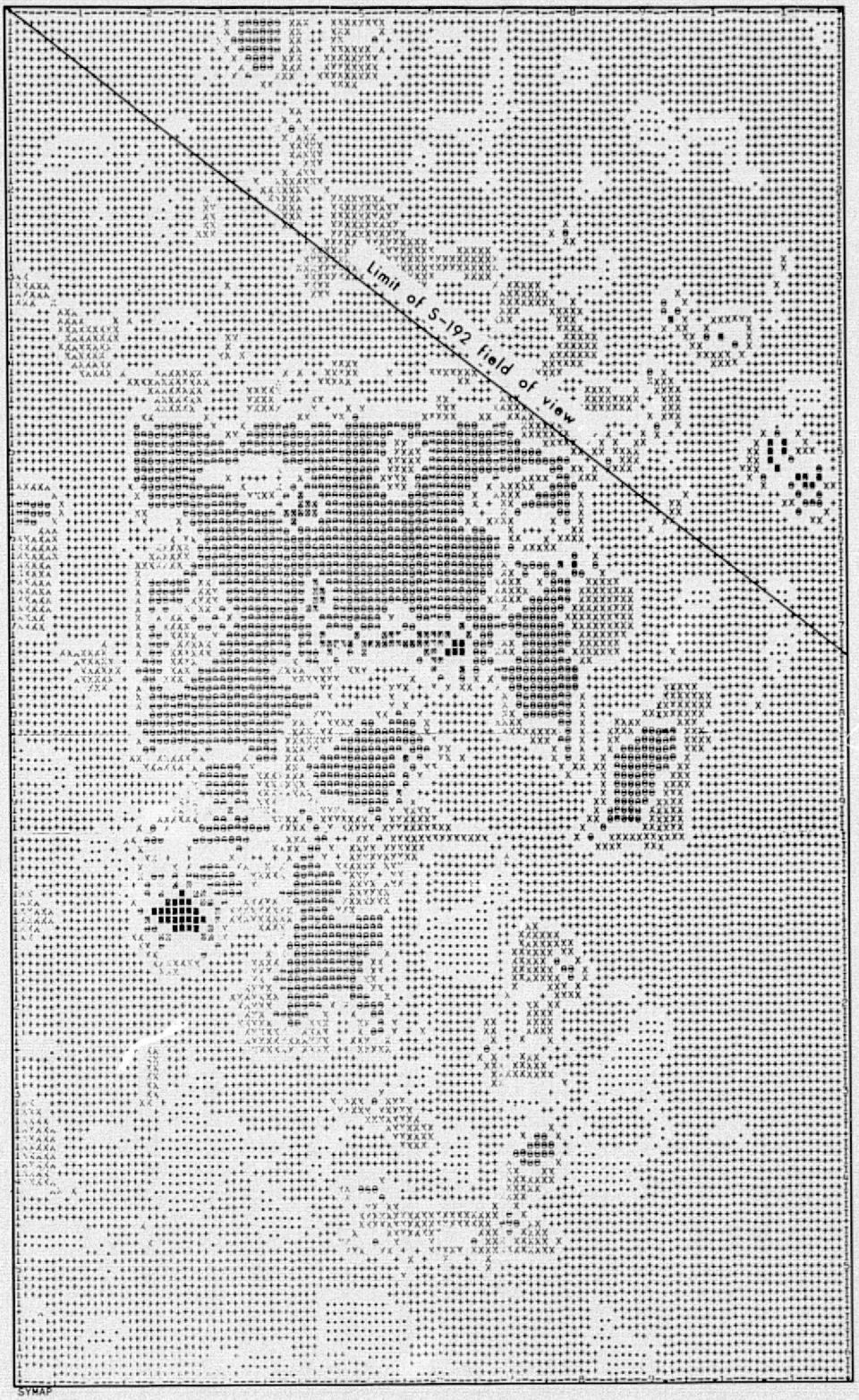


SYMAP

ABSOLUTE VALUE RANGE APPLYING TO EACH LEVEL
('MAXIMUM' INCLUDED IN HIGHEST LEVEL ONLY)

| | | | | | | |
|---|---|---|---|---|---|---|
| MINIMUM | 20.00 | 22.83 | 25.67 | 28.50 | 31.33 | 34.17 |
| MAXIMUM | 22.83 | 25.67 | 28.50 | 31.33 | 34.17 | 37.00 |

| LEVEL | 1 | 2 | 3 | 4 | 5 | 6 |
|---|---|---|---|---|---|---|
| | ..... | +++++++++ | XXXXXXXXX | 000000000 | ■■■■■■■■■ | ■■■■■■■■■ |
| | ..... | +++++++++ | XXXXXXXXX | 000000000 | ■■■■■■■■■ | ■■■■■■■■■ |
| SYMBOLS | ....1.... | ++++2++++ | XXXX3XXXX | 0000040000 | ■■■■■5■■■■ | ■■■■■6■■■■ |
| | ..... | +++++++++ | XXXXXXXXX | 000000000 | ■■■■■■■■■ | ■■■■■■■■■ |
| | ..... | +++++++++ | XXXXXXXXX | 000000000 | ■■■■■■■■■ | ■■■■■■■■■ |

Miles
0 1 2
0 2 4
Kilometres

N

Figure 3.9

REPRODUCIBILITY OF THE
ORIGINAL PAGE IS POOR

Limit of S-192 field of view
SURFACE RADIATION TEMPERATURES
L
25°
28°
31°
34°
37°
40°
377
1237
4121
2748
1277
372
168
NUMBER OF CELLS
Miles
0 1 2
0 2 4
Kilometres
N

Figure 3.10

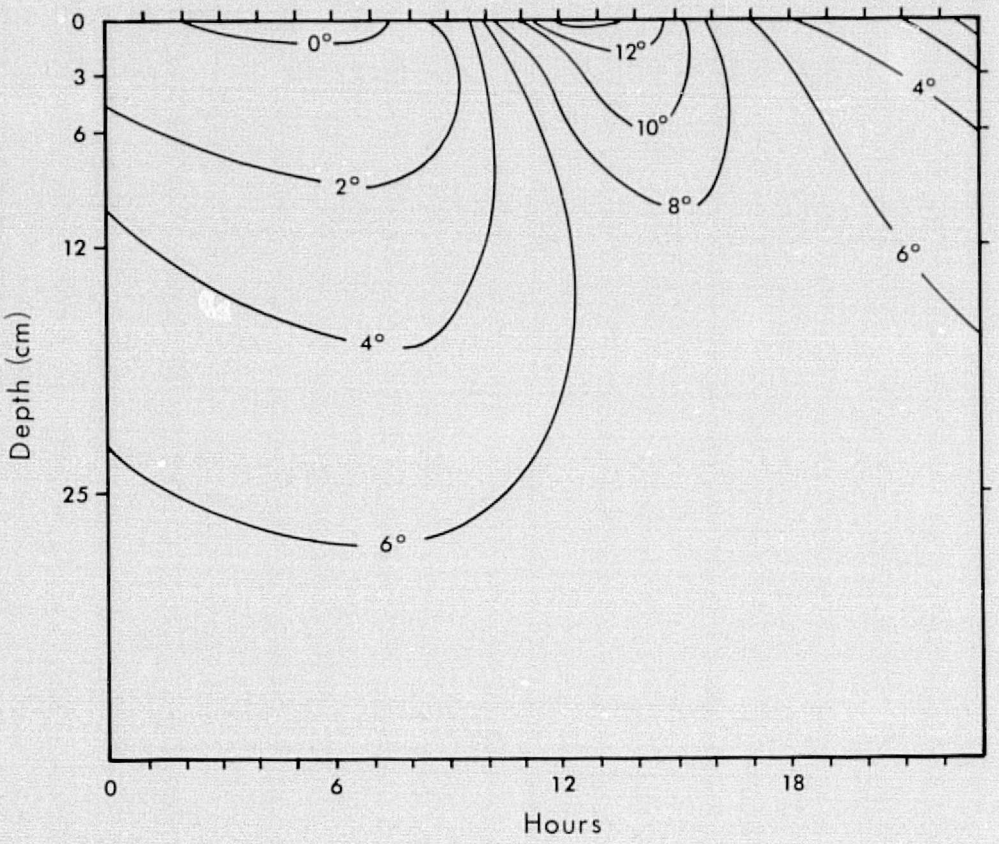


Isotherms in Degrees Celsius

Figure B1--Simulated temperature variations in soil for a 24-hour period.